TÉCNICO LISBOA

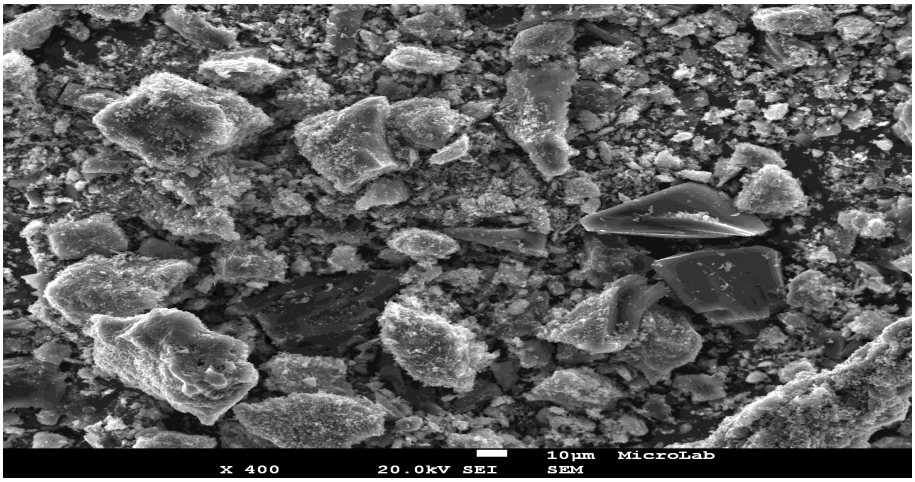

Influence of mineral matter on the gasification kinetics of coal chars in carbon dioxide stream

Paweł Torbus

Thesis to obtain the Master of Science Degree in

Energy Engineering and Management

Supervisors: Dr. Rui Pedro da Costa Neto

Examination Committee

Chairperson: Prof. José Alberto Caiado Falcão de Campos
Supervisor: Dr. Rui Pedro da Costa Neto

Member of the committee: Prof. Mario Manuel Goncalves da Costa

January 2015

"Work performed under task of research No. 3 funded under the Agreement NCBiR No. SP/E/3/7708/10".

The research results presented herein were obtained during the course of the project "*Development of coal gasification technology for high-efficient production of fuels and energy*", Task No. 3 of the Strategic Program for Research and Development: "Advanced energy generation technologies" funded by the **Polish National Centre for Research and Development**.

This thesis is based on work conducted within the **KIC InnoEnergy Master School**, in the MSc programme Clean Coal Technologies. The KIC InnoEnergy supports this programme financially. I have also received financial support from KIC InnoEnergy, which is gratefully acknowledged.

KIC InnoEnergy is a company supported by the European Institute of Innovation and Technology (EIT), and has the mission of delivering commercial products and services, new businesses, innovators and entrepreneurs in the field of sustainable energy through the integration of higher education, research, entrepreneurs and business companies. Shareholders in KIC InnoEnergy are leading industries, research centres, universities and business schools from across Europe.
www.kic-innoenergy.com

The MSc programme Clean Coal Technologies is a collaboration of:
AGH University of Science and Technology, Kraków, Poland,
SUT Silesian University of Technology, Gliwice, Poland
IST Instituto Superior Tecnico, Lisbon, Portugal

ACKNOWLEDGEMENTS

First, I would like to thank Professor **Marek Ściążko** (University of Science and Technology in Kraków, Institute for Chemical Processing of Coal in Zabrze), my supervisor, who gave me the chance to take a part in such an interesting project and guided me through these years into gasification process understanding.

To Doctor **Rui Costa Neto** (Instituto Superior Tecnico in Lisbon), my IST supervisor, who spent a lot of time with me constructing the laboratory scale reactor, and for supporting me with his knowledge when I faced certain design issues. Thank you for time you spent reading my paper I am very grateful for all the meaningful comments you made.

To MSc **Grzegorz Tomaszewicz (**Institute for Chemical Processing of Coal in Zabrze), my co-supervisor, who spent a lot of time to introduce me to the coal gasification topic and industrial work during my internships. I am indebted for all your comments especially those concerning technical details. Thank you for your endorsement of my work in Institute, and for all indulgence you have shown during our cooperation.

To the **Institute for Chemical Processing of Coal in Zabrze**, who made this work possible through their technical and laboratory support. I always enjoyed time of my internship there. Thank you for all the knowledge and practical experience I have gained there.

Special thanks goes to PhD **Ewelina Ksepko** and **Katarzyna Kamińska** who always supported me with their language skills and they did most of the language correction on my papers during the last years.

And last but never least; I would like to thank **my parents** for all the support I have received during my education and for bringing me up in a stimulating environment.

ABSTRACT:

Literature reports that parent coal properties influence kinetics of coal gasification. The reactivity of coal chars towards CO_2 is influenced by coal rank, pyrolysis conditions (heating rate, holding time, final temperature), pressure, surface morphology, pore structure, particle size etc. The role of ash content, content and composition of inorganic constituents likely to catalyse oxygen exchange reactions is still under research.

The main goal was to understand and predict the influence of mineral matter on kinetics of coal char gasification by carbon dioxide. In order to prove the role of certain compounds, they were additionally introduced into studied coals. Experiment results were used for structuring kinetic models.

In this dissertation, integral and differential kinetic models were applied to describe the varying conversion rate: Flynn-Wall-Ozawa, Kissinger-Akahira-Sunose, and Freidman. Obtained from experimental part and further mathematical modelling results show significant influence of mineral matter compounds (iron oxides and limestone) on the kinetics of coal chars CO_2 gasification. Results show that at high conversions, exposure of included minerals on the char surface is mostly caused by fragmentation. In the later stage of gasification, the char particle fragmented into a few particles of *20–30 μm* as indicated by Scanning Electron Microscopes (SEM) pictures. Addition of limestone or iron (III) oxide catalyst does not promoted coal char gasification, but its particles conglomerated and blocked active sites.

Laboratory tests were carried out at Institute for Chemical Processing of Coal in Zabrze, Poland and at Instituto Superior Técnico in Lisbon, Portugal.

Keywords: coal char, CO_2 gasification, isoconversional models, mineral matter, reactivity

RESUMO:

A literatura indica que as propriedades do carvão pai influenciar cinética de gaseificação de carvão. A reatividade de caracteres de carvão em relação CO_2 é influenciada pela classificação de carvão, as condições de pirólise (taxa de aquecimento, tempo de espera, a temperatura final), pressão, morfologia da superfície, estrutura de poros, tamanho de partícula etc. O papel do teor de cinzas, o conteúdo ea composição dos constituintes inorgânicos susceptível de catalisar reações de troca de oxigênio ainda está sob investigação.

O principal objetivo era entender e prever a influência da matéria mineral na cinética de carvão carvão gaseificação por dióxido de carbono. A fim de provar o papel de determinados compostos, eles foram adicionalmente introduzidos em carvões estudados. Os resultados da experiência foram utilizados para estruturar modelos cinéticos.

Nesta dissertação, modelos cinéticos integral e diferencial foram aplicados para descrever a taxa de conversão varia: Flynn-Wall-Ozawa, Kissinger-Akahira-Sunose e Freidman. Obtido a partir da parte experimental e mais resultados de modelagem matemática mostram influência significativa de compostos de matéria mineral (óxidos de ferro e calcário) sobre a cinética da gaseificação do carvão caracteres de CO2. Os resultados mostram que em altas conversões, a exposição de minerais incluídos na superfície do carvão é principalmente causada pela fragmentação. Na última etapa de gaseificação, a partícula de carvão fragmentado em algumas partículas de 20-30 mm, como indicado por figuras SEM. A adição de calcário ou de ferro (III) catalisador de óxido não promoveu carvão carvão gaseificação, mas suas partículas conglomerated e bloqueou sites ativos.
Os exames laboratoriais foram realizados no Instituto de Processamento de Químicos de carvão em Zabrze, na Polónia e no Instituto Superior Técnico, em Lisboa, Portugal.

Palavras-chave: carvão de carvão, a gaseificação CO2, modelos isoconversional, matéria mineral, reatividade

TABLE OF CONTENT:

ACKNOWLEDGEMENTS **3**
LIST OF FIGURES: 7
LIST OF TABLES: ..... **ERROR! BOOKMARK NOT DEFINED.**
LIST OF SYMBOLS AND ABBREVIATIONS: 9

1. INTRODUCTION **10**
1.1. THESIS OUTLINE 12
1.2. OBJECTIVES OF THE THESIS 12

2. COAL GASIFICATION **14**
2.1. HISTORICAL BACKGROUND 14
2.2. OVERVIEW OF COAL GASIFICATION 15
2.2.1. GASIFICATION TECHNOLOGIES *18*
2.3. SYNGAS APPLICATIONS 23
2.4. COAL GASIFICATION IN CO_2 ATMOSPHERE 26
2.4.1. CHARACTERIZATION OF THE BOUDUARD REACTION MECHANISM *27*
2.5. KINETICS OF COAL CHAR GASIFICATION 29
2.6. COAL CHAR GASIFICATION REACTIVITY 30
2.6.1. EFFECT OF COAL RANK *31*
2.6.2. EFFECT OF TEMPERATURE *31*
2.6.3. EFFECT OF PRESSURE *32*
2.6.4. EFFECT OF CO_2 CONCENTRATION *33*
2.6.5. EFFECT OF CATALYST *34*
2.6.5.1. ALKALI AND ALKALINE EARTH METALS *34*
2.6.5.2. SODIUM AND POTASIUM CARBONATES *36*
2.6.5.3. IRON OXIDES *37*
2.6.6. EFFECT OF PARTICLE SIZE *39*

3. METHODS OF HETEROGENOUS REACTION KINETIC ANALYSIS **40**
3.1. FREIDMAN MODEL 41
3.2. KISSINGER-AKAHIRA-SUNOSE MODEL 41
3.3. FLYNN-WALL OZAWA MODEL 42

4. EXPERIMENT **44**
4.1. SAMPLE PREPARATION 44
4.1.1. CHARACTERIZATION OF SELECTED COALS. *45*
4.1.2. COAL CHARS MIXTURES WITH MINERAL OXIDES PREPARATION *47*
4.2. THERMOGRAVIMETRIC RESEARCH 49
4.3. COAL CHARS GASIFICATION RESEARCH 50

5. RESULTS AND DISCUSSION **54**
5.1. THERMOGRAVIMETRIC RESULTS 54
5.1.1. LIMESTONE CATALYST *55*
5.1.2. IRON (III) OXIDE CATALYST *60*
5.2. KINETIC MODELS RESULTS 65
5.2.1. LIMESTONE CATALYST *67*
5.2.2. IRON (III) OXIDE CATALYST *71*
5.3. COAL CHAR GASIFICATION RESULTS 75
5.4. SEM + EDS RESULTS 76

7. SUMMARY AND CONCLUSIONS **82**

REFERENCES **83**

LIST OF FIGURES:

Figure 1. Global power generation and global primary energy mix by source, 2012 [1] 10
Figure 2. Fossil fuel R/P ratios at end of 2012. [3] 10
Figure 3. CO_2 emissions from global electricity generation.[4] 11
Figure 4. Cumulative Synthesis gas units capacities with prognosed increase. [8] 15
Figure 5. Products differences between the pyrolysis, gasification and combustion: based on the needs of the oxidant needed during the process.[7] 16
Figure 6. Coal conversion steps. [9] 16
Figure 7. Classification of gasification technologies. [9] 18
Figure 8. Lurgi process a) gasifier b) gas/solid flows in the gasifier. [9] 19
Figure 9. Fluidized bed gasifiers with recycle. [9] 20
Figure 10. The GE gasifier in: a) quench, b) radiant heat recovery mode. [9] 21
Figure 11. Gasifiers types: operating, construction, planned stage. [8] 22
Figure 12. Syngas applications [9] 23
Figure 13. End use applications of syngas. [8] 24
Figure 14. Integrated Gasification Combined Cycle scheme. 25
Figure 15. Effect of CO_2 introduction in the gasification of solid fuels on relative increase in the CO production, and CO_2 consumption reduction. CO/C, CO_2/C, O_2/C – amount of CO produced, consumed O_2 and CO_2 feed to the system related to the carbon in the fuel. [12] 26
Figure 16. Exemplary installation for CO_2 coal gasification [9]. 27
Figure 17. Carbon oxidation, the Boudouard reaction, and CO oxidation. 28
Figure 18. a) Boudouard equilibrium in a function of temperature and pressure, b) char conversion versus time and pressure. [13] 28
Figure 19. Exemplary reaction rate constant dependence on time. [15] 30
Figure 20. Gasification rates of different ranks of chars at 850°C and 900°C in pure CO_2 [16,17,18]. 31
Figure 21. Effect of temperature on factors: a) carbon conversion and b) gasification rate [3]. 32
Figure 22. Effect of pressure on two factors: a) char conversion histories for Daw Mill bituminous char gasification under 100% CO_2 at 1000°C and b) extent of CO_2 gasification. [20] 33
Figure 23. The effect of CO_2 concentration on two factors: a) carbon conversion and b) gasification rate. [21] 34
Figure 24. Gasification rate vs. conversion curves for the raw and demineralized chars from the SB· and HVB· coals at operating conditions: 1413 K, 70% CO_2 . [23] 35
Figure 25. Catalytic effects of different compounds addition on coal char conversion during CO_2 gasification. [24,25,26,27,28,29] 36
Figure 26. Effect of catalyst loading on reaction rate at 880°C for K_2CO_3 (Δ) and Na_2CO_3 (o). [30] 37
Figure 27. Effect of Fe_2O_3 addition on two factors: a) gasification rate and b) carbon conversion [32]. 38
Figure 28. Effect of particle size on the gasification reaction rate. [36] 39
Figure 29. Kinetic data analysis models. 40
Figure 30. Coal char preparation installation. 45
Figure 31. IChPW's conical ball mill. 47
Figure 32. SEM picture of coal char sample. 48
Figure 33. SEM picture of limestone (*3%$_{wt}$*) particles distribution on the coal char surface. 48
Figure 34. SEM picture of iron (III) oxide (*3%$_{wt}$*) particles distribution on the coal char surface..... 49
Figure 35. Design of the TG 209 F1 Libra. 49
Figure 36. Laboratory reactor scale process arrangement. 50
Figure 37. Reactor cross-section. 51
Figure 38. In-side reaction temperature checks software *LabView* layout. 51
Figure 39. Chromatograph's software *TotalChrom Navigator* layout. 52
Figure 40. Real laboratory reactor scale process set up. 53
Figure 41. Coal char TG results: a) % sample weight, Δ %weight and conversion dependence on the temperature. 54
Figure 42. Coal char with limestone TG results - sample weight vs the temperature. 57
Figure 43. Coal char with limestone TG results – Δ %weight vs the temperature. 59
Figure 44. Coal char with limestone catalyst TG results conversion vs the temperature. 60

Figure 45. Coal char with Fe_2O_3 catalyst TG results % sample weight vs the temperature. 62
Figure 46. Coal char with Fe_2O_3 catalyst TG results Δ %weight **vs** the temperature……63
Figure 47. Coal char with Fe_2O_3 catalyst TG results conversion vs the temperature……64
Figure 48. Flowchart for calculating the activation energy and pre-expotential factor using isoconversional models. [64]……65
Figure 49. Iso-conversion plot of FWO method for coal char at varying degree of conversions. 66
Figure 50. Iso-conversion plot of KAS method for coal char at varying degree of conversions……67
Figure 51. Iso-conversion plot of Friedman method for coal char at varying degree of conversions. .. 67
Figure 52. Coal char with limestone catalyst gasification Flynn Wall Ozawa modeling results: activation energy and pre-exponential factor. 68
Figure 53. Coal char with limestone catalyst gasification Kissinger-Akahira-Sunose modeling results: activation energy and pre-exponential factor……70
Figure 54. Coal char with limestone catalyst gasification Friedman modeling results: activation energy and pre-exponential factor 70
Figure 55. Carbon conversion rate during CO_2 char gasification. 71
Figure 56. Coal char with Fe_2O_3 catalyst gasification Flynn Wall Ozawa modeling results: activation energy and pre-exponential factor. 72
Figure 57. Coal char with Fe_2O_3 catalyst gasification Kissinger-Akahira-Sunose modeling results: activation energy and pre-exponential factor 73
Figure 58. Coal char with Fe_2O_3 catalyst gasification Friedman modeling results: activation energy and pre-exponential factor. 74
Figure 59. Concentration of carbon monoxide in syngas produced during coal char gasification dependence on the temperature. 75
Figure 60. SEM picture of coal char samples……77
Figure 61. SEM picture of coal char samples after gasification. 76
Figure 62. EDS spectrum of mineral matter after gasification……..78
Figure 63. SEM picture of coal char with *3%* of $CaCO_3$ catalyst. 78
Figure 64. SEM picture of limestone catalyst……79
Figure 65. SEM picture of coal char samples with 3% of limestone catalyst after gasification. 79
Figure 66. EDS spectrum of limestone catalyst……80
Figure 67. SEM picture of coal char with 3% of Fe_2O_3 catalyst. 80
Figure 68. SEM picture of Fe_2O_3 catalyst……81
Figure 69. EDS spectrum of Fe_2O_3 catalyst……81

LIST OF TABLES:

Table 1. Comparison of coal gasification technologies. [9] 23
Table 2. Typical composition of synthesis gas [9] 24
Table 3. Example of ash composition (*$\%_{wt}$* of ash, sulfur-free basis). [24] 36
Table 4. Rate constants (*10^{-3} min^{-1}*) with and without catalysts. [30] 37
Table 5. Time vs carbon corversion, for the gasification of Hambach lignite char, in the bed of (I) silica sand and (II) Fe_2O_3. [32] 39
Table 6. Parent coal “Turów” and coal char properties 44
Table 7. Parent coal “Turów” and coal char ash chemical composition 46
Table 8. Market prices of iron (III) oxide and limestone. [60] 46
Table 9. % of sample weight for different limestone catalyst addition vs the temperature……55
Table 10. Process temperature vs. samples conversion. 56
Table 11. % of sample weight for different Fe_2O_3 catalyst addition vs the temperature……60
Table 12. Dependence of process temperature on coal char and coal char with Fe_2O_3 catalyst samples conversion. 61
Table 13. Kinetic methods used in calculating activation energy. 66
Table 14. EDS Acquisition geometry (degrees) of mineral matter after gasification: 77
Table 15. EDS Acquisition geometry (degrees) of $CaCO_3$ catalyst: 79
Table 16. EDS Acquisition geometry (degrees) of Fe_2O_3 catalyst: 81

LIST OF SYMBOLS AND ABBREVIATIONS:

$\emptyset$ $= air\ ratio$

ΔH° $= change\ of\ enthalpy$

vap $= vaporisation$

rxn $= reaction$

(s) $= solid\ state$

(vap) $= vapour\ state$

(g) $= gas\ state$

m_0 $= initial\ mass$

m_t $= temporary\ mass\ at\ time\ t$

m_r $= residual\ mass$

r $= reaction\ rate\ [s^{-1}]$

x $= conversion\ [\%]$

$\%_{wt}$ $= weight\ percent$

k $= reaction\ rate\ constant$

β $= heating\ rate\ [{}^{K}/_{s}]$

R $= gas\ constant\ [8.314\ {}^{J*mol}/_{K}]$

E_a $= activation\ energy\ \left[{}^{kJ}/_{mol}\right]$

T $= temperature\ [K]$

p $= pressure\ [Pa]$

A $= kinetic\ pre\text{-}exponential\ factor$

$^{\circ}C$ $= Celcius\ degree$

K $= Kelvin$

kJ $= kilo\ Joule$

Σ $= sum\ of$

R_{in} $= intristic\ rate$

n $= number\ of\ mols$

1. INTRODUCTION

The world of energy today, and coal industry in particular, is facing complex challenges. Global market becomes significantly more competitive and influenced by different regional approaches to environmental policies.

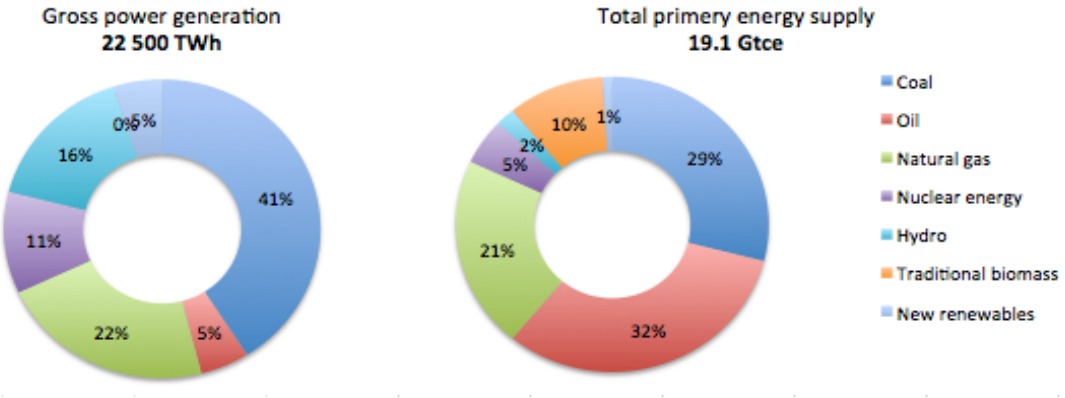

Figure 1. Global power generation and global primary energy mix by source 2012 [1].

Despite many negative factors and predictions, as it is visible in Figure 1, coal is and still will be in the near future one of the most important sources of energy in the world. Global energy use in *29%* depends on coal, and *41%* of gross power generation comes from coal-fired power plants. The European Union is the world's third largest coal consumer, after China and North America. In year 2013, *516.9* millions tones of coal and lignite were used, recalculated for tone of oil equivalent (*toe*). Moreover, in Figure 2 it can be observed that coal remains the most abundant fossil fuel by global reserves-to-production (*R/P*) ratio. It appears that *88%* of Europe's fossil fuels reserves are to be found in a form of coal and lignite. Depending on actual usage they can provide energy security for the next *250* years [2].

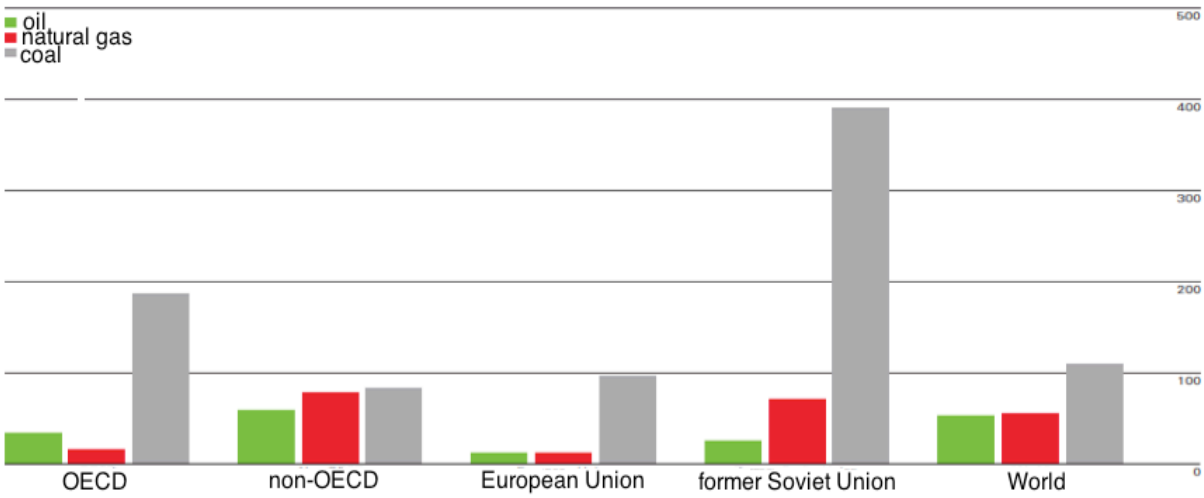

Figure 2. Fossil fuel R/P ratios at end of 2012 [3].

At the same time, coal is the largest anthropogenic contributor to carbon dioxide emissions, shown below in Figure 3. Almost *87%* of European CO_2 emissions come from coal-fired energy production or usage. Global green-house-gases emissions related with energy in 2012 reached a new historic high. There is a direct connection between coal technologies and environmental impact of human activity.

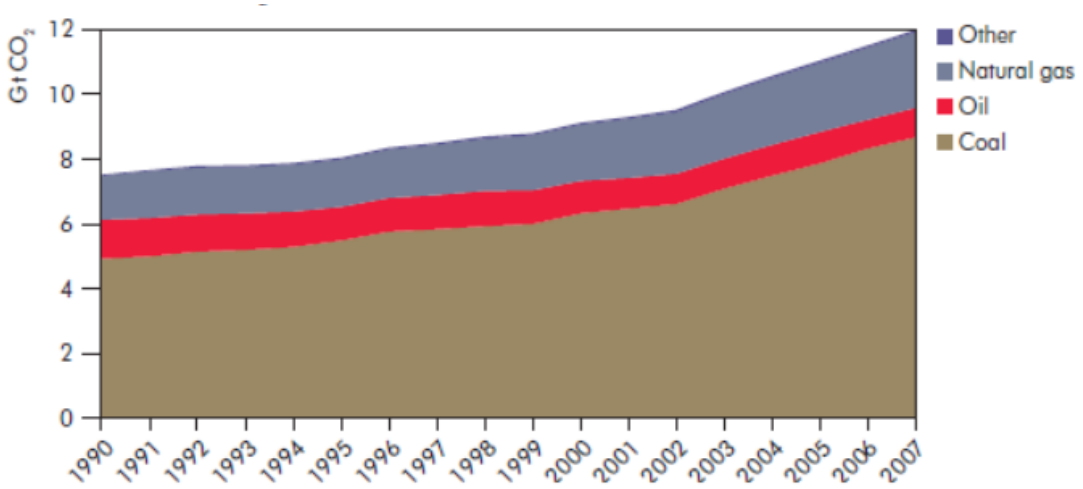

Figure 3. CO_2 emissions from global electricity generation [4].

European policies, due to agreed Kyoto Protocol [5], established the climate and energy package. It is a set of legal acts, which aims to ensure that the European Union meets its ambitious climate and energy targets in for 2020. These targets, known as the "*20-20-20*", establish three key objectives for 2020:

- a *20%* reduction in EU greenhouse gas emissions from 1990 levels;
- raising the share of EU energy consumption produced from renewable resources to *20%*;
- a *20%* improvement in the EU's energy efficiency.

Moreover, European commission and national governments are working for upcoming EU 2030 energy and climate policy framework [6]. Finding the right balance between reducing environmental impact and energy strategy, that answers nowadays economic, social and industrial challenges, is essential for the further European development. Indeed, eco-friendly energy production and industry and available and safe energy should go hand in hand. Many factors show trends for increasing usage and significance of coal. New technologies of energy production like Carbon Capture and Storage (CCS) would allow European Union members, depending on coal, to fulfil environmental challenges without the prejudice to economy and labour market.

Gasification is the key enabling technology in future of low emissions power generation and high efficiency energy systems. Moreover, it is a flexible core technology with many possible applications, like hydrogen, chemicals and liquid fuels production. Current gasification research builds on a strong Research & Development base progression from extended use of combustion technologies.

1.1. THESIS OUTLINE

This thesis includes introduction to the topic that world's energy sector have to be faced, while the demand for power is increasing. Due to all environmental, political, economic and social aspects, coal gasification is regarded as a solution to the increasing energy needs and environmental packages requirements that become more urgent every day.

In *Chapter 2* the historical and technical background of coal gasification is described along with more detailed information about coal gasification in carbon dioxide atmosphere. Literature reports that parent coal properties influence kinetics of coal gasification. The reactivity of coal chars towards CO_2 is influenced by coal rank, pyrolysis conditions (heating rate, holding time, final temperature), pressure, surface morphology, pore structure, particle size etc. The role of ash content, content of inorganic constituents likely to catalyse oxygen exchange reactions is still under research.

In *Chapter 3* methods of heterogeneous reaction kinetic analysis were presented. It contains description of different approaches to the based on the single-step Arrhenius method modelling: differential (Freidman) method, integral methods (Flynn-Wall-Ozawa) and maximum rate method (Kissinger-Akahira-Sunose).

Chapter 4 covers all experimental part. Coal chars sample preparation, they characteristics and treatment during laboratory test are presented. It describes process design, followed procedures and used equipment that were used during thermogravimetric research under isothermal conditions and coal char gasification in laboratory scale reactor.

In *Chapter 5* results from performed test are presented, thermogravimetric curves, SEM + EDS pictures, gas chromatograms and composition. It shows and analyses kinetic details of coal char gasification by carbon dioxide. This data would be used in *Chapter 6,7*, to structure kinetic models. Flynn-Wall-Ozawa, Kissinger-Akahira-Sunose and Freidman models were preformed to understand and predict the influence of mineral matter on kinetics of coal char gasification by carbon dioxide.

Chapter 8 covers summary and conclusions coming from the previous ones. The paper presents analysis of possible application of obtained results and model. It shows the possibilities of industrial implementation and its simplified economy.

1.2. OBJECTIVES OF THE THESIS

The main goal was to investigate, understand and predict the influence of mineral matter on kinetics of coal char gasification by carbon dioxide. In order to achieve this objective literature review, laboratory test and kinetics modelling were used as methods of investigation. It proves the role of certain compounds that were additionally introduced into studied coals.

LITERATURE REVIEW

2. COAL GASIFICATION

Investigation of any new research area should began with comprehension historically situation and achievements performed. Knowledge coming from it is not only key issue for proper process understanding but in addition, enables avoiding mistakes that had been made in the past.

2.1. HISTORICAL BACKGROUND

Process of coal gasification is an old and well-know technology and still under development. First technological applications were performed in the mid-1800s. During the beginning of 20^{th} century gasification was used to produce gas from coal for heating and street lightening, it was know as "town gas".

In England, cradle of Industrial Revolution, both hard coal and brown coal were gasified for streets lightening purposes. Two British engineers - Moordock and Cleek, developed method of hydrocarbons production from coal feedstock, produced gas was named "lighting gas". Process undergo in very simple retort furnaces at the temperature of *1000* ^{o}C. Coal packed inside the tubes was warmed up indirectly by coke combustion. That technology was inefficient and problematic; process gas had caloric value around *25* MJ/m^3. It was abundant due to the discovery and implementation of cheaper source of energy - natural gas.

Modern gasification began in the 1930s with the development of a large-scale cryogenic air separation units for low cost oxygen provided for Lurgi dry ash, moving bed gasifier, generating high-pressure, methane containing gas known as "town gas". It was followed by research leading to the development of Winkler – fluid bed and Koppers-Totzek – entrained flow gasifiers for low-pressure syngas production. Nazi Germans commercialized those technologies during the Second World War, with method developed in the 1920s by two chemists: Franz Fischer and Hans Tropsch, they produced fuel for the *Wehrmacht* and the *Luftwaffe*. In 1944 its production reached level of *124 000* barrels of oil. After World War II, the vast oil fields of Arabia made it uneconomic for most free nations to pursue the technology.

It was not uniform for all world, after the war South Africa was still not a free country. Due to fuel embargo caused by apartheid, in 1950s they were forced to find a way for synthetic gasoline production via Fischer-Tropch synthesis. In the late 1970s, Sasol built an outstanding complex in Secunda. Its annual production was *1.5* billion gallons of gasoline that properties were not different from drilled crude [7].

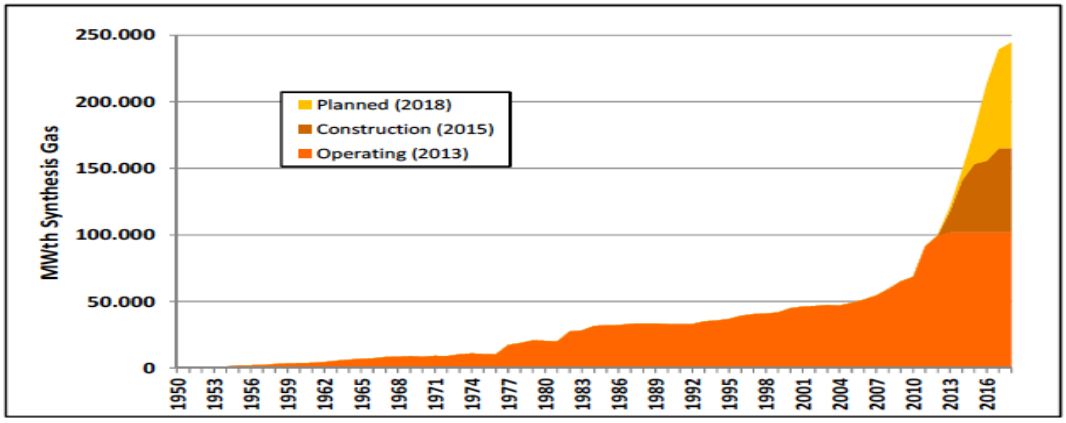

Figure 4. Cumulative Synthesis gas unit's capacities with prognosed increase [8].

This approach was unpopular in the rest of the world, because of low oil prices. Nowadays, when society is aware of fuel reservoirs limits and fossil fuel, environmental impact, coal gasification is once again interesting for scientist, academic, politics and industry. As it is visible in above Figure 4, depicting the 2010 statistics that coal gasification has been experiencing so-called "*renaissance*". Number of operating, constructed and planned installations are increasing distinctly. The most outstanding region of the world is China, their operating capacities are significantly bigger than the rest of the world. Syngas produced via coal gasification is used in different modes, but most popular are: chemicals, liquid fuels, gaseous fuels production and power generation. Number of installations under construction and those planned leaves great opportunity for further research, covering improvement of gasification process. It still may be more efficient, less energy-consuming, less impacting environment impact, and easily controllable [8].

2.2. OVERVIEW OF COAL GASIFICATION

Gasification is a combination of a number of thermal and chemical conversions, happening between organic substances and a gasifying agent – like air, oxygen, steam, carbon dioxide, hydrogen or their mixtures - in high temperature conditions. Quality and composition of process gas is determined by used oxidant, feedstock properties and physiochemical conditions while process is being carried out.

Coal gasification is a process of an incomplete combustion, it is carried out to convert used feedstock into gas fuel. Produced gas, as opposed to gases obtained in combustion reaction, are possible to be further burned to produce energy or chemically converted into other products. Coal gasification is a primary method for chemical processing of low rank coal. Part of the gasification reactions is endothermic, that require heat source. It may be fulfilled by partial coal combustion.

Process of coal gasification, is based on limited excess to the oxidizing medium, as presented below in Figure 5; coal undergoes gasification between pyrolysis (oxygen free atmosphere) and combustion (rich oxygen atmosphere). It could be divided into four main partial reactions:

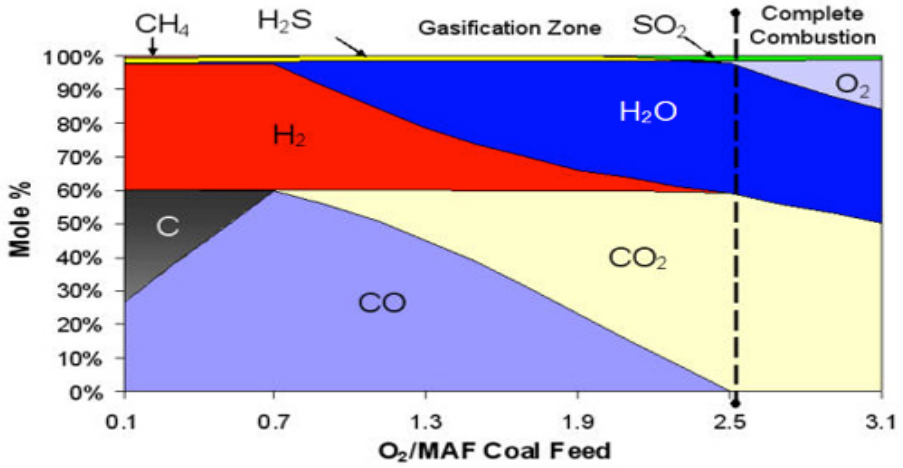

Figure 5. Products differences between the pyrolysis, gasification and combustion: based on the needs of the oxidant needed during the process [7].

- **DRYING**

First step when coal enters a gasifier is it's drying. Moisture in coal matrix decreases its calorific value. It vaporizes during the burning or gasifying processes, but at the same time consumes part of the combustion heat (as it is shown in the reaction below).

$$\boldsymbol{H_2O(l) \rightarrow H_2O(g)} \qquad \boldsymbol{\Delta H^o_{vap} = 43.99\ kJ/kmol} \qquad (1)$$

Dehydration has a very important impact on the overall thermodynamics of the process, especially for coals with high moisture content. Coals with different coal rank, characterizing inter alia moisture content, require individual drying treatment.

- **PYROLYSIS**

Coal also undergoes pyrolysis reactions, which produce coke and volatiles. The reaction shown below illustrates set of complicated and variable reactions. In temperatures greater than *320 °C*, without an oxidizing agent, weak chemical bonds between atoms of carbon and between carbon and oxygen, nitrogen, and sulphur particles in coal matrix break.

$$\boldsymbol{Coal \rightarrow Char(s) + Volatiles(g)} \qquad \boldsymbol{\Delta H^o_{rxn} = possitive, variable} \qquad (2)$$

As it may be seen in below Figure 6, after the first step of pyrolysis, formed fragments may further pyrolyze or undergo reactions leading to forming stable compounds (such as methane, ethane and higher hydrocarbons gases, tar liquids or solids) that with increasing temperature will enter into the second step of gasification.

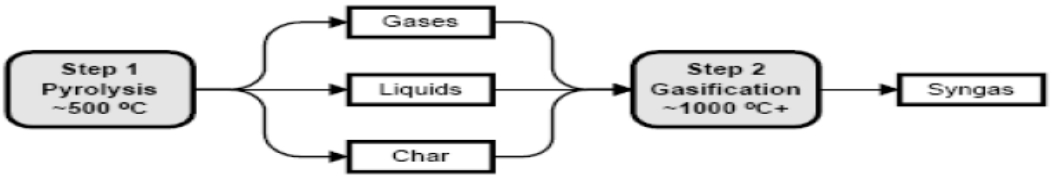

Figure 6. Coal conversion steps [9].

- **COMBUSTION**

Coal char and pyrolysis products formed in closed volume of reactor in contact with an oxidizing agent, that is fed to the gasifier in a form of pure oxygen stream or as air, lead to exothermic combustion reactions (as it is shown in the reactions mentioned below) that provides heat for further gasification. Combustion leads, depending on the amount of provided oxygen, to production of carbon monoxide CO or carbon dioxide CO_2. Carbon monoxide may be further burned to form CO_2 [9].

$$2C(s) + O_2(g) \rightarrow 2CO(g) \qquad \Delta H^o_{rxn} = -221.31\ kJ/kmol \quad (3)$$

$$C(s) + O_2(g) \rightarrow CO_2(g) \qquad \Delta H^o_{rxn} = -293.98\ kJ/kmol \quad (4)$$

$$2CO(g) + O_2(g) \rightarrow 2CO_2(g) \qquad \Delta H^o_{rxn} = -566.65\ kJ/kmol \quad (5)$$

- **GASIFICATION**

Main gasification reactions lead to conversion of carbonaceous fuels into synthesis gases (mixture of hydrogen and carbon monoxide), which are raw chemical materials for final chemical product and as well as fuel for electricity production. Gasification typically uses only *25-40%* of theoretical oxidant to generate enough heat to gasify the remaining unoxidized fuel, producing syngas The overall reaction for coal gasification can be written as following, and can be considered as partial oxidation of hydrocarbon feedstock:

$$C_nH_m + \frac{n}{2}O_2 \leftrightarrow nCO + \frac{m}{2}H_2 \qquad (6)$$

Specific reactions depend on the oxidizing medium used for the process and final temperature of a process. Coal gasification may be undertaken with the usage of: air, oxygen, steam, carbon dioxide, and their mixtures stream. Air and oxygen gasification may be considered as partial oxidations. Reaction 1 is known as steam gasification. Reaction 2 is CO_2 gasification, as well known as the Boudouard reaction.

$$C(s) + H_2O(g) \rightarrow CO(g) + H_2(g) \qquad \Delta H^o_{rxn} = +131.46\ kJ/kmol \quad (7)$$

$$C(s) + CO_2(g) \rightarrow 2CO(g) \qquad \Delta H^o_{rxn} = +172.67\ kJ/kmol \quad (8)$$

Unfortunately coal is not only composed of hydrogen and carbon atoms. In the coal matrix also occur heteroatoms. As the result of gasification they may lead to harmful emissions, like: hydrogen sulfide, ammonia, moreover aromatic hydrocarbons can be formed, but their final fraction does not exceed *1%* of the process gas composition. Coal gasification with usage of oxygen and steam allows production of synthesis gas, and fuel gas with middle calorific value (*16-17 MJ/m^3*), which can be upgraded, to natural gas substitute SNG (*34-35 MJ/m^3*). While carrying out process with air and steam as a product we can obtain a process gas mixture with calorific value in the range of *4-12.5 MJ/m^3* [9].

- **ADDITIONAL GAS PHASE REACTIONS**

Reaction of coal with hydrogen may lead to methanation, as below:

$$C(s) + 2H_2(g) \rightarrow CH_4(g) \qquad \Delta H^o_{rxn} = -74.94\ kJ/kmol \qquad (9)$$

To control in syngas composition carbon monoxide and hydrogen ratios water gas shift reaction is applied, in a catalytic reactor downstream of the gasifier. This reaction may also occur spontaneously due to higher reaction temperature. The reaction follows the equation such as:

$$CO(g) + H_2O(g) \leftrightarrow CO_2(g) + H_2(g) \qquad \Delta H^o_{rxn} = -41.21 kJ/kmol \qquad (10)$$

2.2.1. GASIFICATION TECHNOLOGIES

In a long history of commercial gasification, great number of gasifier designs has been developed. Allo-thermal approach – heat is supplied to the reactor from external source, currently the method is under research and development, however that does not mean that it will be not successful direction in the very near future, particularly when high temperature nuclear reactors are applied. At the moment, auto-thermal process – heat is supplied by internal combustion processes, is dominating. As presented in the following diagram, Figure 7, the process may be classified into 4 groups, characterized by other process arrangement, reactor construction, and gas-solid contacting regime in a reactor:

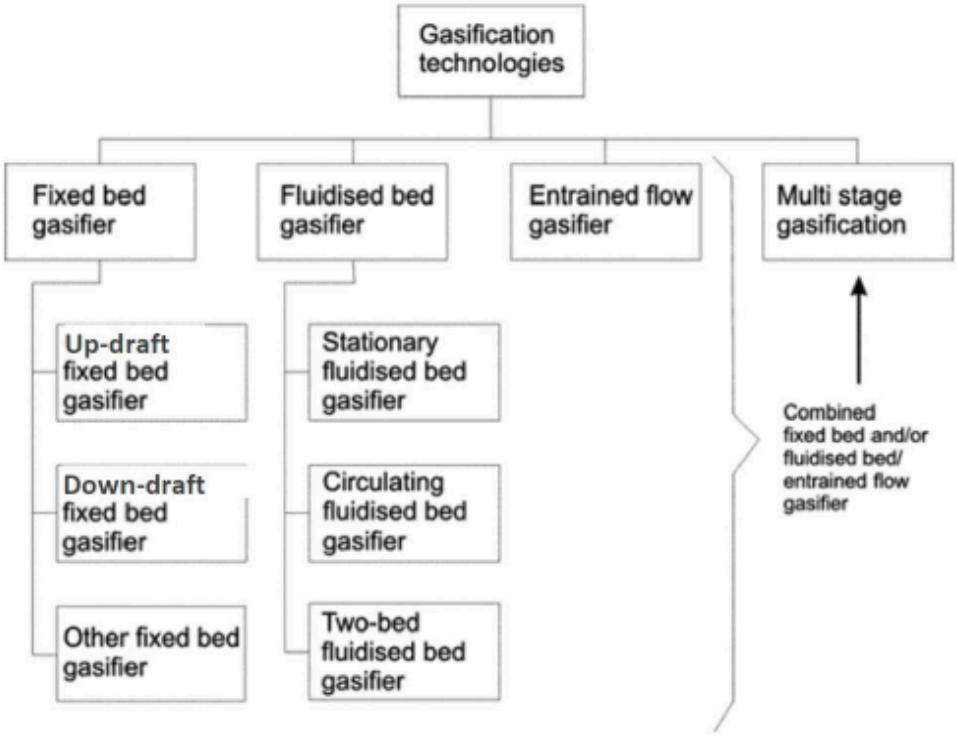

Figure 7. Classification of gasification technologies [9].

- **Fix bed and moving bed gasifiers**

Different types of fixed and moving bed gasifiers occurs, it may be differed into three groups, depending on flow arrangement: updraft, downdraft and cross draft. The most popular one is updraft and most of commercial technologies basses on its assumptions. The gasifier reactor is filled to the certain level with coal; it is fed from an atmospheric pressure bunker above the gasifier, while oxidizing agent flow through the grate and into the coal bed. Coal and gasses moving counter-current are presented in the following Figure 8a; by this construction it is possible to differ drying, pre-heating, combustion, pyrolysis and gasification areas. When the bunker is full, coal lock is pressurized until reaches the gasifier pressure, then valves on the bottom of coal lock opens, and the coal drops into the gasifier. Coal entering from the top of the reactor volume firstly is pre-heated and dried by rising hot syngas. Secondly, in the middle of the bed, rising hot gasses pyrolyse the coal, producing coal char and tars. By-products undergo combustion processes to provide energy for following gasification. What makes this technology especially energy efficient is fact that the highest bed temperature ca. *1100 ^{o}C* occurs just above the grate, where the coal char is gasified. Syngas and coal tar leave top of the gasifier at about *370-590 ^{o}C*.

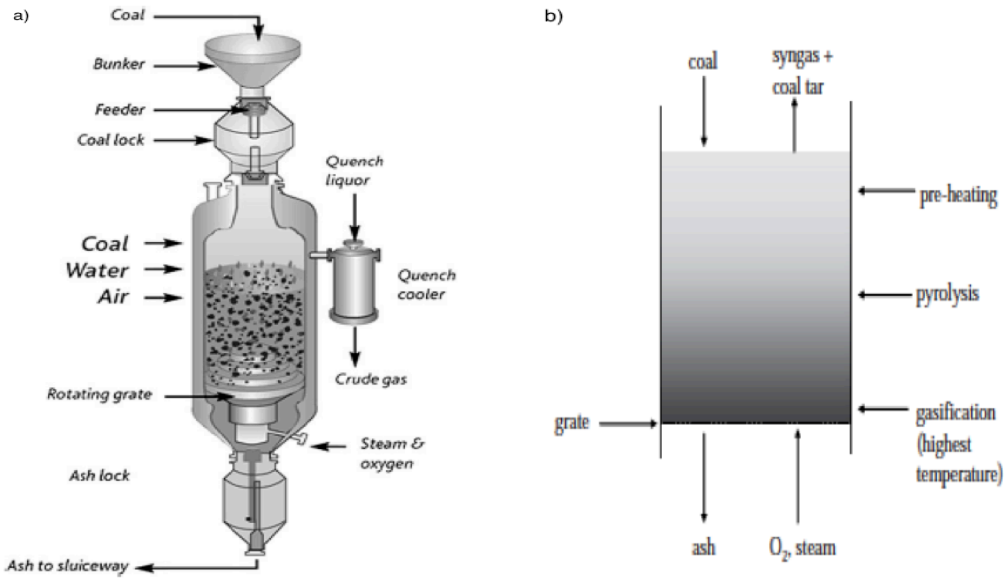

Figure 8. Lurgi process a) gasifier b) gas/solid flows in the gasifier [9].

Comparing to other gasification technologies, this one is operating at relatively low temperatures, it provokes residues in the form of phenols, oleic, tars. It is prevented by gas recirculation. Ash is received in the bottom part of the reactor as slag or dry phase. Exemplary gasifier arrangement is presented below on the Sasol-Lurgi one, in the Figure 8b.

Due to the regime of free-flowing bed and proper heat exchange between the phases, this technology is dedicated to non-coking coals. They have to be characterized by feed coal size *3-30 mm*, to avoid plugging the interstitial spaces between the large coal particles by fine coal; high ash content. Fixed and moving bed technologies found their applications in following commercial usage: Sasol-Lurgi technologies, BGL and BHEL pressurized fluidized bed technologies.

- **Fluidized bed gasifiers**

Gasification process in a fluidized bed reactor is presented in Figure 9. Fine particles of milled coal are fed to a bunker, and a screw feeder withdraws coal from the bunker and injects it into the fluidized bed. The oxidation gas enters to the gasifier split into two streams. Most of the gas is fed underneath the grade. This gas fluidizes and react with the solid bed, formed by ash, additional sand or residue, unreacted coal char. As the coal particles react, they become smaller and less dense, about of *30%* of the ash falls through the grate and is produced as bottom ash, received in the bottom part of the reactor. The remaining *70%* of the ash is entering by the fluidizing gas and is carried into headspace. Rest of the gas feed is injected into the freeboard, where oxidation of gas/solid mixture increase the temperature up to c.a. *1200 ^{o}C*, it melts the ash and causes further increase of carbon conversion from entrained ash. Heat is removed from the top of the gasifier to re-solidify ash, before its leaves the reactor with produced syngas.

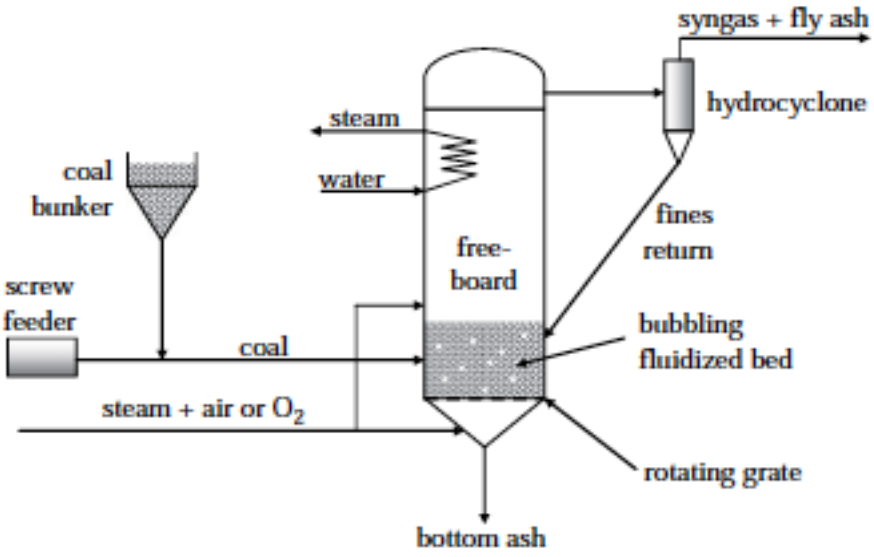

Figure 9. Fluidized bed gasifiers with recycle [9].

Low process temperature causes incomplete coal conversion in a single cycle. To solve this problem, an adjustable cyclone to recycle from the syngas flow some unreacted coal fine particles of entrained ash, back to the fluidized bed to further convert.

Due to the low carbon conversion in a single cycle, this method is especially implemented for high-reactive brown coals. Fluidized bed technologies may find its application in zero CO_2 emission power generation systems because the presence of char allows the reaction with carbon dioxide to proceeds.

Fluidized bed technologies found their applications in following commercial usage: High Temperature Winkler, U-Gas, Foster-Wheeler Partial Gasifier, KBR Transport Gasifier and BHEL pressurized fluidized bed technologies.

- **Entrained bed gasifiers**

Gasification in entrained bed reactors is based on the idea of simultaneous feed of pumpable slurry, mix of a finely grind coal with water, and oxidizing agent into the burner. The slurry and gasses are injected into the top of the pressurized gasifier, and the gas/solid/slag mixture flow downward.

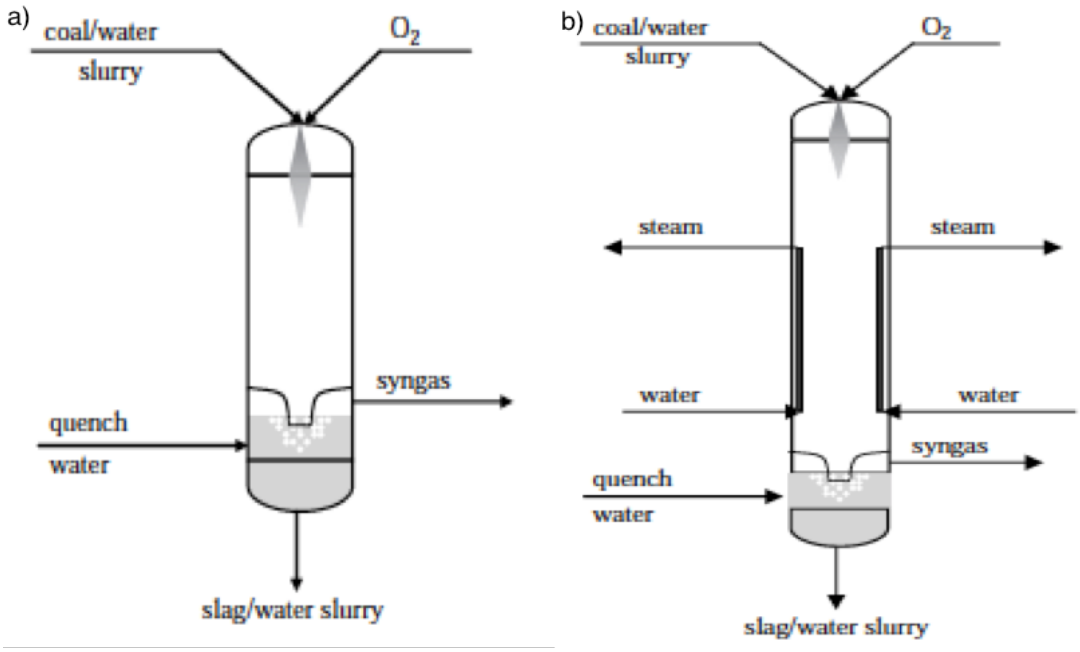

Figure 10. The GE gasifier in: a) quench, b) radiant heat recovery mode [9].

As illustrated in above Figure 10, there are two basic models of operation. First, presented in the Figure 10a is quench mode. Gasification reaction starts at the burners, immediately after injection of previously mentioned mixtures. The mixture of hot gas/slag mixture is bubbled through a water bath that solidifies the slag. Cooled syngas, due to the occurring boiling water, contains increase fraction of steam. The slurry is received in the bottom part of the reactor in a form of slag/water slurry. The gasifier is refractory lined. Hot slag slowly attacks the refractory liner, so the liner must be periodically replaced. Quench mode increases the steam content of the syngas. Second, presented in the Figure 10b is radiant heat recovery mode. In this type of gasifier, longer gasifier body is used. In the walls of the lower part steam tubes are placed, to cool down syngas temperature from *1300 ^{o}C* in reactor to *593 ^{o}C* in first step and finally cooled to *210 ^{o}C* in the water quench. Operating pressure is one of the highest used by most type of gasifiers, it is estimated for *5.6 MPa*. Due to the radiant steam tube heat recovery system, it has greater energy efficiency, but it provokes greater capital cost then quench mode. Frequently, a water shift reactor to increase H_2/CO ratio in syngas composition follows coal gasification process.

High reaction temperatures and short residue time in gasification area provides high carbon conversion and lack of tar produced. The short residence time means the fuel needs to have a larger contact surface, i.e. be more finely ground or be a liquid, which means that system is not economically feasible in smaller scales.

The coal/water slurry feed technique works well with bituminous coals, but not with lower grade coals. Due to the high intrinsic moisture content in low rank coals, the water/coal ratio is often far in excess of optimum. Moreover coal characterized by low ash melting temperatures are used, addition of limestone decreases melting point as well. It enables receiving liquid ash on reactor walls. Due to the high levels of hydrogen and carbon monoxide in produced syngas, entrained bed technologies may find its application in coal-to-liquid fuel production technology.

Construction of mentioned reactors may necessitate enormous investment cost, usage of proper resisting high-temperatures materials and complicated heat exchangers for syngas cooling purposes. Despite those requirements, entrained bed technologies found their applications in following commercial usage: Shell, GE- Texaco, E-Gas, GSP, MHI technologies.

- **Multi stage gasification**

Multi stage gasification technology bases on combined fix bed and/or fluidized bed/entrained bed gasifier.

As it may be seen in following Figure 11, nowadays entrained bed gasifiers, especially Shell and GE/Texaco types, are the most popular ones in industrial application

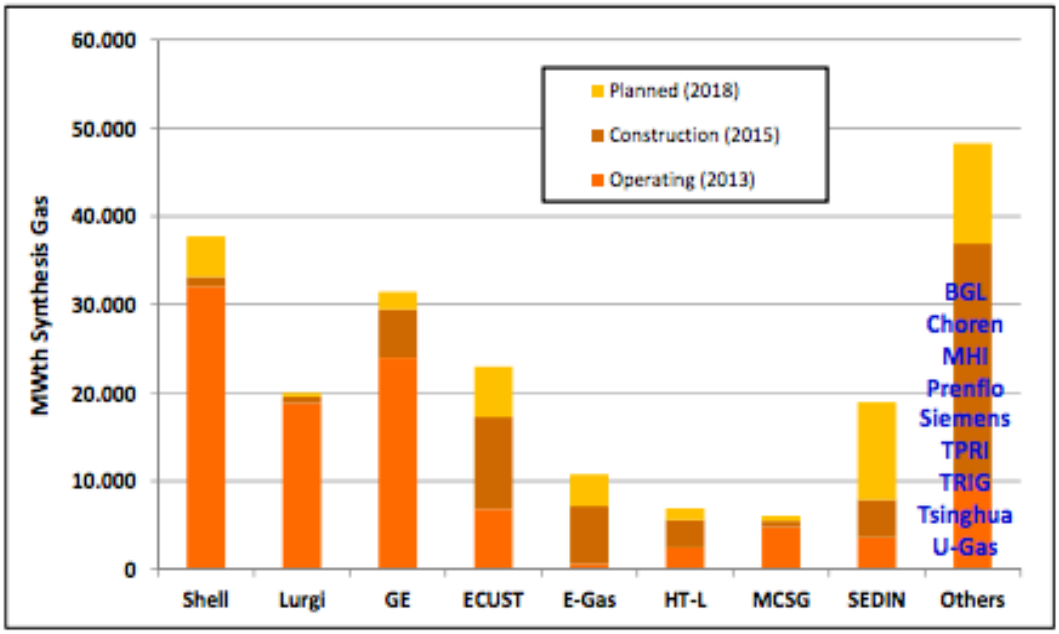

Figure 11. Gasifiers types: operating, construction, planned stage [8].

Brief summary comparison of above-mentioned technologies, with listed application examples, process requirements (gasification agent, fuel, particles size), temperature and pressure regime, heat exchangers, and final carbon conversion, energetic efficiency is presented in Table 1.

Table 1. Comparison of coal gasification technologies [9].

Parameter	Gasifier type				Gasifier type				
	Fixed bed	Fluidized bed			Entrained bed				
	Lurgi/BG	HTW	KRW	U-Gaz	GE/Texaco	Shell	DOW	PREN FLO	VEW
Agent	O_2 + Steam	Air	Air + Steam	Air + Steam	O_2 + Steam	O_2 + Steam	O_2 + Steam	O_2 + Steam	Air
Fuel form	dry coal	dry coal	dry coal		coal slurry	dry coal	dry coal	dry coal	dry coal
Particles size [mm]	3 -50	6	5	6	0.5	0.1	-	0.1	0.1
Ash recieving	slag	dry ash	ash char	ash char	slag	slag	slag	slag	slag
Heat exchangers	water	adiabatic	adiabatic	adiabatic	adiabatic	water	adiabatic	water	adiabatic
Reaction temp [°C]	1800	950	1100	1100	-	up to 2000	1430-	up to 2000	2000
Syngas temp [°C]	430-500	900	1000	1000	1300-1500	900		900	1400-1440
Pressure [MPa]	2.5-3	1-2.7	2	2.5	3-8	"2-3"	2.2	2.3	2-2.5
Carbon conversion [%]	99,7	90-92	96.5	97	99	99.7	99.3	99.7	60
Energetic efficiency [%]	89-91	70-75	69.7	69.6	76	81.6	77	74.5	-

2.3. SYNGAS APPLICATIONS

Synthesis gas (syngas) is the product of carbonaceous materials gasification and is considered as a very versatile energy product. It has a great number of possible industrial applications, as may be seen in following Figure 12.

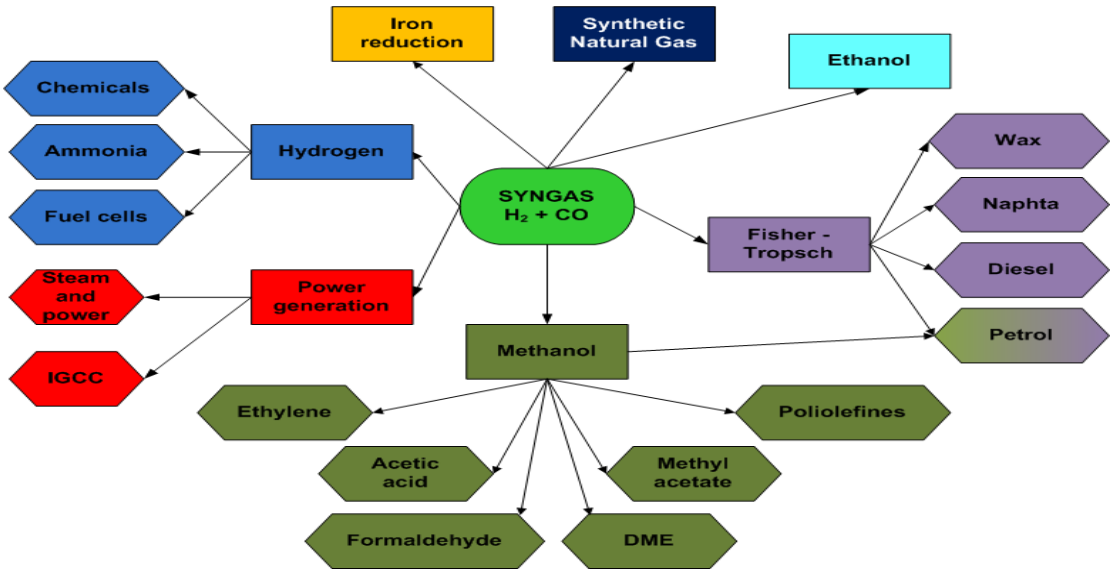

Figure 12. Syngas applications [9]

Syngas is a feedstock for a range of different products and processes, naming main ones presented below in Figure13: chemicals, liquid fuels, gaseous fuels production, and electricity generation.

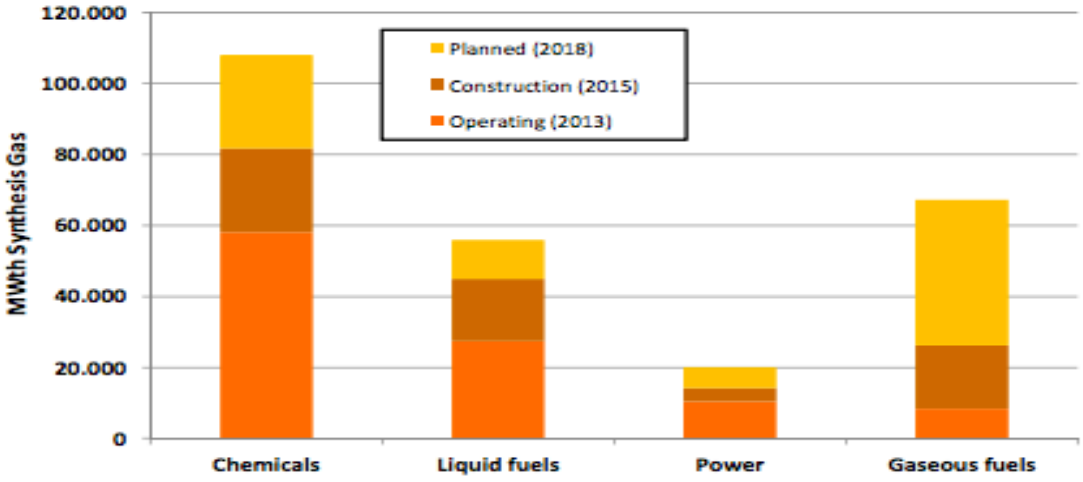

Figure 13. End use applications of syngas [8].

Gasification technology, process environment and material properties have a great impact on the specific syngas composition. It varies, with respect of dedicated application. Typical composition of synthesis gas is presented below, in Table 2, it is a mixture of mostly hydrogen, carbon monoxide with additional methane and unwanted components: nitrogen and carbon dioxide. A number of the components of syngas causes challenges like tar generation, hydrogen level and moisture content.

Table 2. Typical composition of synthesis gas [9].

Gas substance	Composition			
	fixed bed	fluidized bed	entrained bed	
			dry	coal-slurry
Hydrogen	39.1	35	28	36
Carbon monoxide	18.9	40	66	42
Carbon dioxide	29.7	20	2	20
Methane	7	3	0	0
Nitrogen	4.3	2	4	2
C_nH_m	1	0	0	0

Syngas has a long and demonstrated in the *Introduction Chapter* history in power generation. In last century before natural gas become viable cities and towns were powered on "*town gas*". Syngas provides opportunities for power generation. Unfortunately, direct natural gas substitution is not possible, due to hydrogen properties; it burns much quicker than methane. Under normal circumstances, faster combustion in the engine cylinders would provoke to the potential danger of pre-ignition, knocking and engine backfiring. Number of technical adjustments needed to be performed in order to answer this challenge. The most promising, with possible on wide range scale application in power generation sector is, presented below in Figure 14 *Integrated Gasification Combined Cycle.*

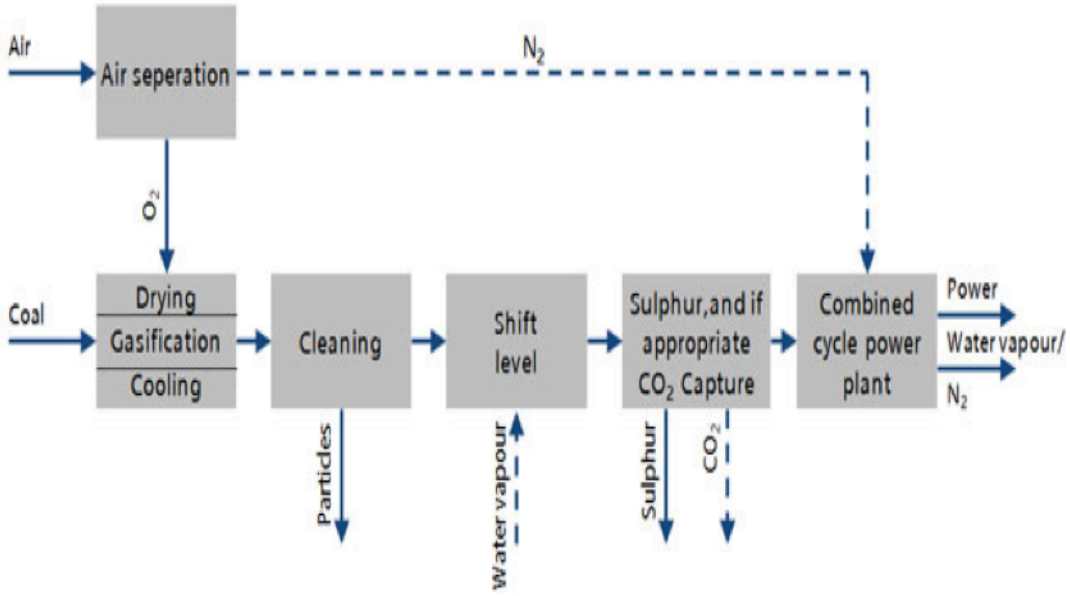

Figure 14. Integrated Gasification Combined Cycle scheme [7].

The technology bases on combined cycle, where coal feedstock is not burnt in a conventional steam power plant, but is initially dried and supplied to a gasifier, produced syngas after subsequent cooling down, preliminary cleaning, calorific value increasing via Water-Gas-Shift reaction, sulphur, and if appropriate CO_2 capture, is a fuel in the gas turbine combined cycle power plant. This approach is characterized by outstanding efficiency of carbon dioxide sequestration, and after adequate research and development into final efficiency of the system, may be the answer for nowadays pro-environmental policy needs.

Conversion of syngas into Fischer-Tropsch (FT) liquid fuel brings an alternative fuel to the energy mix, as it was reported in *Introduction Chapter* those technologies are well tested and had their implementation into industrial scale previously in the history. Fuel derived via gasification process meets most important requirements for alternative fuels. It has superior combustion and air pollutant properties. FT diesel can be used in existing engines, without any large-scale fleet adjustment or replacement [98].

Moreover, due to main growth in China of Coal-to-Chemicals industry, nowadays *25%* of world ammonia and *35%* of world methanol production are bases on gasification process [8].

Syngas is the favoured feedstock for the major development of clean coal technologies, amount of produced synthesis gas and its usage is increasing in last years, and as it may be seen in above Figure 13, due to the planned and constructed units, number of operating ones will increase and will have significant impact on the industry.

2.4. COAL GASIFICATION IN CO_2 ATMOSPHERE

Coal gasification with carbon dioxide use as oxidizing medium is considered today as a very modern, innovative direction of gasification technology development. Carbon dioxide has a great share in flue gases composition, due to the Carbon Capture and Storage (CCS) technologies. Regardless its geological storage, the possibility of utilization, implementation and usage as a feedstock for chemical processes is inevitable.

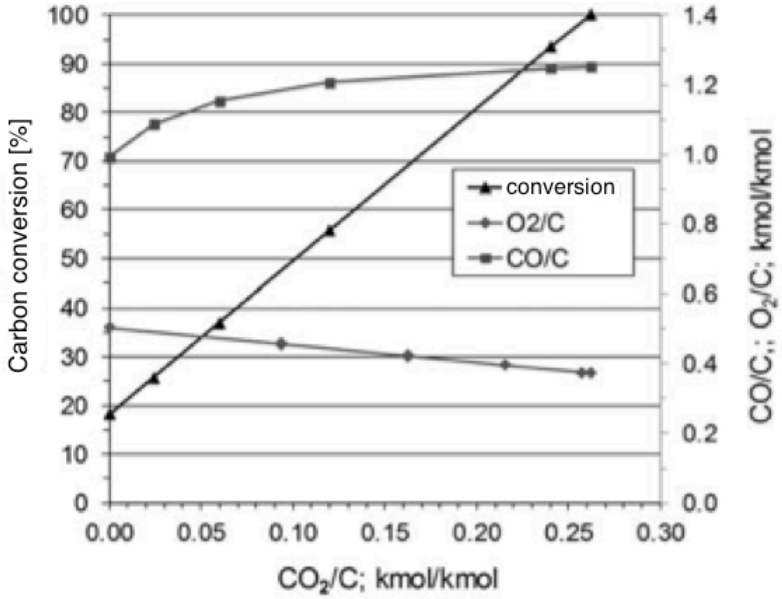

Figure 15. Effect of CO_2 introduction in the gasification of solid fuels on relative increase in the CO production, and CO_2 consumption reduction. CO/C, CO_2/C, O_2/C – amount of CO produced, consumed O_2 and CO_2 feed to the system related to the carbon in the fuel [12].

Coal gasification in CO_2 atmosphere is based on the Boudouard reaction. There were performed thermodynamic calculations for coal gasification at the temperature of *1000 °C*, which results are presented in Figure 15 [12]. Its use may lead to the increase in process efficiency and economic enhancement of syngas production, due to reduction of feedstock coal and oxidizing medium consumption. Moreover, it can decrease environmental footprint, provoked by carbon dioxide emitted into atmosphere. Comparing classic gasification to one with carbon dioxide, CO_2 implementation into chemical reactor enhance carbon conversion with following increase of carbon monoxide fraction in process syngas.

Effective carbon dioxide introduction to coal gasification process requires several fundamental conditions. One of the most important is requirement of high process temperature. Chemical reactor with circulating fluidized bed (CFB), as one presented in Figure 16 below, guarantees proper conditions of mass and heat exchanges, that is the second important factor of coal gasification by CO_2.

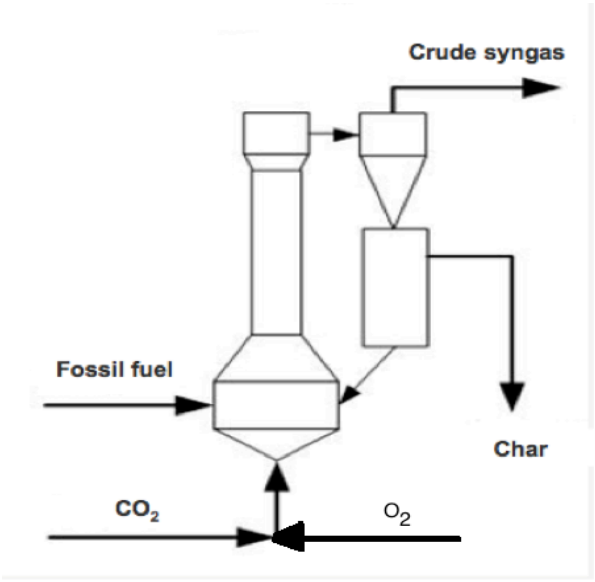

Figure 16. Exemplary installation for CO_2 coal gasification [9].

Recycle of partial converted coal char (separated from crude syngas in the preliminary cyclone), establishes conditions of high concentration of solid phase (coal char and coal), well mixed in gas flow. Occurring in reactor, reactive, high carbon-content coal char allows at its surface conversion of feed CO_2 into carbon monoxide, so desired in syngas composition. Moreover, produced in circulating fluidized bed (CFB) reactor coal char, may be used for energetic purposes. Oxygen is feed to the reactor to provide proper temperature, due to the coal combustion.

2.4.1. CHARACTERIZATION OF THE BOUDUARD REACTION MECHANISM

The Boudouard reaction is a main reaction of uncatalysed carbon gasification involving CO_2. It is an endothermic reaction, resulting in a production of carbon monoxide. Due to the large positive enthalpy (c.a. *172 kJ/mol* under standard conditions), thermal equilibrium does not favour CO production until the temperature range over $700\ ^{o}C$, when the entropic term, $-T\Delta S$, begins to dominate and the Gibbs free energy becomes negative. Correlation between carbon oxidation, the Boudouard reaction, and CO oxidation is presented below in Figure 17.

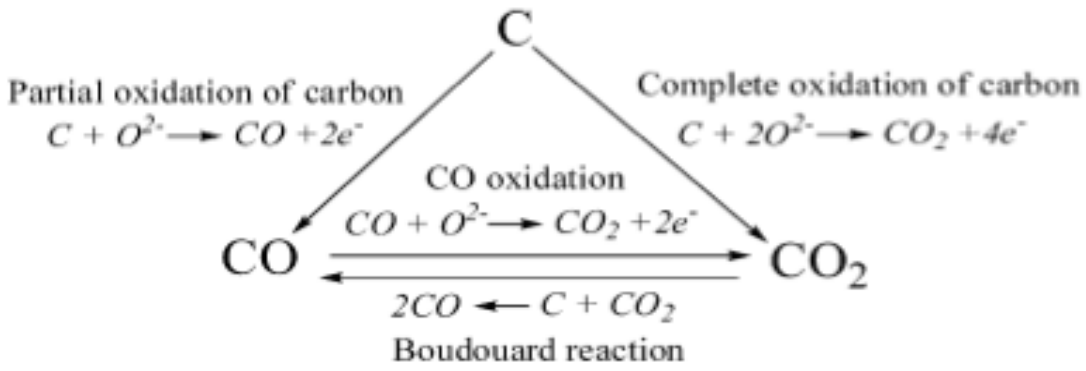

Figure 17. Carbon oxidation, the Boudouard reaction, and CO oxidation.

The mechanism for the Boudouard reaction may be presented in a simple two-step oxygen exchange mechanism, described by Ergun [9]:

$$C_f + CO_2 \overset{k_{-1}}{\underset{k_1}{\longleftrightarrow}} C(O) + CO \qquad (11)$$

$$C(O) \overset{k_2}{\rightarrow} CO + C_f \qquad (12)$$

In the first step carbon dioxide dissociates at free active site C_f, releasing carbon monoxide and forming and oxidized surface complex C(O). Secondly, the carbon-oxygen complex produces a molecule of CO, intrinsic decomposition rate constant and active site density product characterize Boudouard rate constant.

Under steady conditions, in the atmosphere of CO_2, the reaction is driven to the right, production of one carbon monoxide's molecule for each active site is reached. Second molecule of CO is formed due to complex decomposition. As may be seen in Figure 18, high temperatures, above *650 °C* promotes Boudouard reaction direction to the carbon monoxide production. Increasing pressure causes need of higher temperature, as may be seen in Figure 18a, to obtain the same mole fraction of carbon monoxide.

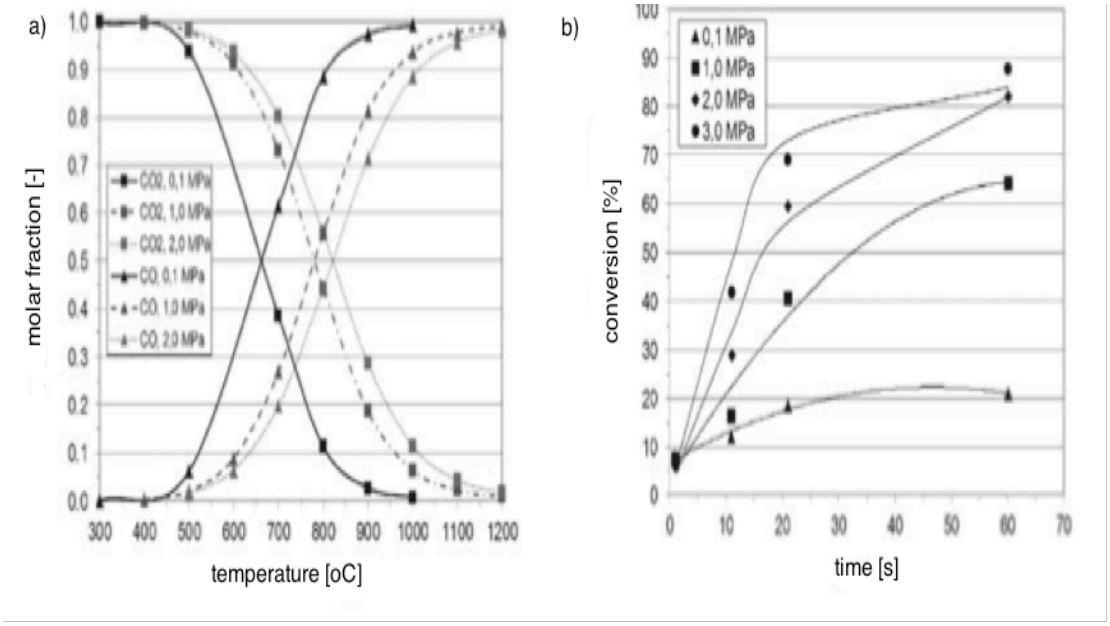

Figure 18. a) Boudouard equilibrium in a function of temperature and pressure, b) char conversion versus time and pressure [13].

Despite the thermodynamic limitations (influence of pressure on the temperature), as presented in Figure 18b, elevated pressures promote the Boudouard reaction and enhance carbon conversion. For the reaction to be performed properly several factors are necessary to be provided: reactive coal char, adequate reaction time (determined by kinetic conditions) and intensive contact gas-solid surface.

2.5. KINETICS OF COAL CHAR GASIFICATION

Several carbon – carbon dioxide reactions mechanisms have been proposed in the literature, however there seems to be a common attitude towards it. Those reactions listed below are complex, partially reversible. The mechanism is given in 5 steps, of which two are assumed reversible. Oxygen and carbon monoxide can appear in a form of complexes at the carbon surface [C(O) and C(CO)]. The rate-limiting step is the desorption of the carbon–oxygen surface complex.

$$C_f + CO_2 \leftrightarrow C(O) + CO \quad (13)$$

$$C(O) \rightarrow CO \quad (14)$$

$$CO + C_f \leftrightarrow C(CO) \quad (15)$$

$$CO_2 + C(CO) \rightarrow 2CO + C(O) \quad (16)$$

$$CO + C(CO) \rightarrow CO_2 + 2C_f \quad (17)$$

The forward and the reverse reactions take places simultaneously and at different rates. The rate of the Boudouard reaction can be determined using the following equations [14]:

$$r = -\frac{1}{m_{carbon}}\frac{dm_{carbon}}{dt} \quad (18)$$

$$r = fT + g \quad (19)$$

f and *g* have the units of K^{-1} s^{-1} and s^{-1}, respectively. Carbon – carbon dioxide reactions depend on partial pressures of CO and CO_2, its correlation may be understood by application of the Langmuir-Hinshelwood model. Partial pressures are calculated as follows:

$$p_i = p_{tot}\frac{n_i}{\sum n_i} \quad (20)$$

where p_{total} is system total pressure, $\frac{n_i}{\sum n_i}$ molar fraction, and constant of proportionality (k_f) temperature-dependent occurs forward reaction rate (r_f) is proportional to the concentrations of CO. It looks analogous for reverse reaction.

$$r_f = k_f * [CO] * [H_2O] \quad (21)$$

$$r_r = k_r * [CO_2] * [H_2] \quad (22)$$

Furthermore, the intrinsic reaction rate equation was transformed into the form of a Langmuir-Hinshelwood expression as follows:

$$R_{in} = \frac{k_1 P_{CO_2} + k_4 P_{CO_2}^2}{1 + k_2 P_{CO_2} + k_3 P_{CO}} \quad (23)$$

where k_1, k_2, k_3 and k_4 are the temperature-dependent constants obtained from the above reactions. It could be generated in a form of the Arrhenius-type equation as given below:

$$k_i = A_i \exp\left(\frac{-E_a}{RT}\right) \quad (24)$$

where A_i is pre-exponential coefficient, E_a - activation energy, R - gas constant. The *n*th order intrinsic rate equation is expressed as:

$$\boldsymbol{R_{in} = kP_{CO_2}^{n}} \qquad (25)$$

When compared to the *n*th order equation, the Langmuir– Hinshelwood model has three important features:

- the intrinsic reactivity is a non-linear function of CO_2 partial pressure, it does not use an uncertain pressure order *n*;
- it has a mechanistic basis due to the consideration of an adsorption–desorption two-step reaction;
- it includes the inhibiting effect of the product gas (CO), which may become significant at a high CO partial pressure.

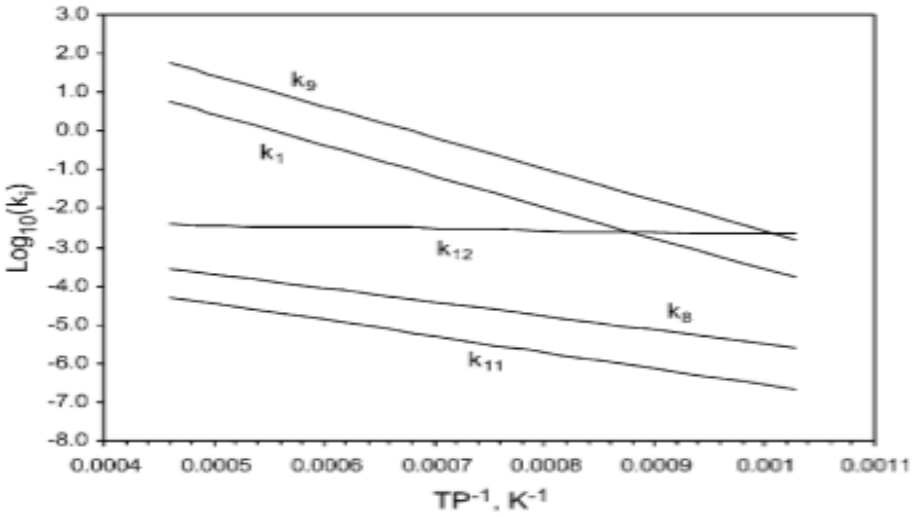

Figure 19. Exemplary reaction rate constant dependence on time [15].

2.6. COAL CHAR GASIFICATION REACTIVITY

Coal chars gasification has been intensively studied all over the world with main goals: to develop efficient, environmentally friendly and economically attractive clean technology of coal conversion process. Kinetics of coal char gasification had a significant role since it provides valuable information that can be used for proper design and operation of gasifiers.

Literature reports that several factors related to char and process conditions have a great impact on coal char conversion and reaction rate of coal chars under gasification in a CO_2 atmosphere. Among them could be considered: coal rank, process temperature, process and gas pressure, gas composition (CO_2 concentration), coal and ash chemical composition, additional mineral catalyst, pore structure, and particle size.

2.6.1. EFFECT OF COAL RANK

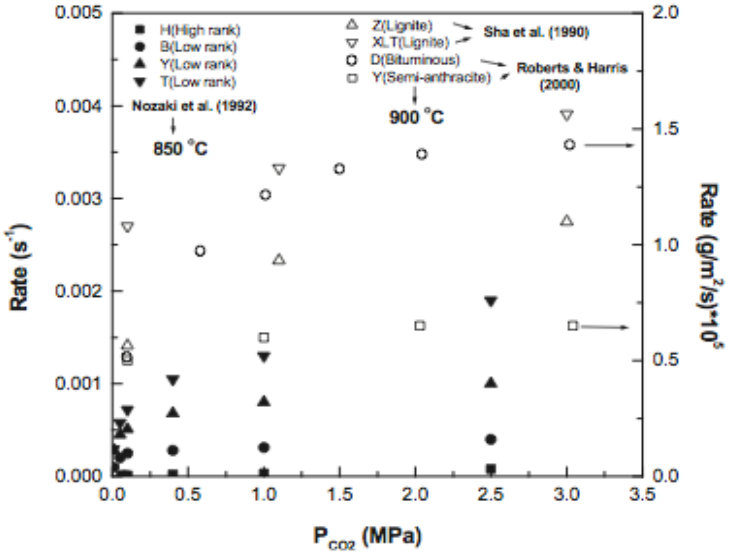

Figure 20. Gasification rates of different ranks of chars at 850°C and 900°C in pure CO_2 [16,17,18].

Nozaki [16] investigated the gasification rate measured at *850 °C*, the same done Sha [17] and Roberts and Harris [18] at *900 °C*. Each of tests was performed under pure CO_2 in a PTGA (pressurized thermo-gravimetric analysis). Together, eight different coal chars with ranks ranging from the sub-bituminous to the anthracite as shown in above Figure 20.

As it may be seen, that all of mentioned researches observed that the gasification rate of the high-rank coal was less than the rate of the low-rank coals i.e. the coal reactivity decreases as coal rank increases.

2.6.2. EFFECT OF TEMPERATURE

There is an evident correlation between increasing temperature of coal char gasification and carbon conversion and reaction rate. Chinese researches Tie-feng Lui, Yi-tian Fang, Yang Wang performed empirical investigation on the influence of temperatures on gasification reactivity of chars [19]. They used Chinese Binxian coal in their study; sample preparation was very similar to one that is used in this work. Coal char was gasified by carbon dioxide, to achieve the experiment's goal; gasification was performed in temperature range from *1100 °C* to *1300 °C* with a rise of *50 °C* in each test.

In Figure 21a obtained curves of carbon conversion as a function of gasification time are shown. It can be seen that with the same reaction time, raising temperature causes increase of carbon conversion. There is a visible significant difference, between curves of gasification in *1100 °C* and rest of temperatures. Higher temperature promotes increase of carbon conversion especially in the first 2 minutes of the test. It is possible to observe the overlapping of the curves at high temperatures. The time to obtain complete conversion is shorter for progressively higher temperature.

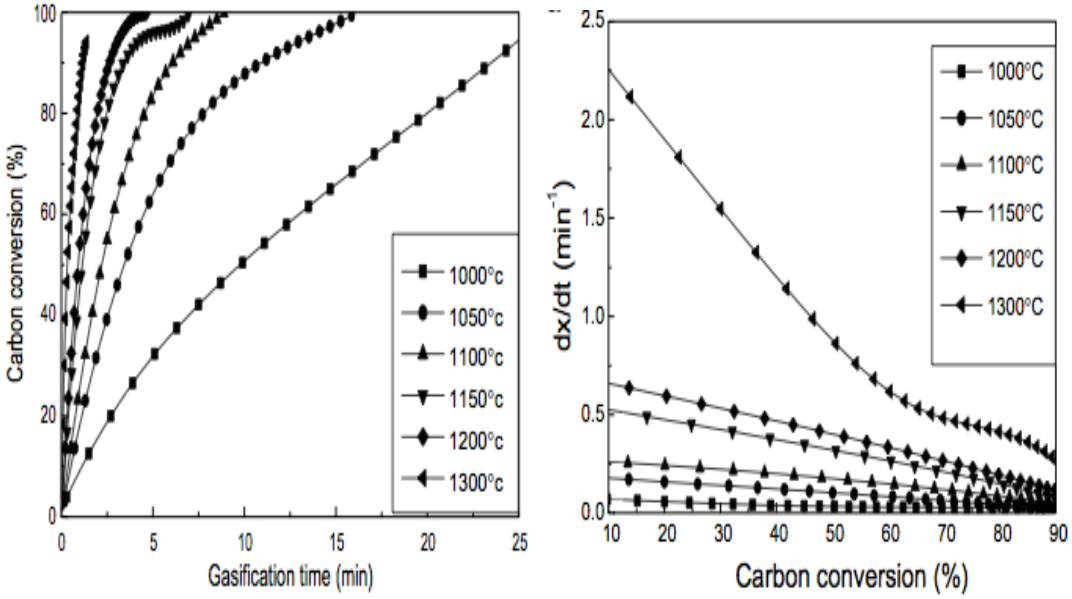

Figure 21. Effect of temperature on factors: a) carbon conversion and b) gasification rate [3].

Dependence of gasification rate on carbon conversion is presented in Figure 21b. It is possible to observe that raising temperature increases gasification rate and in the opposite, gasification rate decreases with increasing carbon conversion. The maximum rate increases with raising temperature. The correlation between the gasification rate and the carbon conversion is nearly linear for temperatures *1100 -1250 °C*, but it changes significantly for the highest *1300 °C*. It can be observed that higher temperatures cause a more evident reaction rate drop with increasing carbon conversion. It is effect of diffusion in pores, provoking so-called “apparent rate”.

2.6.3. EFFECT OF PRESSURE

Change of process pressure has a significant influence on gasification, it may effect both directly, by changing partial pressures of reactants and indirectly, by affecting transport rates. To check this dependence a British research group: R.C. Messenbock, D.R. Dugwell, R. Kandiyoti [20] performed investigation of the reactivity of coal during CO_2 gasification in high-pressure wire-mesh reactor. They preformed experiments on a bituminous coal char for different pressures from *0.1* to *3.0 MPa*.

As presented in Figure 23 increasing pressure diametrically influences gasification reaction; both char conversion (a) and extend of CO_2 gasification (b) are higher with increasing pressure. Pressure dependency is not linear for the entire process course; however there is visible pattern. The increase of pressure precipitates reaction rate especially reaction in the first *20* seconds, dependence in this time region is linear. After longer hold time its influence is not so significant, gasification’s rate slows down. After *60* seconds hold time conversion rates of coal chars were *24, 65.2, 78.6*, and *86 %$_{wt}$* at pressures of *0.1, 1.0, 2.0,* and *3.0 MPa*, respectively. Due to the progressively high pressures, the reaction sensitivity is weaker.

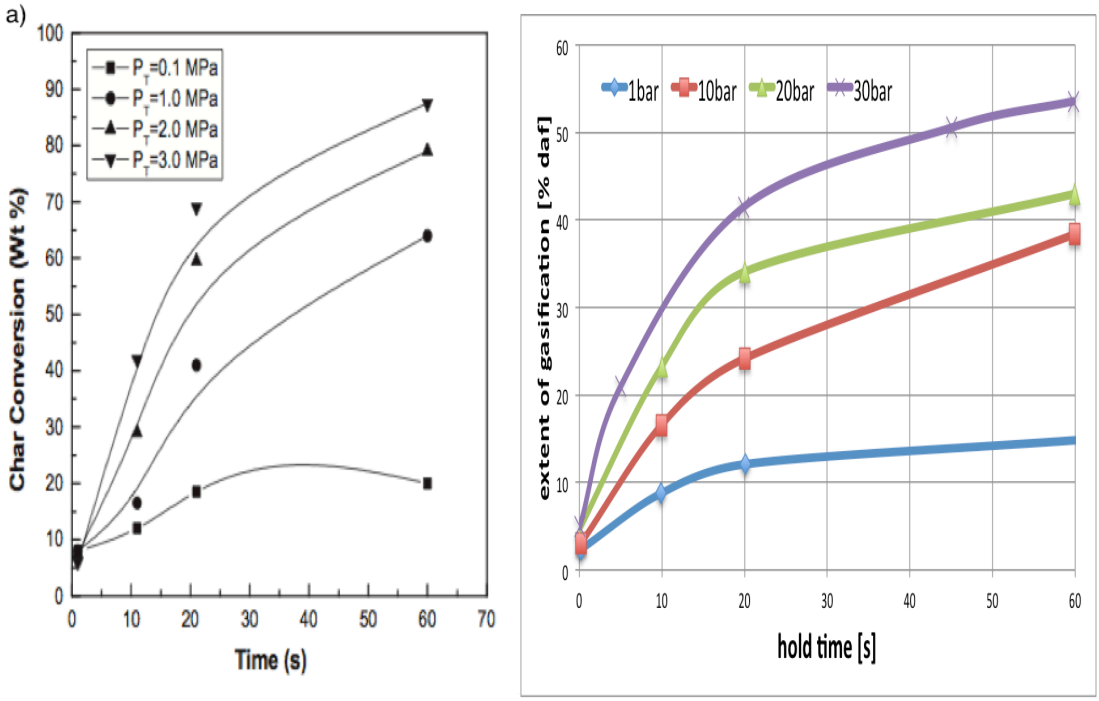

Figure 22. Effect of pressure on two factors: a) char conversion histories for Daw Mill bituminous char gasification under 100% CO_2 at 1000°C and b) extent of CO_2 gasification [20].

2.6.4. EFFECT OF CO_2 CONCENTRATION

Main reactant gas in the reviewed gasification type is CO_2. Additionally it may occur as a pure gas or as a mixture. Presented below results of researches present influence of CO_2 concentrations on coal char gasification, its conversion and reaction rate. American scientists Gui-Su Liu, Stephen Niksa [21] performed deep investigation into parameters influencing New Zealand's coal char gasification in CO_2 atmosphere at *0.5 MPa* in a PDTF (Pressurized Drop Tube Furnace). They reported the following effect of CO_2 concentration on the gasification reaction rate.

As it may be seen in Figure 24a, coal char conversion depends directly on CO_2 concentration. With the increasing concentration, the higher conversion is obtained at the same time, for example after *40* minutes of gasification with CO_2, *0.6, 0.7, 0.8* coal char conversions reached $20\%_{wt}$, $60\%_{wt}$ and $100\%_{wt}$ respectively. Relation between conversion and concentration is not linear but with the increasing concentration, the conversion rate is also increasing.

At the same time, as shown in Figure 24b, the gasification rate shows increase proportionally to the CO_2 mole fraction range from *8* to $25\%_{wt}$. Further increase from $25\%_{wt}$ to $58\%_{wt}$ enhances reaction in a relatively lower rate. Reaction order assumed and calculated differs depending on quoted research group. Mainly, the reaction order varies from the zero order at high CO_2 partial pressures to the first order at low CO_2 partial pressure. For example a South Korean research group, headed by D.H. Ahm [22] investigated CO_2 gasification kinetics of a sub-bituminous coal char at elevated pressures. They

reported that with the partial pressure of CO_2 in the range of *0.1-0.5 MPa* and *0.2 MPa* caused order value of *0.4* and *0.69* respectively. Both tests were performed at the temperature of *1300 °C* and at total system pressure of *1.0 MPa* and *0.5-1.5 MPa* respectively.

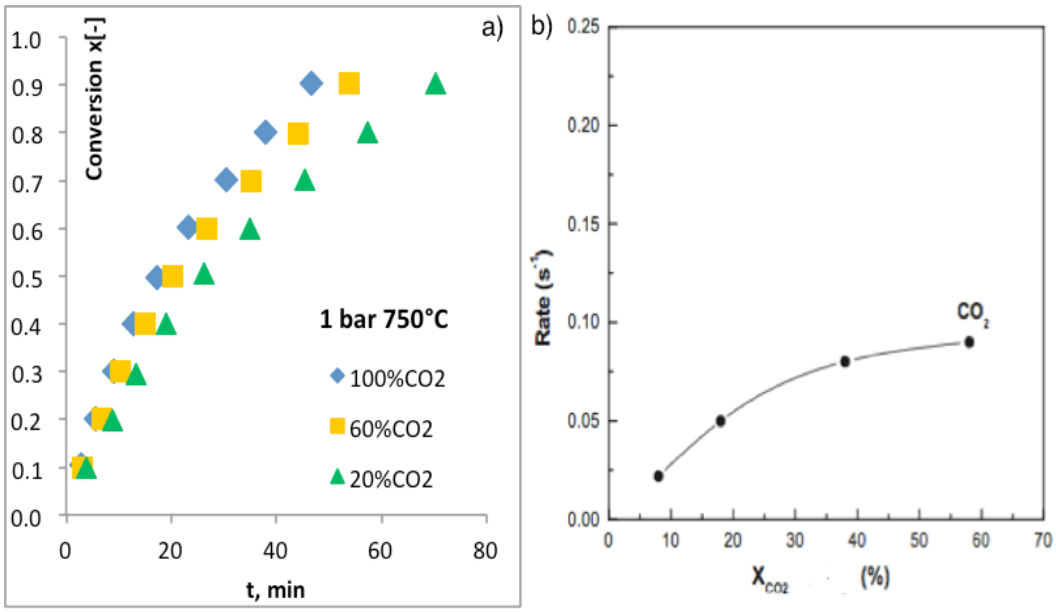

Figure 23. The effect of CO_2 concentration on two factors: a) carbon conversion and b) gasification rate [21].

2.6.5. EFFECT OF CATALYST

In recent years, catalytic coal gasification has been studied extensively. Various research groups examined the effect of various compounds on promoting coal conversion. From economical point of view, obtaining coal gasification in lower temperatures without qualitive and quantitive losses is desired. Manifold studies have shown that mostly group VIII metals, alkali and alkaline metals are effective in CO_2 gasification of coal.

2.6.5.1. ALKALI AND ALKALINE EARTH METALS

Alkali and alkaline earth metals (AAEM) mainly occur as organically associated cations or in discrete minerals. For low rank coals, these highly dispersed metals are forming the mineral matter naturally present in the carbon matrix, they also act as catalysts for the gasification reaction. An Argentinian group of scientists J. Ochoa, M.C. Cassanello, P.R. Bonelli and A.L. Cukierman [23] performed research on influence of mineral matter occurring in coal matrix on gasification kinetics of the Argentinean subbituminous (SB) and high volatile bituminous (HVB) coal chars. To achieve the test goals, they investigated differences in kinetics of raw coal char and chars that were demineralized. As presented in Figure 25 below, subbituminous char with mineral matter has a higher reaction rate then the demineralized one in the initial conversion range. The reaction rate of demineralized coal decreases steadily, which is a quite different behaviour from raw coal, which discloses maximum. It is

clearly seen that ash in coal needs time to be activated as catalyst and this results in a increasing rate and in a later stage catalytic effect becomes weaker because ash layer blocks reaction surface. The opposite trend may be observed for the high volatiles bituminous char, where reactivity in all conversion range is higher for demineralized coal char,

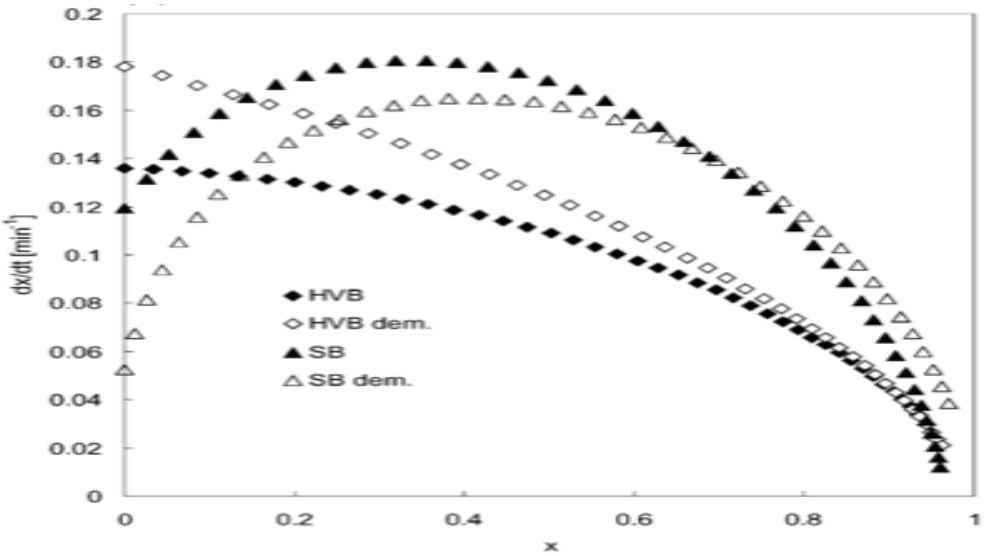

Figure 24. Gasification rate vs. conversion curves for the raw and demineralized chars from the SB. and HVB. coals at operating conditions: 1413 K, 70% CO_2 [23].

A Japanese Koichi Matsuoka's research group [24] reported that the alkali and alkaline earth metal AAEM species in SB coals, used in the tests, occur mostly in a form of dispersed species. The way that AAEMs were released from coal matrix during gasification process depended on the type of metals.

Sodium and Potassium vaporized during the gasification and their interaction with other materials was very weak. The main part of Calcium and Magnesium remained in the residue char, despite the fact that the major part of carbon underwent gasification reaction. Calcium has the biggest share in the alkali and alkaline earth metal species. It has a great influence on the formation of low temperature melting ash. Dispersed species of Calcium were converted into submicron particles during pyrolysis and then they reacted with clay minerals to form alumni-silicates complexes.

Table 3 presents coal ash composition, investigated components occur in metal's oxides form. Most of ash is composed of silica, aluminium, iron and calcium oxides (total *73.7%*$_{wt}$), but there also occur magnesium, titanium, sodium, phosphorus oxides and several others, not mentioned in a table below.

Table 3. Example of ash composition ($\%_{wt}$ of ash, sulfur-free basis) [24].

	SiO_2	Al_2O_3	Fe_2O_3	CaO	K_2O	MgO	TiO_2	Na_2O	P_2O_5
SS012	35,7	23,4	14,7	14,7	0,9	5,3	1,3	1,1	3
SS070	47,4	20,1	10	13,8	0,8	3,9	1,1	2,3	0,5

Literature reports that metals catalysing the Boudouard reaction are: Potassium (K), Sodium (Na), Calcium (Ca), Iron (Fe), Magnesium (Mg), Vanadium (V), Lithium (Li), Cesium (Cs), Chromium (Cr), Manganese (Mn), Barium (Ba), Strontium (Sr), Nickel (Ni), Copper (Cu). [24,25,26,27,28,29] As presented below in Figure 26, those metals decrease activation energy and in the same time decrease gasification temperature. Those catalysts cause increase of coal char conversion at the same temperature, for example: for presented results at the temperature of *800 °C*, the conversions obtained are *0.22, 0.4, 0.65, 0.83, 0.84* and for coal char with addition of Magnesium (Mg), Iron (Fe), Calcium (Ca), Sodium (Na), and Potassium (K) compounds respectively, comparing to the *0.1* conversion for pure coal char.

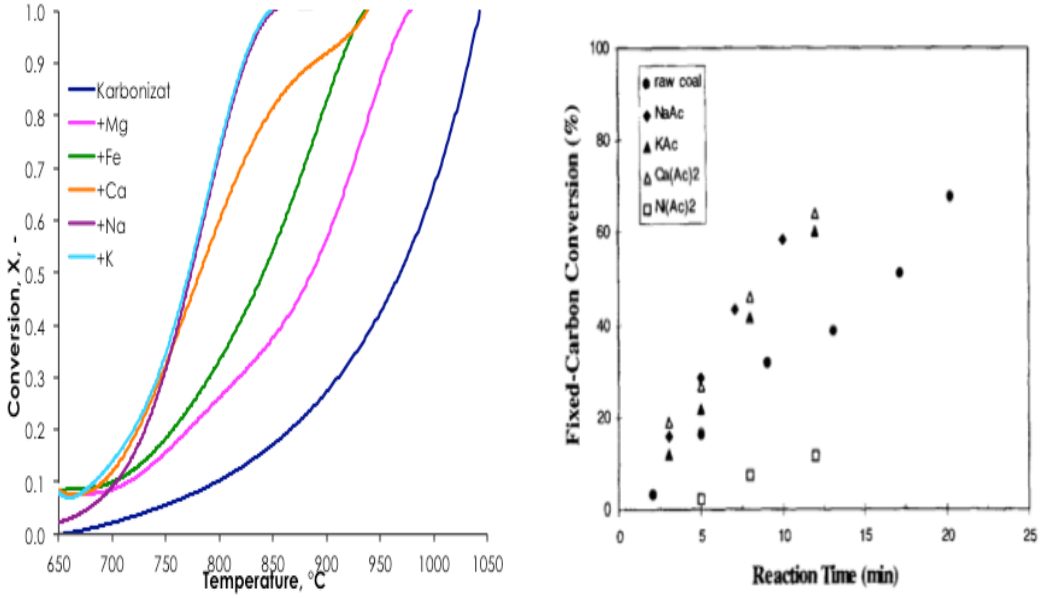

Figure 25. Catalytic effects of different compounds addition on coal char conversion during CO_2 gasification [24,25,26,27,28,29].

2.6.5.2. SODIUM AND POTASIUM CARBONATES

Chinese scientists Shufen Li and Yuanlin Cheng [30] investigated the catalytic effect of Na_2CO_3 and K_2CO_3 addition on the rate of the coal char CO_2 gasification. It may be deducted from the presented Table 4 that the conversion of coal chars increases and the activation energy decreases with the increasing catalyst loading. The catalytic effect of K_2CO_2 is greater that of Na_2CO_3.

Table 4. Rate constants (10^{-3} min^{-1}) with and without catalysts [30].

Catalyst (%)	Na_2CO_3 catalyst							K_2CO_3 catalyst						
	Reaction temperature (°C)													
	850	880	900	930	960	E [kJ/mol]	A [min^{-1}]	850	880	900	930	960	E [kj/mol]	A[min^{-1}]
0	5,06	6,66	6,75	8,32	10,8	122	1480							
1	5,83	6,05	7,13	8,6	9,1	118,2	1313	6,09	6,44	7,02	12,2	11,4	112,3	866
5	5,8	7	7,88	9,82	13,1	101,8	260	6,25	7,67	10,8	11,9	14,7	91,9	116
9	8,2	8,56	8,56	12,5	16,9	80,3	75,1	17,3	16,7	18,3	16,9	30,7	75,3	18,4
16	12,7	20,1	20,1	23,6	23,8	75,8	24,3	36,6	38,1	33,6	49,7	73,7	52	4,04
20		21,4	21,4						35,1					
25		30,9	30,9						26,2					
32		28,8	28,8											

As presented in Figure 27, for CO_2 gasification at *790-1020 °C* and *0.2 MPa* catalyst additions is enhancing gasification reaction rate up to the certain loading level (*5-20%$_{wt}$* for K_2CO_2 and *9-25%$_{wt}$* for Na_2CO_3) after reaching this point it drops again. Below *9%$_{wt}$* for Na_2CO_3 and *5%$_{wt}$* for K_2C0_3 the loading has little effect.

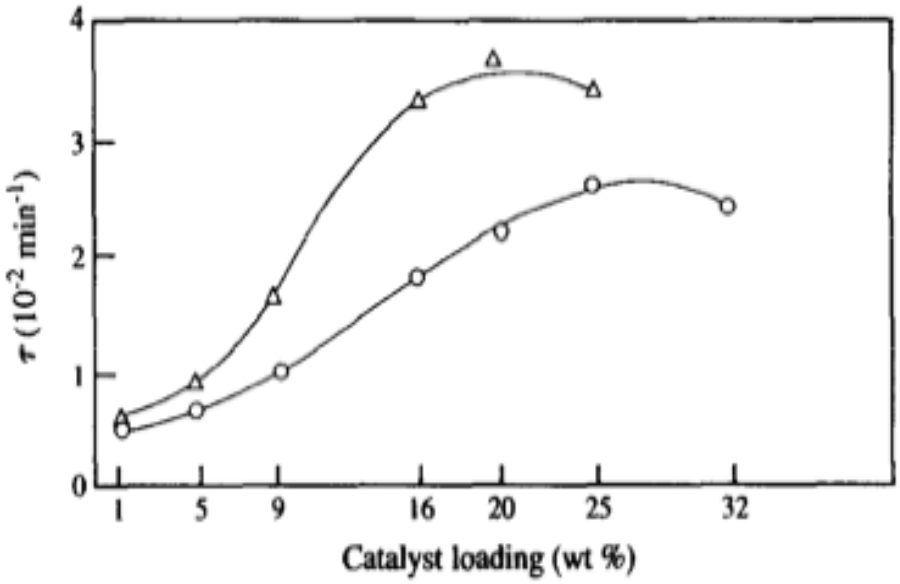

Figure 26. Effect of catalyst loading on reaction rate at 880°C for K_2CO_3 (**Δ**) Na_2CO_3 (***o***) [30].

2.6.5.3. IRON OXIDES

Dispersed iron catalysts were also considered as promising material for promoting coal char CO_2 gasification. Japanese scientists K.Asami, P.Sears, E.Eurimsky, Y.Ohtsuka [31] investigated gasification of brown coal and char with carbon dioxide using iron catalysts precipitated from an aqueous solution of $FeCl_3$. They concluded that the presence of iron catalyst can decrease the temperature, at which maximum rate of CO formation is achieved by *130-160 °C* lower temperatures or even a more significant lowering could be observed with higher loading in the range of ≤ *3%$_{wt}$* Fe.

Iron increased char conversion, specific rates in isothermal gasification. It resulted in complete gasification within a short reaction time. Precipitated iron occurs as fine oxide-hydroxide (FeOOH) particles, which are mainly reduced to the form of Fe_3C and then transformed in the initial phase of gasification reaction into α-Fe and γ-Fe and finally oxidized into iron oxides FeO and Fe_3O_4. Iron cations reactions during gasification are discussed in terms of solid-gas and solid-solid reactions.

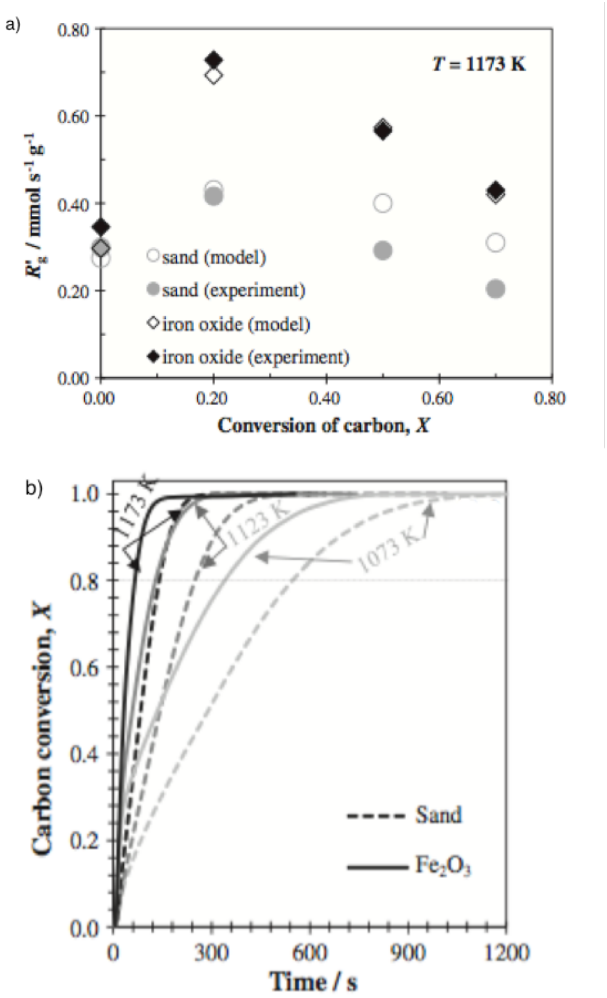

Figure 27. Effect of Fe_2O_3 addition on two factors: a) gasification rate and b) carbon conversion [32].

British Marco A. Saucedo's [32] research group investigated influence of iron-based oxygen carrier for CO_2 gasification of lignite coal. As presented in Table 5, at *1073 K*, time needed to exceed *50,80,95%$_{wt}$* of conversion are just slightly lower for the usage iron oxide bed instead of bed of silica sand. However, at both *1123* and *1173 K*, time needed to exceed *80%$_{wt}$* of coal conversion was *45%$_{wt}$* lower in a bed of Fe_2O_3. For experiments performed at the same temperature, the time to reach equal conversion of coal was evidently shorter when iron oxide was used as a bed material instead of sand. This dependence increased with raising gasification temperature. Coal char conversion dependence on iron oxide addition is also presented in Figure 28a.

Table 5. Time vs carbon corversion, for the gasification of Hambach lignite char, in the bed of (I) silica sand and (II) Fe_2O_3 [32].

x	Silica sand			Fe_2O_3		
	1073K	1123K	1173K	1073K	1123K	1173K
50%	995	480	240	915	300	150
80%	2520	980	420	2080	550	230
95%	>3710	1525	585	3180	910	355

Moreover, as it may be seen in Figure 28b Fe_2O_3 addition caused increase of gasification rate, at higher temperatures, (*1173 K*), its value, during first *60-120 s*, when devolatization takes place, could be even 2 times higher in experiments with Fe_2O_3 than in a bed of sand.

$$Fe_mO_n + CO_2 \rightarrow Fe_mO_{n+1} + CO \qquad (26)$$

$$Fe_mO_{n+1} + C \rightarrow Fe_mO_n + CO \qquad (27)$$

The equation is the catalytic reduction. Carbon dioxide used in coal gasification is an oxidizing agent of some mineral compounds fixed in coal matrix, such as a metal iron (Fe), pyrrhotite ($Fe_{1-x}S$), and oldhamite (CaS). Form of iron oxide produced depends on the reaction conditions, at low oxygen levels, the stable iron forms at *900 °C* (metallic iron and wustite (FeO)). Wustite decomposes into metallic iron and magnetite (Fe_3O_4) below temperature of *570 °C*. Pyrrhotite, depending on the atmosphere, in inert one it undergoes further decomposition to metallic iron or is oxidized to iron oxide in low oxygen concentrations. Oldhamite in the presence of CO_2 at *900 °C* forms calcium oxide. [33,34,35] Due to the diametric effect of coal char with CO_2 reaction on its structure and mineral composition, some minerals disappear and new ones like [fayalite ($(Fe,Mg)_2SiO_4$), hercynite ($FeAl_2O_4$), rankinite ($Ca_3Si_2O_7$)) and anorthite ($(Ca,Na)(Si,Al)_4O_8$] are formed. Those minerals have great influence on reaction kinetics.

2.6.6. EFFECT OF PARTICLE SIZE

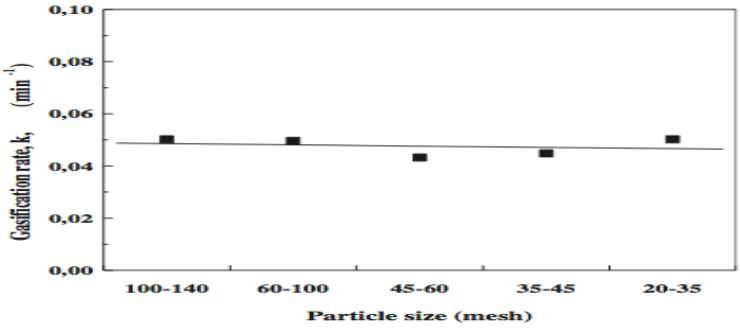

Figure 28. Effect of particle size on the gasification reaction rate [36].

According to the Australians D. P. Ye, J. B. Agnew [37] researches, who performed for Bowman's coal during CO_2 gasification at temperature of 765°C and Greek G. Skodras [36] at 800 °C. They concluded as presented above in Figure 29 that particle size does not influence the rate of gasification under the examined experiment conditions.

3. METHODS OF HETEROGENOUS REACTION KINETIC ANALYSIS.

Thermogravimetric analysis is recording a weight-change of a sample at a constant heating rate. It has a great advantage over measurement at a constant temperature as thermogravimety shows changes of sample during heating to the desired temperatures. The application of the dynamic TG methods are considered to be a promising tool for understanding the mechanisms of physical and chemical processes that occur during degradation of solid matter. Gasification process is simple one, initial structure in the sample is not changed during degradation of solid matter, it may be represented by the following reaction scheme:

$$\boldsymbol{A_{solid} \rightarrow B_{solid} + C_{volatile}} \qquad (28)$$

The rate of conversion, $r = \frac{dx}{dt}$ for TG experiment at constant rate of the temperature change, $\beta = \frac{dT}{dt}$ may be expressed by the following equation:

$$\boldsymbol{\frac{dx}{dt} = \beta \frac{dx}{dT} = k(T) f(x)} \qquad (29)$$

where x is the degree of conversion, *f(x)* is the function of conversion and *k(T)* is the rate of weight loss on temperature. Arrhenius equation can be applied successfully to obtain kinetic parameters:

$$\boldsymbol{k(T) = Aexp(\frac{-E}{RT})} \qquad (30)$$

where *E* is the apparent activation energy, *A* the pre-exponential factor and *T* the gas constant.

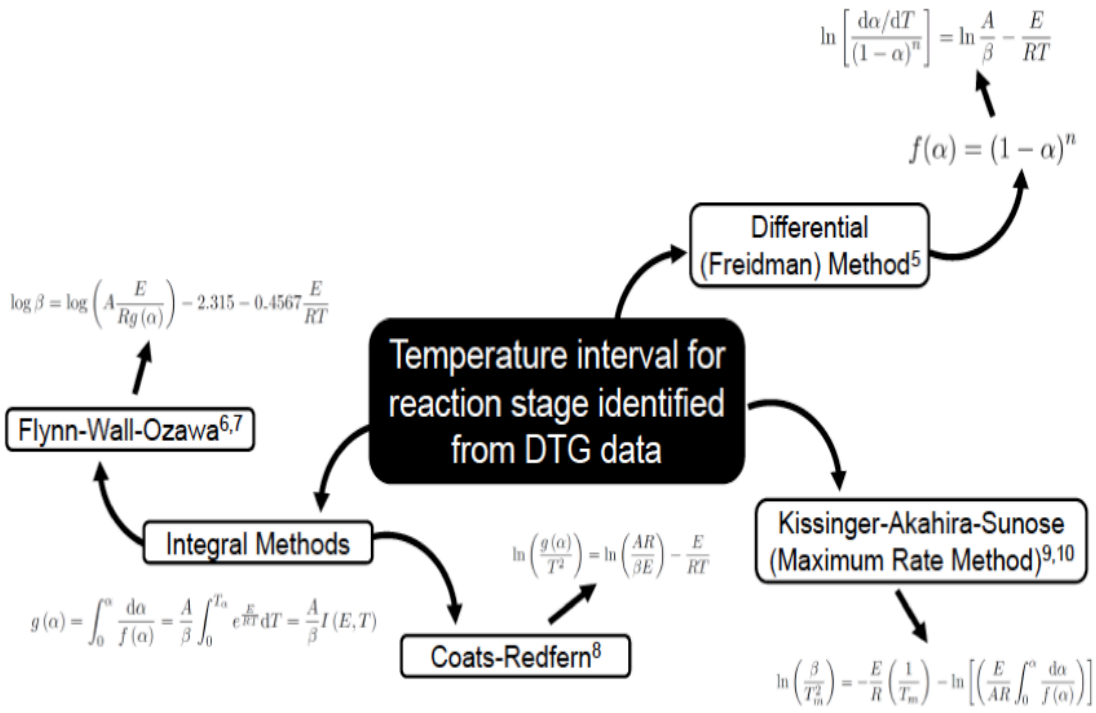

Figure 29. Kinetic data analysis models.

There are many methods applied for obtaining the kinetic parameters from the thermogravimetric data. Typically, all kinetic models require assumption of specific order of reactions and regression analysis, and are based on a single-step Arrhenius method, presented by above equations [38,39]. Isoconversional and multi-heating methods can be particularly useful on describing kinetics of complex material reactions [63]. Based on the results of thermogravimetric measurements with multiple heating rates (β), three main modes may be applied. As presented in Figure 30, they solve Arrhenius equation by different mathematical approach to build kinetic model:

- Friedman differential method,
- Kissinger-Akahira-Sunose maximum rate method,
- Flynn-Wall-Ozawa integral method.

3.1. FREIDMAN MODEL

Friedman method [40], named after researcher who first derived this method, stands for isoconversional differential methods. The method treats Arrhenius equation as a differential one; it simply derives from taking the logarithm of Arrhenius equation:

$$\ln\left[\beta_i\left(\frac{dx}{dT}\right)_{x,i}\right] = \ln[A_x f(x)] - \frac{E_{a,x}}{RT_x} \qquad (31)$$

The apparent activation energy (E_a) is determined for wide range of conversions from the slope of the plot of $ln[\beta_i(dx/dT)_{x,i}]$ vs. $1/T_x$, based on fact that under the isoconversional assumption the function $f(x)$ reaches a given, constant x value. Subscript i is the ordinal number of the experiment performed at a given heating rate. Lack of any mathematical approximations makes Friedman method an accurate one.

3.2. KISSINGER-AKAHIRA-SUNOSE MODEL

To obtain the Kissinger-Akahira-Sunose model [41,42] the standard Arrhenius equation can be shown as follows:

$$\frac{dx}{f(x)} = \frac{A}{\beta}\exp\left(\frac{-E}{RT}\right)dT \qquad (32)$$

after integration with the initial conditions of $x=0$ at $T=T_o$, the function obtain the following form:

$$g(x) = \int_0^x \frac{dx}{f(x)} = \frac{A}{\beta}\int_{T_0}^{T} \exp\left(\frac{-E}{RT}\right)dT = \frac{AE}{\beta R}p\left(\frac{E}{RT}\right) \qquad (33)$$

The most essential for this technique is the assumption that the pre-exponential factor A, activation energy E and function of conversion are independent of temperature, while A and E_a are independent of x.

The KAS method is based on the equation derived from the condition of the maximum of reaction rate and assumption that the reaction rate *dx/dt* reaches maximum at the temperature T_p, where the curve displays the peak. It was taken into consideration when the formulation following Coats-Redferm approximation of the temperature integral [43] and relationship [44]:

$$\boldsymbol{ln\frac{\beta}{T_P{}^2} = ln\frac{AR}{Eg(x)} - \frac{E}{RT_P}} \qquad (34)$$

The value of apparent activation energy E may be obtained from the slope of the plot $ln\beta/T_P{}^2$ vs. $(1/T_p)$, for a series of experiments at different heating rates. Its evaluation is based on the slope of straight line that the plot $ln\beta/T_P{}^2$ vs. $(1/T_p)$ for a constant value of *x* should be. Further, from the intercept one also obtains the pre-exponential factor *A*.

3.3. FLYNN-WALL OZAWA MODEL

The Flynn–Wall–Ozawa (FWO) method [45,46] is derived from the integral isoconversional method and it uses the Doyle approximation [47] for the temperature integral, which allows formation of following equation:

$$\boldsymbol{lnp(a) = -5.331 - 1.052a} \qquad (35)$$

where $x = \frac{E}{RT}$, that after substitution with previous relations lead to:

$$\boldsymbol{ln\beta_i = \ln\left(\frac{A_x E_a x}{Rg(x)}\right) - 5.331 - 1.052\frac{E_{a,x}}{RT_x}} \qquad (36)$$

Thus, for *x* = *const*., a plot of ln β_i vs. $1/T_X$, obtained from themograms recorded at several heating rates, should be a straight line which slope allows evaluation of the apparent activation energy.

As far as the pre-exponential factor is concerned, its value can be obtained from the intercept if the form of the integral conversion function is known. For $x < 0.2$, Doyle's approximation leads to errors higher than $10\%_{wt}$. For such cases Flynn [48] suggested corrections in order to obtain correct activation energy values. Professor Ozawa made an assumption that the degree of reaction is a constant value independent of the heating rate when a DSC curve reaches its peak, and derived the following equation:

$$\boldsymbol{ln\beta_i = const - 1.052\frac{E_{a,x}}{RT_x}} \qquad (37)$$

EXPERIMENTAL PART

4. EXPERIMENT

4.1. SAMPLE PREPARATION

The brown coal from the Turów minefield, located in Lower Silesia coalfield (Poland), was used for the experiments. Its proximate and ultimate characterizations are presented below in Table 6. This specific type of coal was chosen due to the outstanding low ash content in the coal matrix.

Table 6. Parent coal "Turów" and coal char properties

Indicated parameter	Symbol	Unit	Parent coal "Turów"		Coal char "Turów"	
			Value	Uncertainty +/-	Value	Uncertainty +/-
Moisture (tot.) content	W_t^r	%	36.9	0.7	-	-
Moisture content	W^a	%	6.4	0.1	2.0	-
Ash content	A^a	%	27.7	0.2	51.1	-
Ash content	A^r	%	18.7	0.2	52.1	-
Ash content	A^d	%	29.6	0.2	-	-
Volatile content	V^a	%	38.06	0.17	0.61	-
Volatile content	V^d	%	40.66	0.17	0.62	-
Volatile content	V^{daf}	%	57.75	0.25	1.30	-
High Heating Value	Q_s^a	%	17842	83	15719	-
High Heating Value	Q_s^d	%	19062	101	16040	-
Low Heating Value	Q_i^a	%	16860	101	15607	-
Low Heating Value	Q_i^r	%	10571	246	-	-
Low Heating Value	Q_i^d	%	18180	119	15975	-
Low Heating Value	Q_i^{daf}	%	25822	168	33381	-
Sulfur content	S_t^a	%	1.52	0.04	1.16	-
Sulfur content	S_t^r	%	1.02	0.04	-	-
Sulfur content	S_A^a	%	0.07	0.06	0.10	-
Sulfur content	S_C^a	%	1.45	0.05	1.06	-
Carbon content	C_t^a	%	44.2	0.6	45.8	-
Carbon content	C_t^r	%	29.8	0.7	-	-
Carbon content	C_t^d	%	47.2	0.6	46.7	-
Hydrogen content	H_t^a	%	3.78	0.27	0.29	-
Nitrogen content	N^a	%	0.44	0.15	0.46	-
Oxygen content (cal.)	O_d^a	%	16.03	0.69	-	-
Phosphorus content	P^a	%	0.027	0.002	0.039	-
Chlorine content	Cl^a	%	0.013	0.017	0.009	-
Chlorine content	Cl^r	%	0.009	0.017	-	-
Fluorine content	F^a	%	0.036	0.017	0.055	-
Mercury content	Hg^d	mg/kg	0.157	0.028	-	-

Chars were prepared via pyrolysis process that leads to devolatization of the parent coals in a fixed-bed reactor heated by an electric furnace under a nitrogen stream. *4 kg* of coal in 2 samples (*2 kg* each sample), were crashed under *200 µm size* and placed in the reactor. Nitrogen stream was controlled by the Bronkhornst mass flow meter connected to the computer and with usage of FDD software it was possible to set constant flow at the level of *0.6 l/min*. Samples were submitted to a heating rate of *5 K/min* up to *1273 K* and held at this temperature for half an hour. The thermocouple type *K* located in the middle of the reactor checked temperature regardless of the oven controllers. Gases produced during the process were cooled down to condensate all liquids. All device arrangement is visible in Figure 30 below.

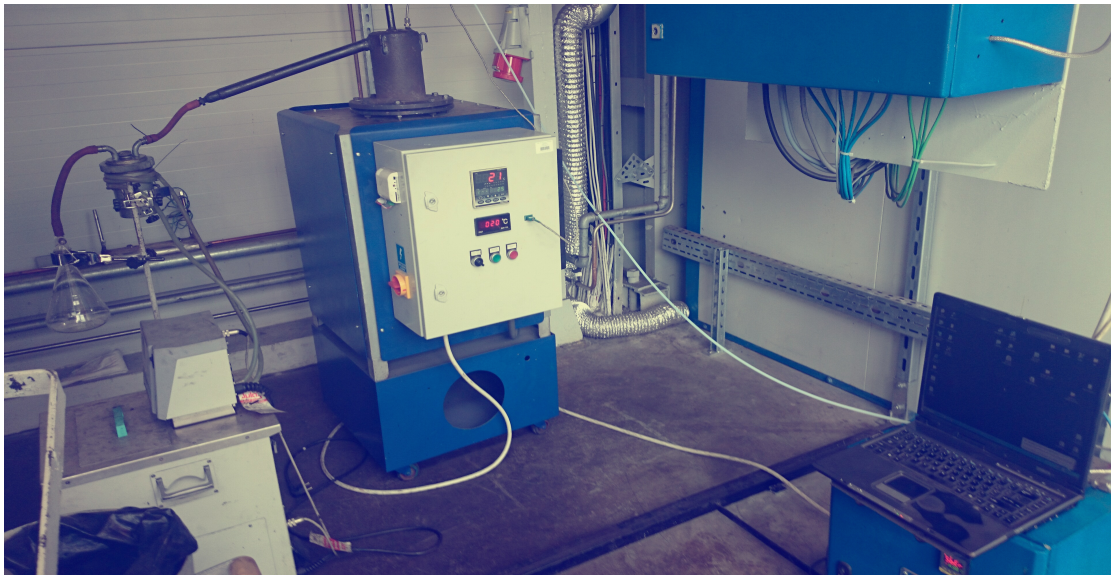

Figure 30. Coal char preparation installation.

After the process coal chars were milled with usage of agate mortar and mills, sieved and for further usage only fractions with size below *100 µm* were obtained.

4.1.1. CHARACTERIZATION OF SELECTED COALS.

Coal chars were also examined to check the ultimate and proximate analysis. All of the parent coal and coal char characterization tests were performed under the supervision of MSc Grzegorz Tomaszewicz, in Institute for Chemical Processing of Coal in Zabrze, Poland, with respect to the Polish governmental and own Institutes standards and procedures [49-59]. Those results are presented in the Table 6.

As it is possible to conclude from above Table 6 the pyrolysis process devolatilized (volatile content diametrically falls from *38.06%$_{wt}$* to *0.62%$_{wt}$*) and dehydrogenated (hydrogen content drops from *3.78%$_{wt}$* to *0.29%$_{wt}$*) parent coal. In contrast to that, it could be observed that increasing mass fraction of carbon (increased from *29.8%$_{wt}$* to *46.7%$_{wt}$*) and ash (from *27.7%$_{wt}$* to *52.1%$_{wt}$*). All parameters were compared in the analytic state of coal.

For depth understanding of these findings relevance of, chemical composition of ash content for parent coal and coal char had to be performed [54]. As presented in the following Table 7 their composition is very similar. Silica oxide, aluminium oxide, iron (III) oxide, calcium oxide, magnesium oxide, sodium oxide and potassium oxide have the largest share. For my experiment, investigating influence of mineral matter on the coal char gasification kinetics, I had to choose certain mineral compounds to test. With the respect to results from other research groups, presented in the literature part, it is known that silicon and aluminium compounds have no catalytic activity on the Boudouard reaction. From the rest of the compounds I had to choose the ones that are possible to implement in the industry due to their low price, easy accessibility, supply ability and characterized by high catalytic activity documented in the literature part.

Table 7. Parent coal “Turów” and coal char ash chemical composition

Indicated parameter	Symbol	Unit	Parent coal "Turów"		Coal char "Turów"
			Value	Uncertainty +/-	Value
Silicon oxide content	SiO_2	%	50.4	1.92	48.14
Aluminium oxide content	Al_2O_3	%	33.64	1.54	33.04
Iron (III) oxide content	**Fe_2O_3**	**%**	**5.98**	**0.56**	**5.96**
Calcium oxide content	**CaO**	**%**	**1.34**	**0.21**	**1.11**
Magnesium oxide content	MgO	%	1.60	0.13	1.37
Phosphorus (V) oxide content	P_2O_5	%	0.22	0.04	0.18
Sulphur (III) oxide content	SO_3	%	0.39	0.22	0.43
Manganese oxide content	Mn_3O_4	%	0.03	0.02	0.03
Titanium oxide content	TiO_2	%	2.39	0.04	2.19
Barium oxide content	BaO	%	0.07	0.01	0.07
Strontium oxide content	SrO	%	0.03	0.01	0.02
Sodium oxide content	Na_2O	%	1.54	0.03	1.28
Potassium oxide content	K_2O	%	1.93	0.06	1.88

With the respect of above composition and prices listed below in Table 8, materials were chosen. Iron (III) oxide, due to the fact it has the highest fraction in mineral matter composition from compounds influencing gasification, and calcium carbonate, because of relative low price were chosen.

Table 8. Market prices of iron (III) oxide and limestone. [60]

Compound	Symbol	Price [€/ton]
Iron (III) oxide	Fe_2O_3	350.00-700.00
Limestone	$CaCO_3$	10.00 - 40.00

4.1.2. COAL CHARS MIXTURES WITH MINERAL OXIDES PREPARATION

For further research investigating mineral matter influence on the kinetics of coal chars gasification 6 mixtures of specified coal chars with different addition of minerals were selected and prepared:

- Coal char + artificial *1%$_{wt}$* of iron oxide (Fe_2O_3)
- Coal char + artificial *3%$_{wt}$* of iron oxide (Fe_2O_3)
- Coal char + artificial *5%$_{wt}$* of iron oxide (Fe_2O_3)
- Coal char + artificial *1%$_{wt}$* of limestone
- Coal char + artificial *3%$_{wt}$* of limestone
- Coal char + artificial *5%$_{wt}$* of limestone

To provide conditions simulating distribution of mineral matter a small as possible of compound powders were needed. For this purpose Sigma Aldrich's iron oxide (Fe_2O_3) was used. It was characterized by *99%* purity and particles were sized *<5* micrometres. As the second type of catalyst representing mineral matter , compound limestone was used. Limestone catalyst was mainly (>90%) composed from calcium carbonate ($CaCO_3$), however it contained some contaminants (SiO_2 + NR, Fe_2O_3, $MgCO_3$, Al_2O_3). It was milled to the size of particles *<200* micrometres. This guaranteed the accomplishment of particle's distribution goals.

Coal char particles were mixed with synthetic mineral matter in a conical ball mill, presented in Figure 32 below, by the time of *8* hours for each sample. To check if the distribution goals were achieved three random samples of *1 g* of coal char mixed with iron oxide were weighted. The ash content tests were performed. They were heated up to *850 ^{o}C* in air atmosphere. The ash residues in each sample were very similar and it proved that the performed mixing method turned out to be successful.

Figure 31. IChPW's conical ball mill.

Coal char, obtained mixtures with artificial catalysts, and after gasification residues samples were tested by Scanning Electron Microscopes (SEM) with Energy Dispersive X-ray Spectroscopy (EDS) analysis. Pictures of coal char and mineral oxides distribution on coal char are presented in following Figure 32 and Figure 33, 34.

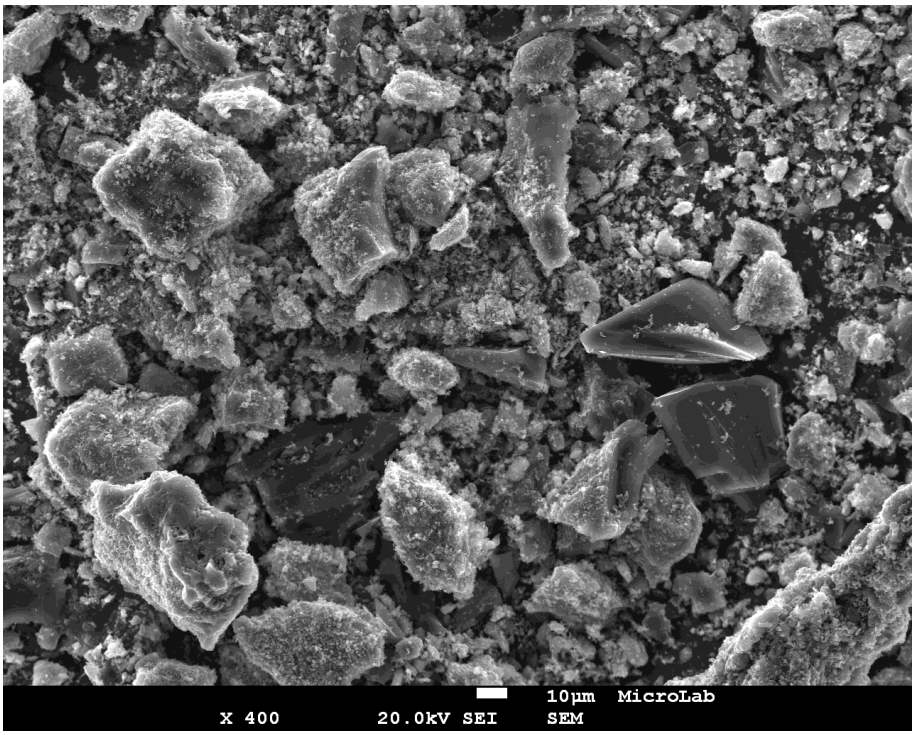

Figure 32. SEM picture of coal char sample.

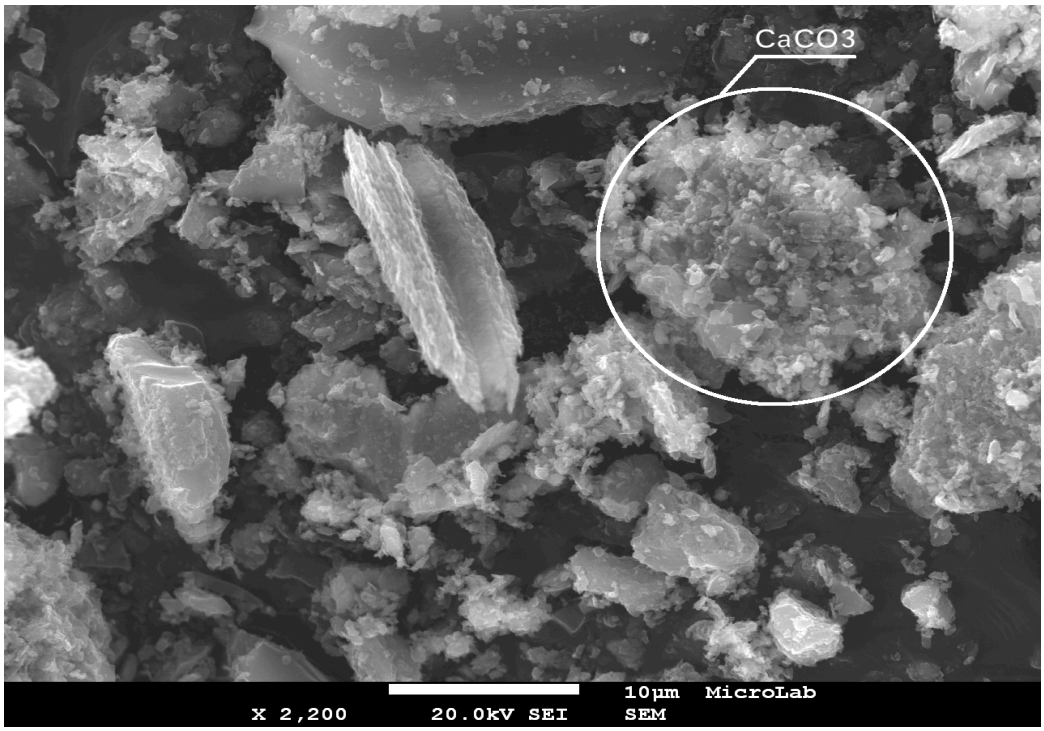

Figure 33. SEM picture of limestone ($3\%_{wt}$) particles distribution on the coal char surface.

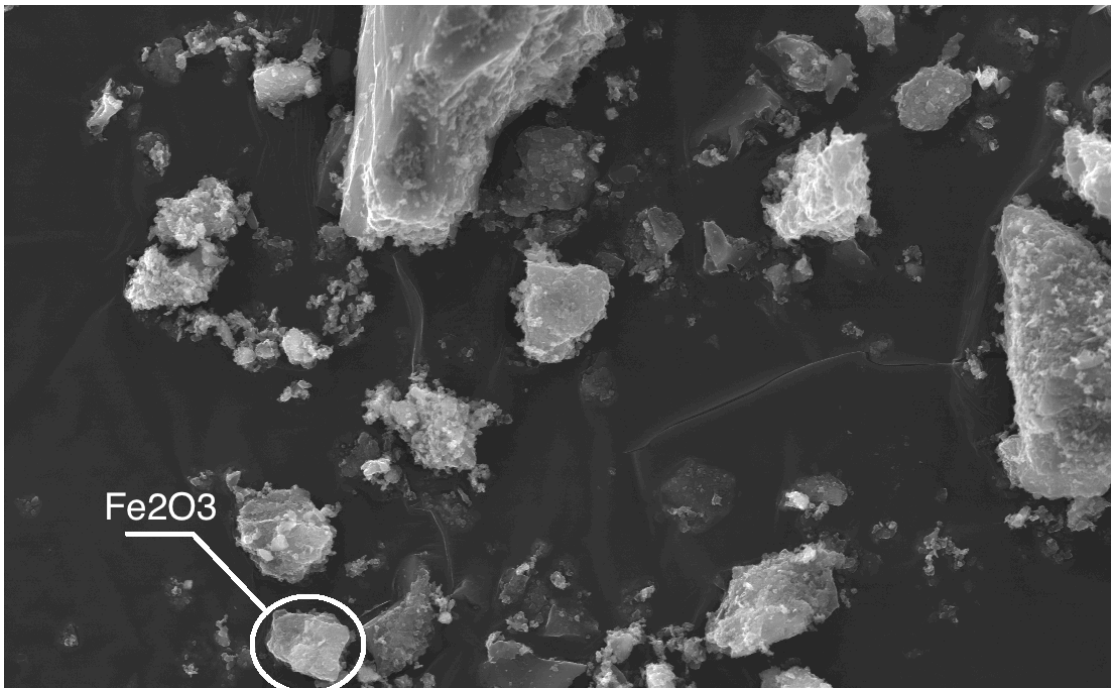

Figure 34. SEM picture of iron (III) oxide (*3%$_{wt}$*) particles distribution on the coal char surface.

4.2. THERMOGRAVIMETRIC RESEARCH UNDER ISOCONVERSIONAL CONDITIONS

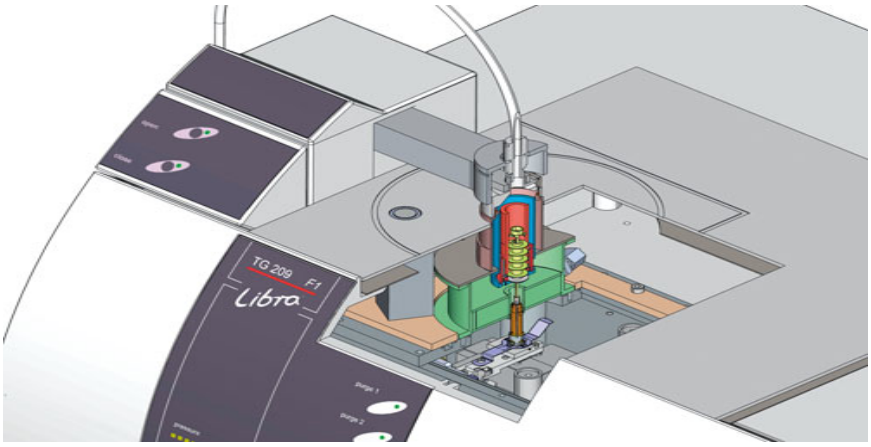

Figure 35. Design of the TG 209 F1 Libra.

For thermogravimetric research under isoconversional conditions produced by Netzsch TG 209 ***F1*** *Libra* was used. It is designed for heating the sample up to *1100 ^{o}C* with very specified heating and cooling rates (*0.001 K/min* to *200 K/min*). This device was chosen also due to its high resolution *0.1µg*. It allows performing processes under different atmospheres (inert, oxidizing, reducing, static, dynamic). TG Libra has a gas supply unit with integrated mass flow controller for two purge gases and one protective gas and can guarantee vacuum, by tight assembly up to *10^{-2} mbar (1 Pa).* The most practical advantage of this unit is the automatic sample changer (ASC) for up to *64* sample crucibles.

5 mg samples of the aforementioned coal char and the coal char's mixtures were tested. To investigate deeply the area of the influence of the temperature and the heating rate, gasification with CO_2 flow (supplied by gas supply unit at the level of *50 ml/min*). For each type of sample tests were performed with three different heating rates: *1 K/min, 3 K/min* and *5 K/min*.

Samples were weighted with precision of +/- *0.01mg*. They were placed in ceramic crucibles. Those crucibles are taken by automatic sample changer and placed into red tube oven, presented in Figure 35 above. The firm software also controls heating up rate and carbon dioxide flow. Thermogravimetric method is based on changes of the sample mass in time function. The gasification reaction rates($r[s^{-1}]$) and char conversions ($x[-]$) were calculated by following equations:

$$x = \frac{m_0 - m_t}{m_0 - m_r} \qquad (38)$$

$$r = \frac{dx}{dt} \qquad (39)$$

where m_0 *[mg]* denotes the sample mass at the beginning of the gasification, m_t *[mg]* is the sample mass at the reaction time *t [s],* and m_r *[mg]* is residual mass after gasification.

4.3. COAL CHARS GASIFICATION RESEARCH

To investigate deeply the mechanism of coal char gasification and mineral matter's influence on it research in laboratory scale chemical reactor was performed as well. This part of the dissertation investigation took place in Instituto Superior Tecnico in Lisbon at the Department of Mechanical Engineering (DEM) under the supervision of Doctor Rui Costa Neto.

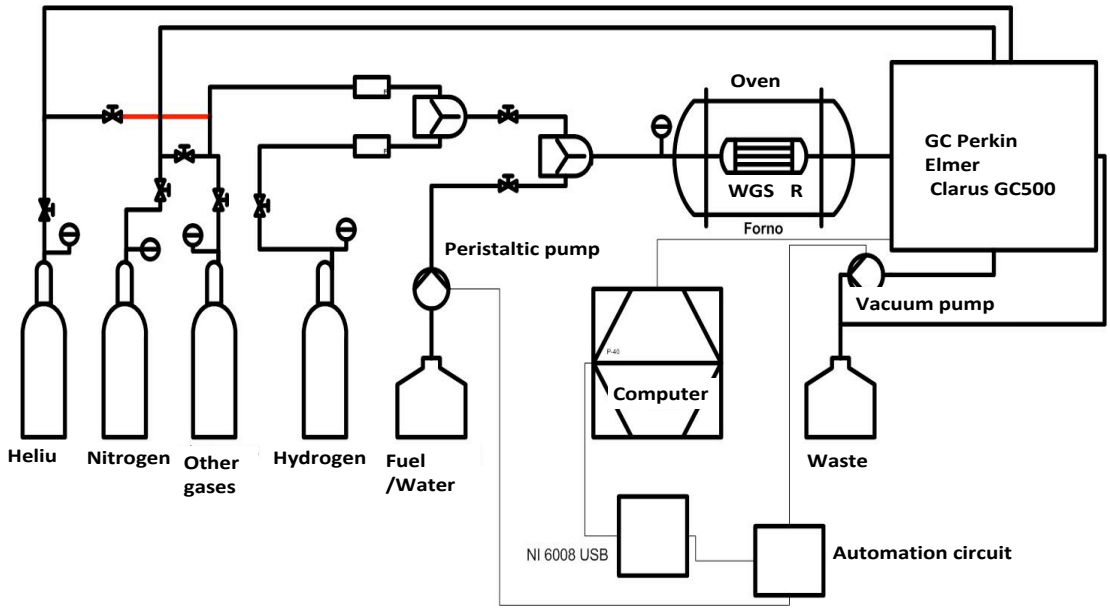

Figure 36. Laboratory reactor scale process arrangement.

There occurred certain challenges of process design and its implementation into reality. The main goal of this part of research was to scale up the process from the thermogravimetric weight to the laboratory installation with chemical reactor. For this purpose, installation's arrangement was necessary for tests undergoing with carbon dioxide gas flow in a ceramic reactor placed in the oven enabling heating up the sampled fixed into it up to *1100 °C*.

With respect of the belonging to the university facilities and devices available, installation presented in Figure 36 above, was constructed. It contained the following main devices:

- **Oven and the reactor**

Due to the possibility to use the electric oven, I choose the ceramic tube reactor, characterized by *40mm* diameter. Ceramic material guarantees proper heat convection and high-temperature resistance. This size of reactor allowed tests on the *12 g* weights range samples. To build a fixed-bed the reactor tube was filled with aluminium oxide balls with the diameter of *1 mm*. Those balls with special a high-temperature resistance fibber and a metal net were placed coal chars samples directly and still in the heating area of the oven and allowed constant, even gas flow. The mentioned arrangement and reactor cross-section are presented in the following Figure 37.

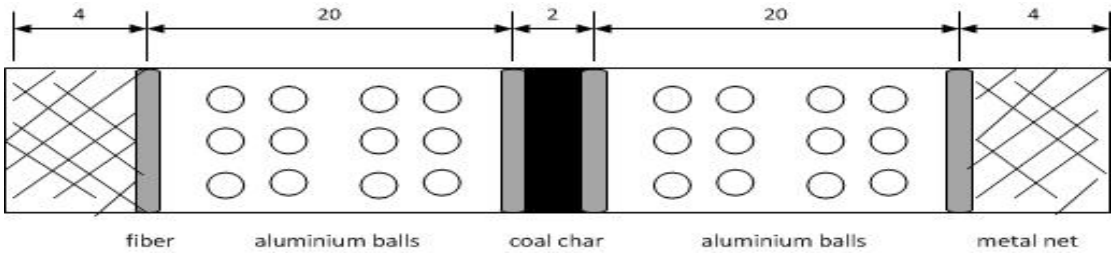

Figure 37. Reactor cross-section.

Due to the fact that final temperature (*950 °C*) and the heating rate (*10 K/min*) have a great impact on the reaction behaviour and its kinetics, the temperature control was one of the most important issues to solve. To control process temperature, there was prepared a special, individual *LabView* software overlay. It was connected with thermocouple type K, placed in side the reactor. Temperature and its horizontal distribution were checked online (record rate was set every *10* seconds). Below, in the Figure 38. The used *LabView* layout is presented.

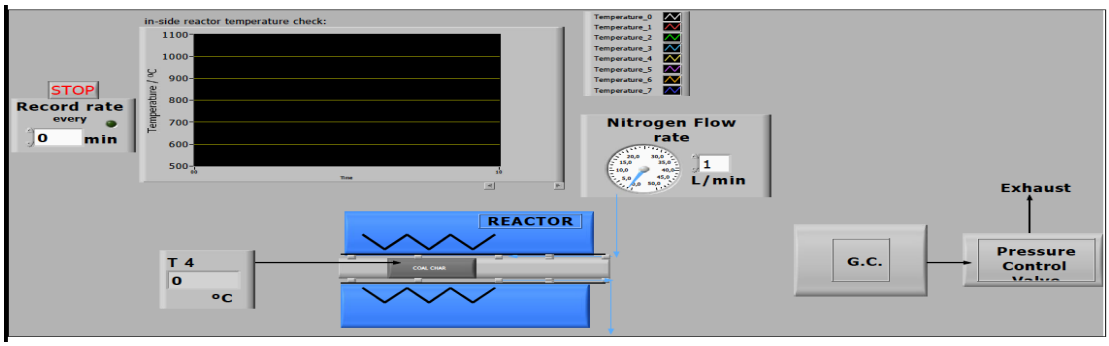

Figure 38. In-side reaction temperature checks software *LabView* layout.

- **Gas chromatograph**

To analyse the conversion coefficient process gas composition and its correlation with flowing time is needed. To obtain this information Gas chromatograph application is necessary. It gave feedback not only about qualitative data, but also about quantitive. Instituto Superior Tecnico was in possession of *Clarus 500* Gas Chromatograph, which was used to perform required tests.

The Gas chromatograph was connected by the loop to the output of process gas from the chemical reactor. Every *15* minutes the automotive valves sucked a small portion of the process gas for the composition test. For the proper usage in firm software *TotalChrom* dedicated to the *Clarus 500* Gas Chromatograph, there was a necessity to built a method, sequence based on set of methods and setup the instrument with those. Programmed method collects information about opening the valves, circuits and pressures that occur during the process; there is also information about the data files and exporting the results. Sequence is a set of methods, which was programmed to repeat cycle every *15* minutes during all *3*-hours test (*12* times). Those steps are presented below in Figure 39.

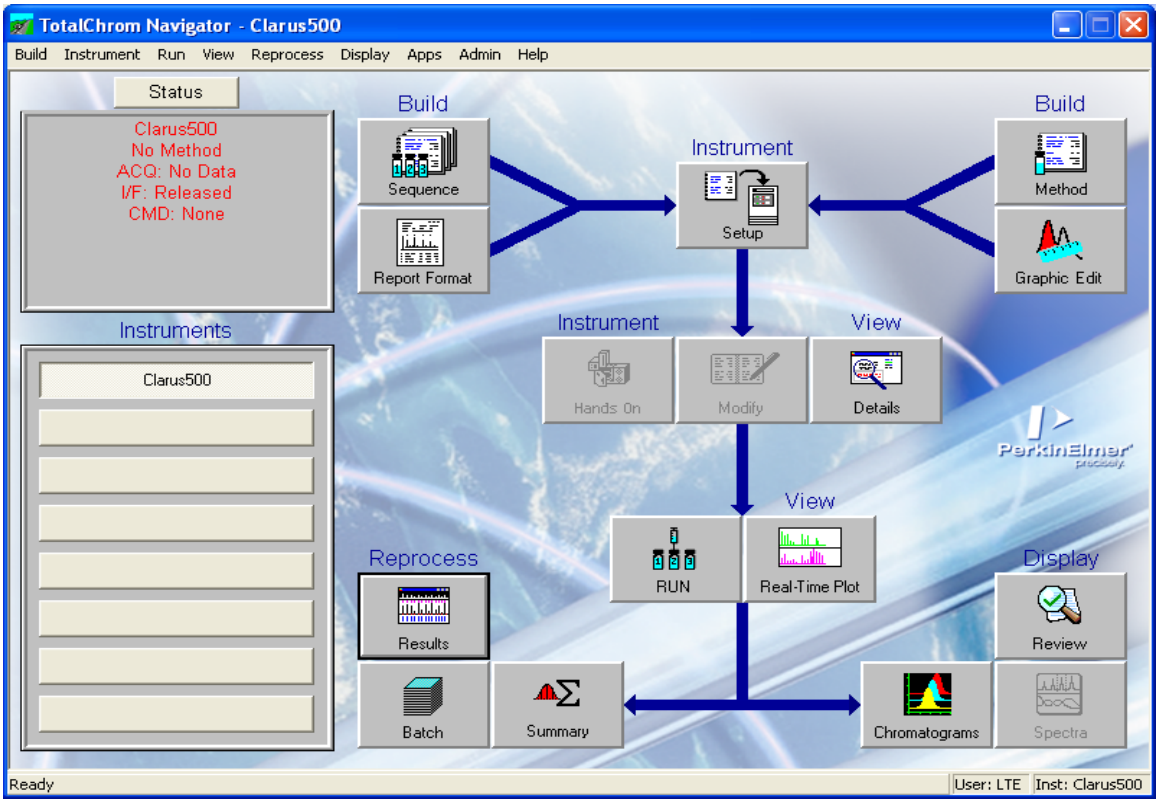

Figure 39. Chromatograph's software *TotalChrom Navigator* layout.

Due to the fact that gas chromatograph had a limit of test frequency, there occurred a need to solve the issue of intensive changes in gas composition during the first hour of the reaction. Data collected every *15* minutes was not representing properly the pattern of changes, which is why there were collected *1 ml* syringes every *2* minutes during reaction (*800-1000* ^{o}C) and afterwards their composition was analysed.

- **Gas Supply gases**

For heating up the reactor minimal nitrogen flow, for the coal char gasification *2 dm^3/min* carbon dioxide flow, for proper work of Gas Chromatograph minimal hydrogen, air and nitrogen flows are necessary. Those gases are supplied to the installation from the certified gas canisters.

As presented below in Figure 40, both gas inputs into the reactor and outputs to the Gas Chromatograph were controlled by proper scale manual flow meter, which guarantees the possibility of flow control at the expected level. The flow meters were checked before the tests with the reverse pipette method.

To protect from overheating the gas supplies valves, end flanges of ceramic tube reactor were cooled down by cold water flowing thru the rubber hose. Water flow was driven by electric water pomp.

- **Computer**

To control the Gas chromatograph, the in-side reactor temperatures and for mastering the raw chromatography results, a computer with adequate software is necessary. As mentioned above, *LabView* and *TotalChrom Navigator,* belonging to the university, were used.

All laboratory reactor scale installation set up, which were prepared and constructed by me, is presented in Figure 40 below.

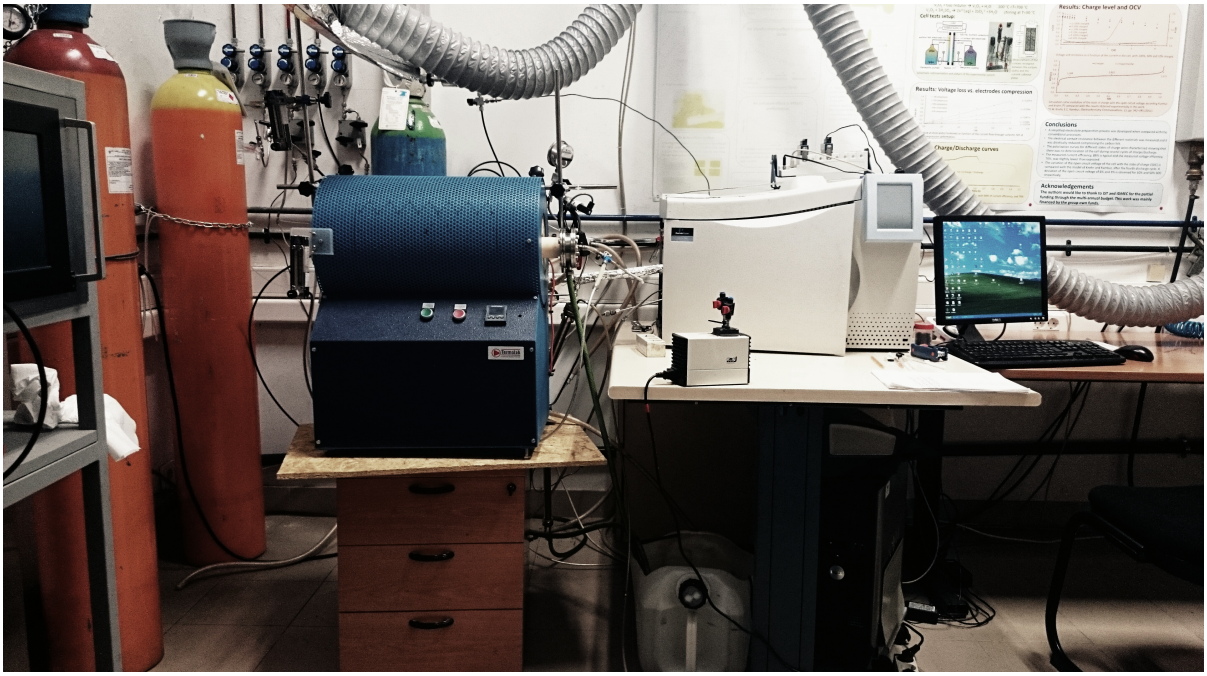

Figure 40. Real laboratory reactor scale process set up.

5. RESULTS AND DISCUSSION

5.1. THERMOGRAVIMETRIC RESULTS

Results obtained from thermogravimetric research, were exported into MS Excel files. It showed dependence of samples weight on time. After processing with respect of mass ratios and heating rates, following dependences on temperature were obtained: % of sample weight, Δ% of sample weight, sample conversion. Firstly coal char samples were tested to establish reference results for further investigation of catalyst addition effect. Results of coal char samples and its mixtures with increasing loading of artificial catalysts are presented below.

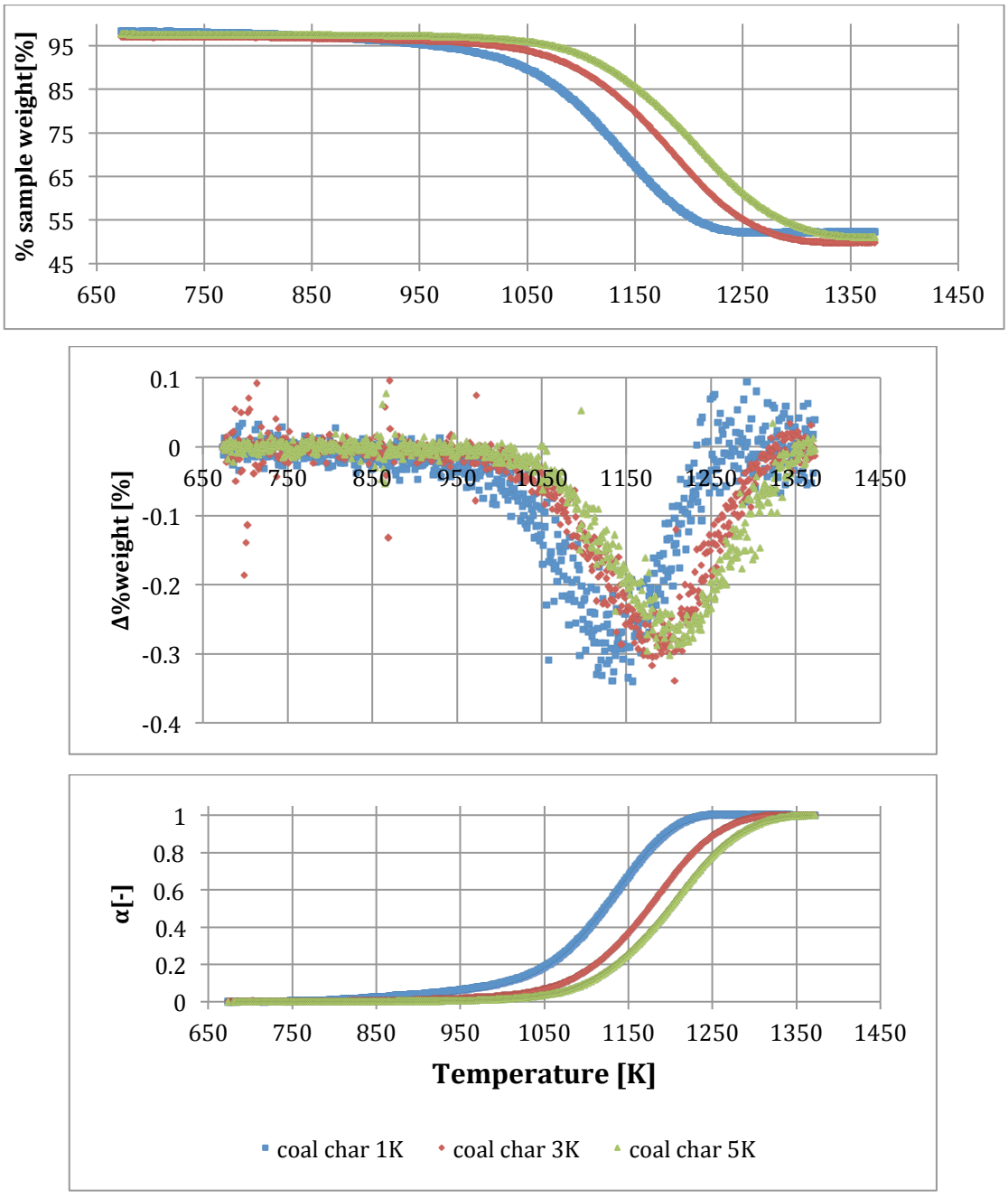

Figure 41. Coal char TG results: a) % sample weight, Δ %weight and conversion dependence on the temperature.

Judging from above Figure 41 main coal char gasification reaction took place in the temperature range from about *973 K* to *1273 K*. Labojko [61] research group found coal char gasification in the similar range from *1000 K* to *1273 K*. From the thermogravimetric results for all heating rates, it seems that fraction of coal char sample weight started to decrease significantly in temperatures higher then *1000K*. Likewise change of sample weight dependence on temperature increased and sample conversion increases as well. In Figure 41a it may be seen that for all tests, sample weight drops from *100%$_{wt}$* at the temperature *973 K* to *50-52%$_{wt}$* at *1273 K*. From Figure 41b it may be seen that the highest reaction rate is obtained at the temperature range from *1073 K* to about *1223 K* depending on the heating rate. Sample conversion presented in Figure 41c starts increasing in the temperature range from *873 K* for heating rate *1 K/min* to *750 K* for *5 K/min*. Final conversion *(>99%$_{wt}$*) is achieved at the temperature range from *1231 K* for heating rate *1 K/min* to *1334K* for *5K/min*.

As regards the introduced results: sample weight decrease in lower temperatures for reaction performed with lowest heating rate (*1 K/min*), then for middle heating rate (*3 K/min*) and in highest temperatures with highest heating rate. Accordingly for coal char gasification it may be said that lower heating rate enable higher reaction rate and higher conversion in lower temperatures. It was caused by the fact, that with lower heating rate sample was exposed on carbon dioxide for longer time, needed for the reaction. Because the reaction is endothermic and lowest heating rate provides a better heat rate transfer to the reaction region. Other research groups [61] confirmed this conclusion.

5.1.1. LIMESTONE CATALYST

Results of thermogravimetric test performed on mixtures of coal char with limestone catalyst loading (1,3,5%) were compared to the reference pure coal char results. As it may be concluded from Figure 42 sample weight started to decrease significantly at lower temperature was observed for lowest heating rate (1 K/min), then for middle heating rate (3 K/min) and in highest temperature sample weight started to decrease for highest heating rate (5 K/min). For example, coal char with artificial 1% of limestone catalyst samples weight in the temperature 1123K were 74,6041; 87,2528; 89,0604 for 1K/min, 3 K/min and 5 K/min heating rates respectively. All samples weights decreased to the range from 50% to 54% of residual weight, depending on the catalyst loading. Higher catalyst loading, higher residual weight was. Thermogravimetric results showed catalytic effect of limestone addition.

As it may be seen in Figure 42 and in Table 9, with increasing catalyst loading the conversion of tested char samples is larger for higher catalyst load. Some deviations in presented data can be noticed at highest temperature applied. However comparison with pure coal char conversion shows that generally the catalytic effect is very small. Smaller values of the yield of solid residue can be attributed lower content of mineral components. Those results were compared for reaction conducted at *3 K/min* heating rate.

Table 9. % of sample weight for different limestone catalyst addition vs the temperature.

T [K]	% sample weight			
	coal char	1%$_{wt}$ limestone	3%$_{wt}$ limestone	5%$_{wt}$ limestone
1023	94,97887	96,21844	95,13057	94,62296
1073	92,25735	93,68866	92,46682	91,79259
1123	85,49191	87,25281	85,87547	84,86882
1173	73,79691	75,82863	74,54957	73,07571
1223	60,33299	62,50726	61,53216	60,0706
1273	52,30441	51,96249	53,80364	52,59563
1323	49,94436	51,96249	51,51387	50,6309

From Figure 43 it may be seen that biggest change of sample weight occurred at the temperature range from *1073 K* to *1273 K*. Bigger changes of sample weight per Kelvin in lower temperatures were obtained with lower heating rate. As well, reaction rates were promoted in lower temperatures for *3, 5, 1%$_{wt}$* of limestone catalyst loading respectively. Maximum rate was obtained for sample with *3%$_{wt}$* limestone addition at *1095 K*. Sample conversion started to increase from *900 K* to final conversion in the temperature range from *1200 K* to *1300 K*. With usage of *B-spline* interpolation [62], temperatures for each of constant conversion were established. Results are presented in below Table 10.

Table 10. Process temperature vs. samples conversion.

x	coal char			coal char + CaCO3								
				1% add			3% add			5% add		
	1K/min	3K/min	5K/min	1K/min	3K/min	5K/min	1K/min	3K/min	5K/min	1K/min	3K/min	5K/min
0,05	922,783	1031,49	1067,433	925,0335	1043,992	1008,216	903,4389	1032,214	1059,436	926,1701	1029,251	1057,51
0,1	997,7328	1072,091	1100,278	998,2394	1078,89	1072,58	987,5185	1072,21	1097,538	1001,312	1069,715	1095,404
0,15	1032,587	1094,209	1119,898	1033,809	1099,365	1100,968	1027,58	1094,36	1117,767	1035,535	1091,947	1115,148
0,2	1055,715	1110,52	1135,508	1055,521	1115,081	1120,191	1051,584	1110,603	1133,81	1056,377	1107,981	1131,028
0,25	1070,196	1124,073	1148,512	1072,282	1127,981	1135,631	1068,661	1124,135	1147,387	1070,689	1121,489	1144,242
0,3	1083,065	1136,163	1160,203	1084,968	1139,333	1148,934	1082,016	1135,988	1159,268	1083,25	1133,061	1157,337
0,35	1094,585	1146,627	1170,653	1096,311	1149,724	1160,829	1094,407	1146,599	1170,111	1094,698	1143,331	1167,31
0,4	1104,013	1156,416	1180,68	1106,302	1159,19	1171,569	1104,16	1156,184	1180,057	1104,115	1153,212	1177,203
0,45	1113,08	1165,45	1190,001	1115,648	1168,17	1181,48	1113,416	1165,519	1189,379	1113,139	1162,041	1186,579
0,5	1121,429	1174,225	1198,985	1124,309	1176,487	1190,784	1122,491	1174,226	1198,242	1121,636	1170,585	1195,481
0,55	1129,947	1182,517	1207,535	1132,645	1184,9	1199,702	1130,935	1182,595	1206,889	1130,016	1179,163	1204,197
0,6	1138,008	1190,889	1216,098	1141,217	1193,218	1208,513	1139,295	1191,013	1215,45	1138,146	1187,559	1212,703
0,65	1146,094	1199,413	1224,787	1149,349	1201,334	1217,287	1147,429	1199,466	1224,075	1146,242	1195,804	1221,56
0,7	1154,398	1208,311	1233,841	1157,714	1210,032	1226,401	1156,253	1208,321	1233,179	1154,727	1204,605	1230,588
0,75	1163,126	1217,233	1243,517	1166,665	1219,201	1236,054	1164,984	1217,344	1242,94	1163,729	1213,928	1240,383
0,8	1172,125	1227,402	1254,256	1176,411	1229,28	1246,917	1174,473	1227,691	1253,936	1172,977	1224,264	1251,015
0,85	1182,635	1239,283	1266,632	1187,292	1240,716	1259,193	1184,788	1239,772	1266,476	1183,758	1235,851	1263,89
0,9	1194,3	1253,971	1281,887	1199,459	1254,48	1274,71	1197,41	1254,725	1282,358	1196,39	1250,515	1279,403
0,95	1209,726	1273,453	1302,739	1212,714	1273,621	1294,987	1212,404	1275,006	1303,826	1209,939	1269,591	1300,937

As it may be seen in above Table 10 and Figure 45 sample conversion increases firstly for lowest heating rate (*1 K/min*) then for *3 K/min* and *5 K/min*. Highest conversion of constant steps occurs in lowest temperatures for *3%$_{wt}$* addition of artificial limestone to the coal char sample, then for *5%$_{wt}$* addition and in highest temperatures for *1%$_{wt}$* addition. Furthermore, addition of *3%$_{wt}$* of limestone seems to have catalytic effect on coal char gasification. It may be seen that for all heating rates limestone catalyse reaction in the first stage, up to *0.4* sample conversion. Exemplary for reactions performed with lowest - 1K/min heating rate constant conversions: *0.1; 0,2; 0,3; 0,35*; occurred in following temperatures: *997.7328K* and *987.5185K*; *1055.715K* and *1051.584K*; *1083.065K* and *1082.016K*; *1094.585K* and *1094.407K* for coal char and coal char with *3%$_{wt}$* artificial limestone addition samples respectively.

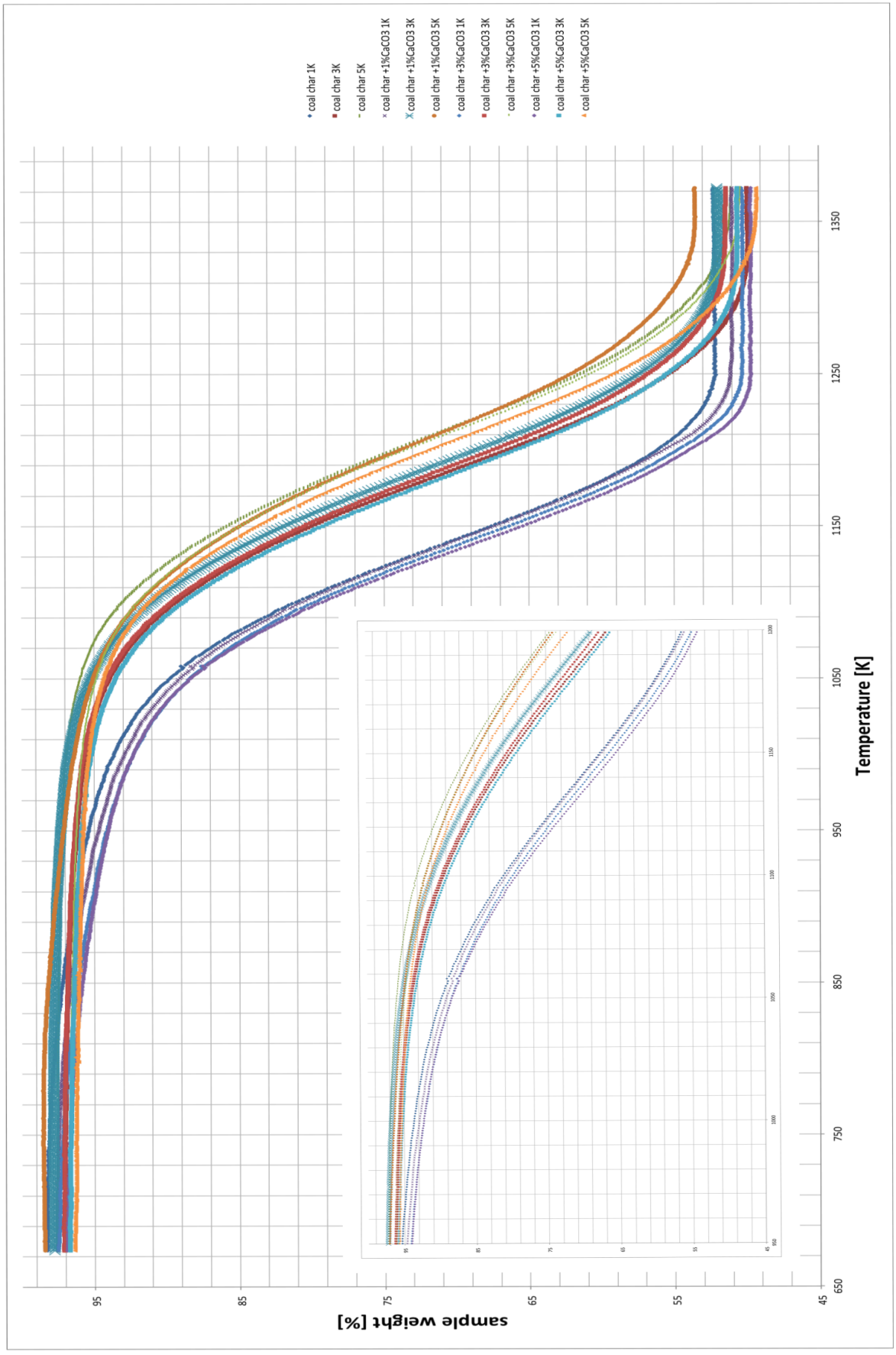

Figure 42. Coal char with limestone TG results - sample weight vs the temperature.

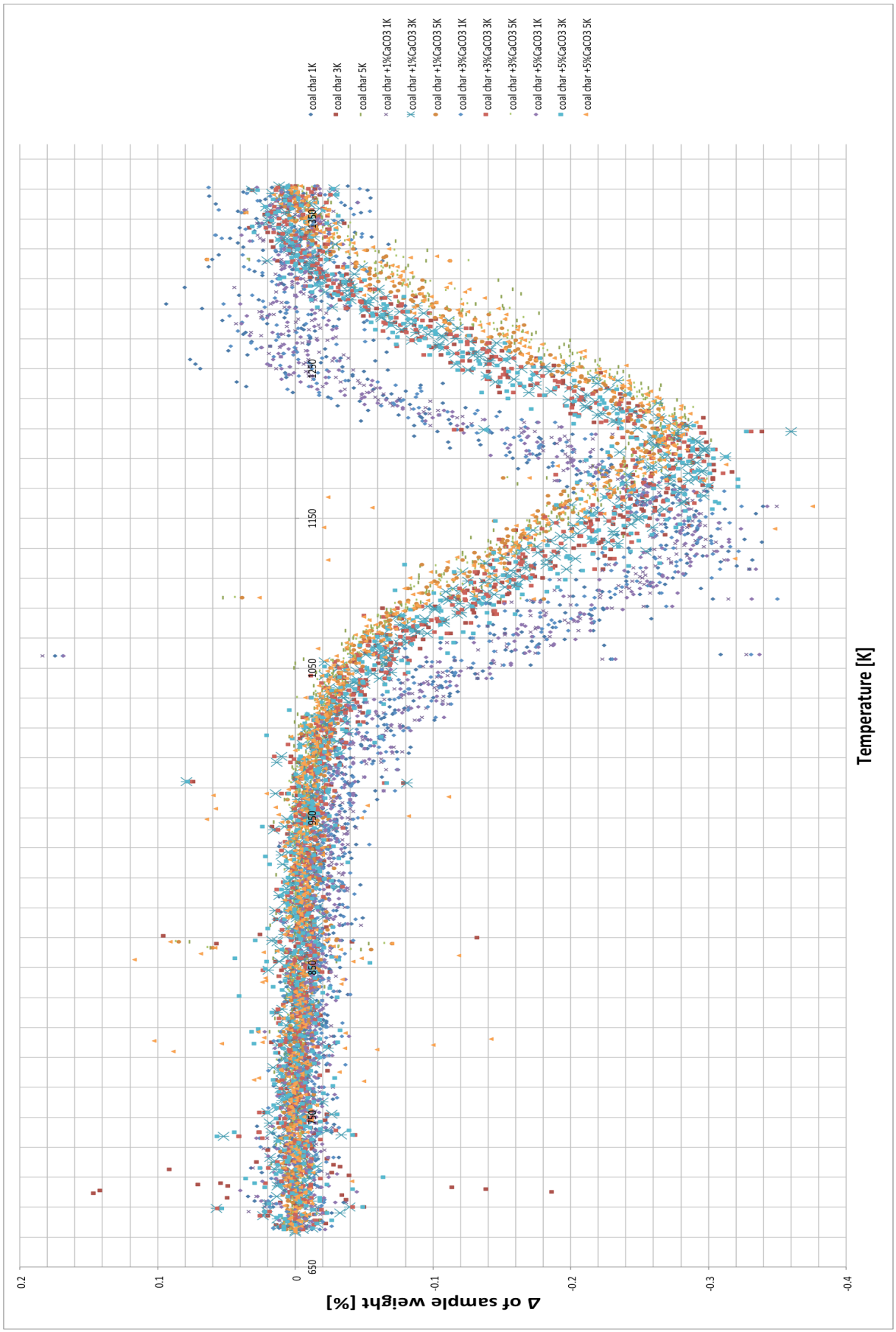

Figure 43. Coal char with limestone TG results – Δ %weight dependence on the temperature.

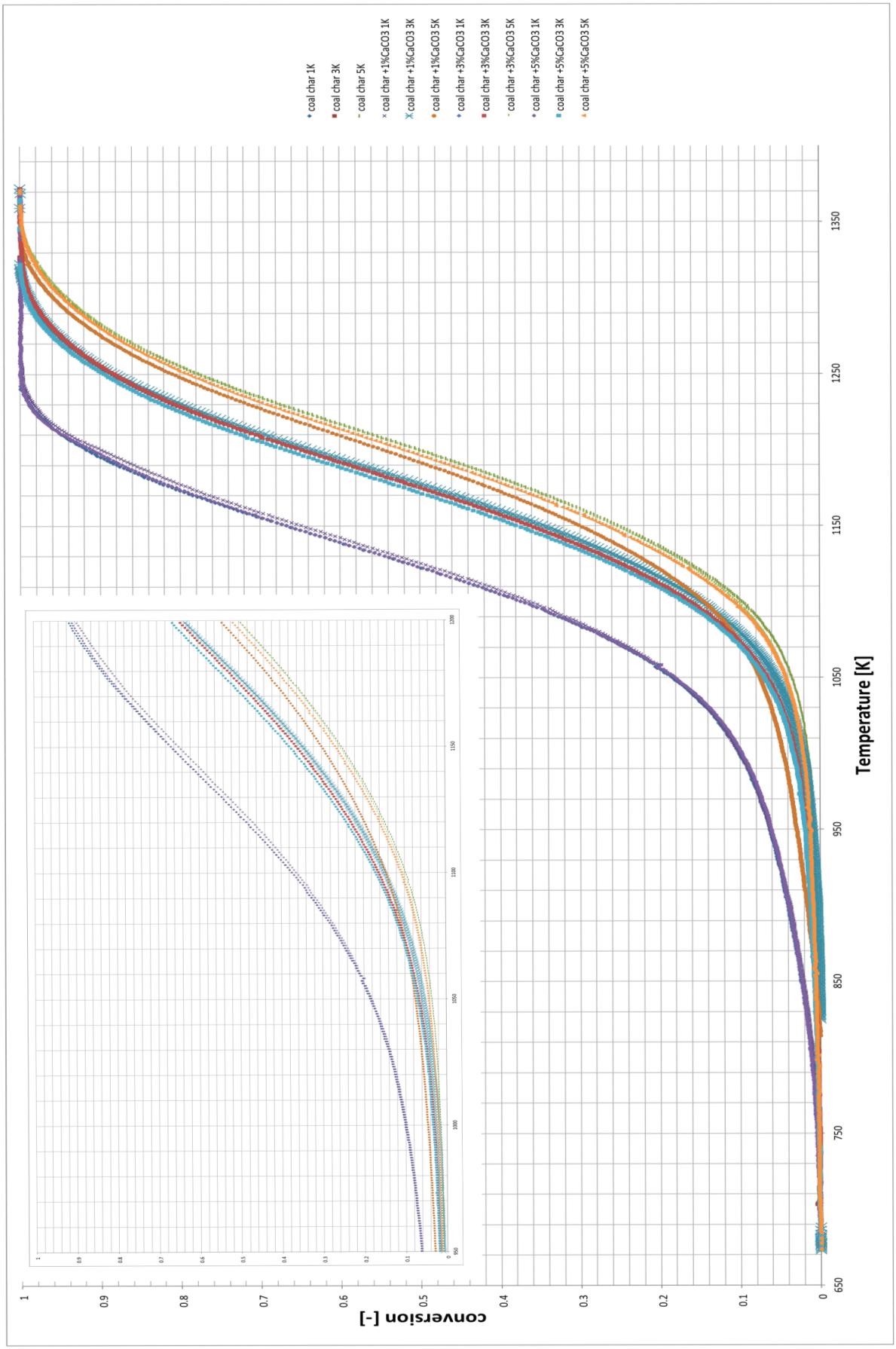

Figure 44. Coal char with limestone catalyst TG results conversion vs the temperature.

5.1.2. IRON (III) OXIDE CATALYST

Results of thermogravimetric test performed on mixtures of coal char with artificial iron (III) oxide catalyst loading (*1,3,5%$_{wt}$*) were compared to the reference pure coal char results. As it may be concluded from Figure 45 highest decrease of sample weight in lower temperature was observed for lowest heating rate (*1 K/min*), then for middle heating rate (*3 K/min*) and in highest temperature sample weight started to decrease for highest heating rate (*5K/min*). For example, coal char with artificial *1%$_{wt}$* of Fe_2O_3 catalyst samples weight in the temperature *1123 K* were: *73.5937; 85.9297; 87.5171* for *1 K/min, 3 K/min and 5 K/min* heating rates respectively. Similarly to the samples with limestone catalyst, all samples weights decreased to the range from *50%$_{wt}$* to *54%$_{wt}$* of residual weight, depending on the catalyst loading. Higher catalyst loading, higher residual weight was. Thermogravimetric results showed catalytic effect of iron (III) oxide addition in a limited range.

Table 11. % of sample weight for different Fe_2O_3 catalyst addition vs the temperature.

T [K]	% sample weight			
	coal char	1% Fe2O3	3% Fe2O3	5% Fe2O3
1023	94,97887	95,14127	94,68256	94,80092
1073	92,25735	92,45334	92,03392	92,05889
1123	85,49191	85,74615	85,44959	85,24096
1173	73,79691	74,17271	73,95123	73,69243
1223	60,33299	60,78464	60,83059	60,71585
1273	52,30441	52,77446	52,93538	53,42189
1323	49,94436	50,44602	50,7798	51,57891

As it may be seen in below Figure 45 and above Table 11, with increasing catalyst loading % of sample weight obtained in the reaction temperature were lower. However iron (III) oxide addition showed catalytic effect in the limited range of temperatures. For an addition of *1%$_{wt}$* of Fe_2O_3 sample weight was lower then coal char sample weights only in the temperature of *1023 K*. For *3%$_{wt}$* Fe_2O_3 addition samples with catalyst weights were lower range up to *1123 K*. Finally addition of *5%$_{wt}$* of Fe_2O_3, catalysed and lowered down samples weight in the biggest range - up to *1173 K*. The difference of sample weights was bigger in lower temperatures. Those results were compared for reaction for *3 K/min* heating rate.

From Figure 46 it may be seen that biggest change of sample weight occurred at the temperature range from *1073 K* to *1273 K*. Bigger changes of sample weight per Kelvin in lower temperatures were obtained with lower heating rate. As well, reaction rates were promoted in lower temperatures for *3, 5, 1%$_{wt}$* of Fe_2O_3 catalyst loading respectively. Maximum rate was obtained for sample with *3%$_{wt}$* Fe_2O_3 addition at *1157 K*. Sample conversion started to increase from 900K to final conversion in the temperature range from *1200 K* to *1300 K*. With usage of same as in limestone TG results, *B-spline* interpolation [62], temperatures for each of constant conversion were established. Results are presented in below Table 12.

Table 12. Dependence of process temperature on coal char and coal char with Fe_2O_3 catalyst samples conversion.

x	coal char			coal char + Fe2O3								
				1% add			3% add			5% add		
	1K/min	3K/min	5K/min	1K/min	3K/min	5K/min	1K/min	3K/min	5K/min	1K/min	3K/min	5K/min
0,05	922,783	1031,49	1067,433	913,1099	1031,935	950,74	909,8013	1026,16	1041,979	921,8804	1025,883	1055,747
0,1	997,7328	1072,091	1100,278	994,3905	1072,332	1048,642	991,445	1069,994	1090,052	996,2	1068,072	1093,609
0,15	1032,587	1094,209	1119,898	1031,332	1094,627	1089,233	1030,552	1093,125	1113,145	1031,098	1091,067	1114,702
0,2	1055,715	1110,52	1135,508	1053,338	1110,523	1112,48	1053,123	1109,774	1130,02	1052,49	1107,382	1130,647
0,25	1070,196	1124,073	1148,512	1069,776	1124,17	1130,343	1069,162	1123,598	1144,01	1068,44	1120,833	1144,069
0,3	1083,065	1136,163	1160,203	1083,059	1136,132	1145,052	1082,72	1135,42	1156,573	1081,768	1132,673	1155,967
0,35	1094,585	1146,627	1170,653	1094,855	1148,29	1158,228	1094,471	1145,698	1167,762	1093,34	1143,214	1166,787
0,4	1104,013	1156,416	1180,68	1104,748	1156,453	1169,852	1104,445	1155,497	1178,012	1103,463	1153,118	1176,811
0,45	1113,08	1165,45	1190,001	1114,19	1165,549	1180,411	1113,531	1164,749	1187,717	1112,369	1162,006	1186,106
0,5	1121,429	1174,225	1198,985	1122,733	1174,269	1190,713	1122,306	1173,59	1196,847	1121,237	1170,544	1194,981
0,55	1129,947	1182,517	1207,535	1131,161	1182,656	1199,883	1130,622	1181,937	1205,788	1129,502	1179,098	1203,621
0,6	1138,008	1190,889	1216,098	1138,699	1190,921	1209,148	1138,784	1190,337	1214,606	1137,725	1187,182	1212,171
0,65	1146,094	1199,413	1224,787	1147,221	1199,417	1218,309	1147,109	1198,838	1223,385	1145,687	1195,456	1220,793
0,7	1154,398	1208,311	1233,841	1155,97	1208,042	1227,758	1155,405	1206,944	1232,647	1153,933	1204,169	1229,766
0,75	1163,126	1217,233	1243,517	1164,326	1217,141	1237,754	1164,144	1216,642	1242,424	1162,578	1213,128	1239,359
0,8	1172,125	1227,402	1254,256	1173,337	1227,306	1248,787	1173,263	1226,688	1253,302	1171,42	1223,1	1250,193
0,85	1182,635	1239,283	1266,632	1183,729	1238,961	1261,27	1183,458	1238,223	1265,624	1181,893	1234,47	1262,293
0,9	1194,3	1253,971	1281,887	1196,254	1253,252	1276,631	1195,428	1252,552	1280,928	1193,448	1248,499	1276,967
0,95	1209,726	1273,453	1302,739	1212,482	1272,516	1297,952	1212,005	1271,122	1301,541	1209,423	1267,28	1297,43

As it may be seen in above Table 12 and below Figure 47 sample conversion increases firstly for lowest heating rate (*1K/min*) then for *3 K/min* and *5 K/min*. Highest conversion of constant steps occurs in lowest temperatures for *3%$_{wt}$* addition of artificial Fe_2O_3 to the coal char sample, then for *5%$_{wt}$* addition and in highest temperatures for *1%$_{wt}$* addition. Furthermore, addition of *3%$_{wt}$* and *5%$_{wt}$* addition of Fe_2O_3 seems to have catalytic effect on coal char gasification. It may be seen that for all heating rates Fe_2O_3 catalyse reaction in the first stage, up to *0.4* sample conversion. Exemplary for reactions performed with lowest - *1K/min* heating rate constant conversions: *0.1; 0,2; 0,3; 0,35;* occurred in following temperatures: *997.7328 K, 991.445 K,* and *996.200 K; 1032.587 K, 1030.552 K*, and *1031.098 K; 1055.715 K, 1053.123 K,* and *1052.490 K; 1070.196 K, 1069.162 K, 1068.440 K; 1083.065 K, 1082.720 K,* and *1081.768 K; 1094.585 K, 1094.471 K,* and *1093.34 K* for coal char, coal char with *3%$_{wt}$* , coal char with *5%$_{wt}$* of artificial limestone addition samples respectively.

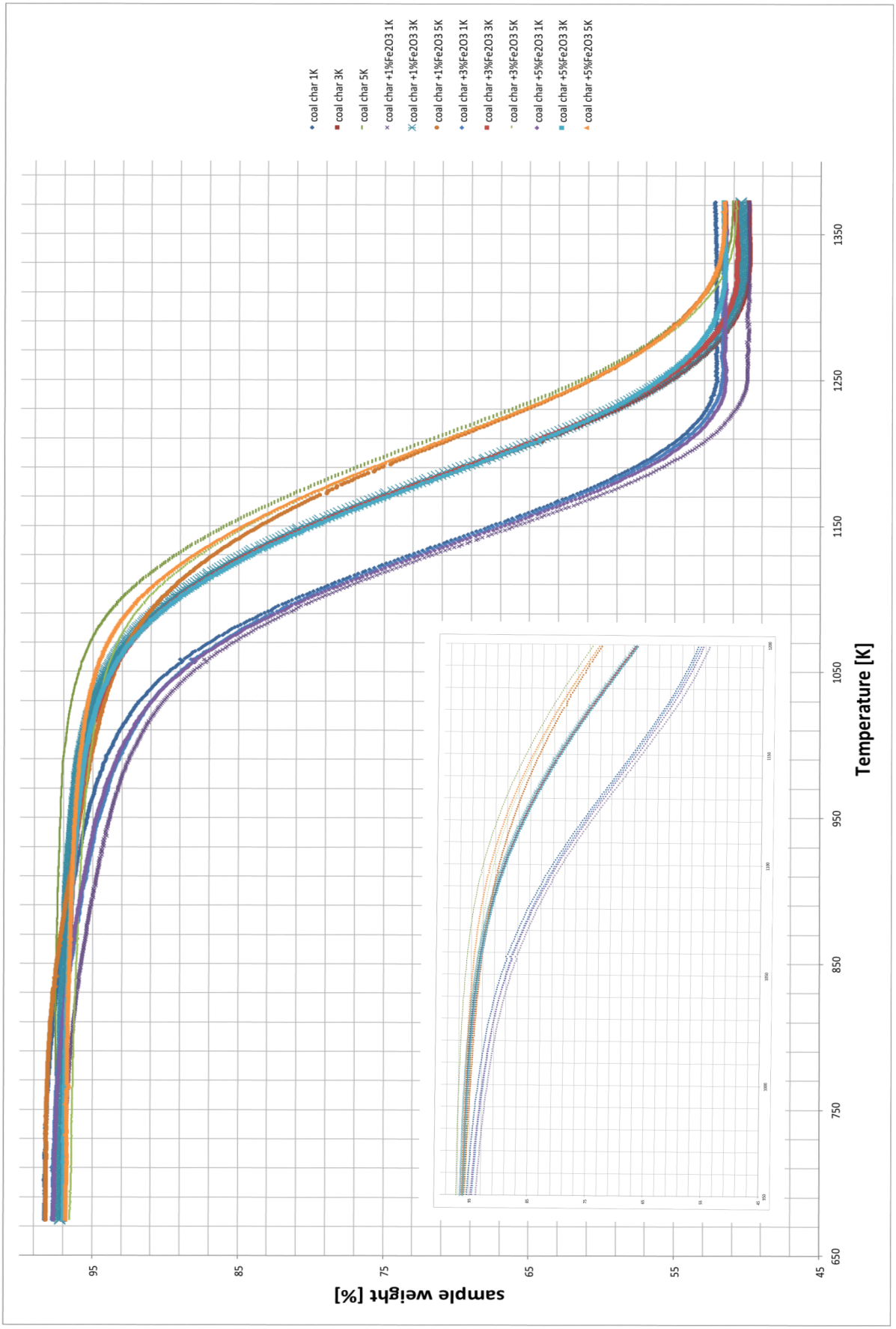

Figure 45. Coal char with Fe_2O_3 catalyst TG results % sample weight vs the temperature.

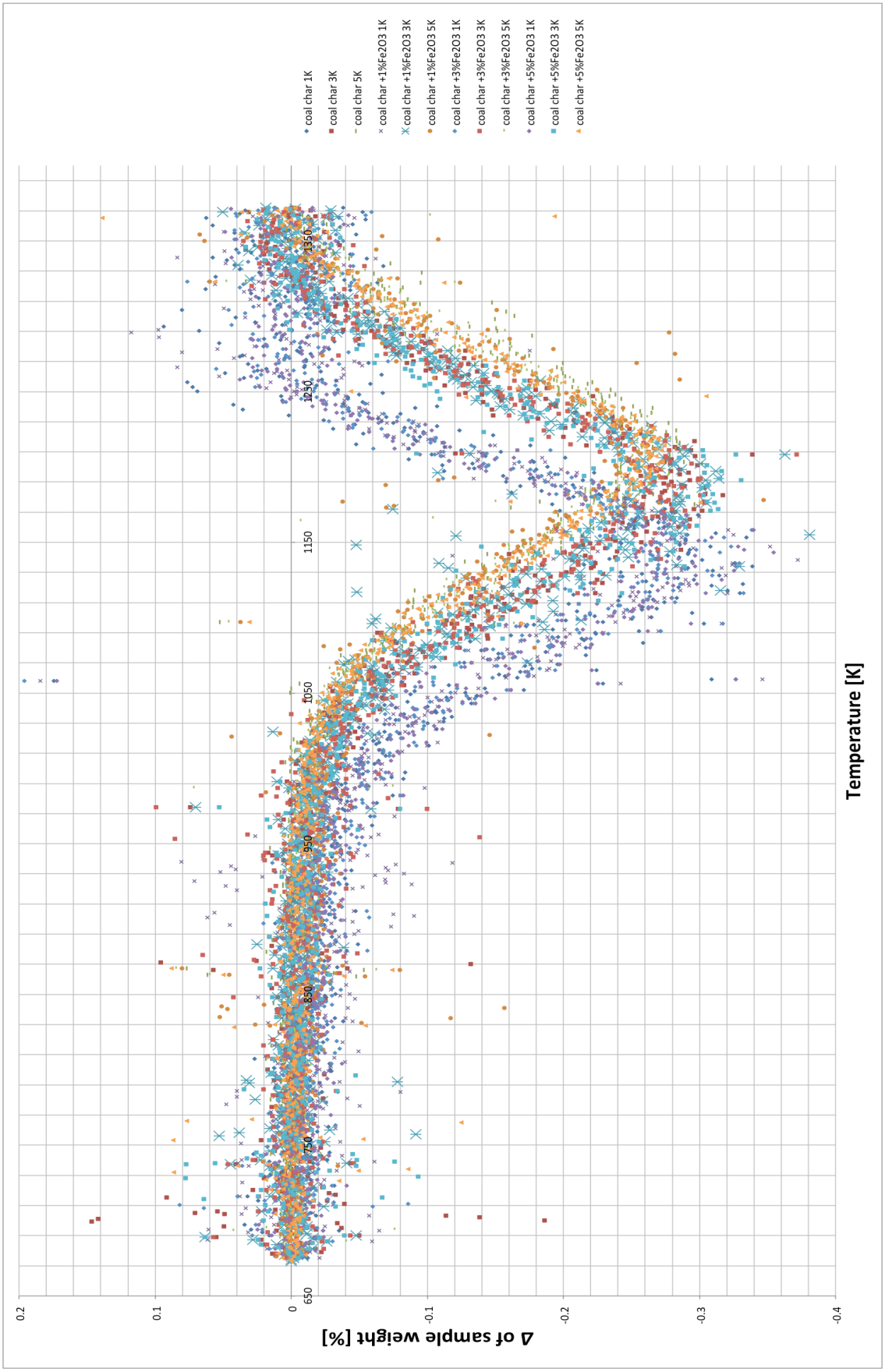

Figure 46. Coal char with Fe_2O_3 catalyst TG results Δ %weight vs the temperature.

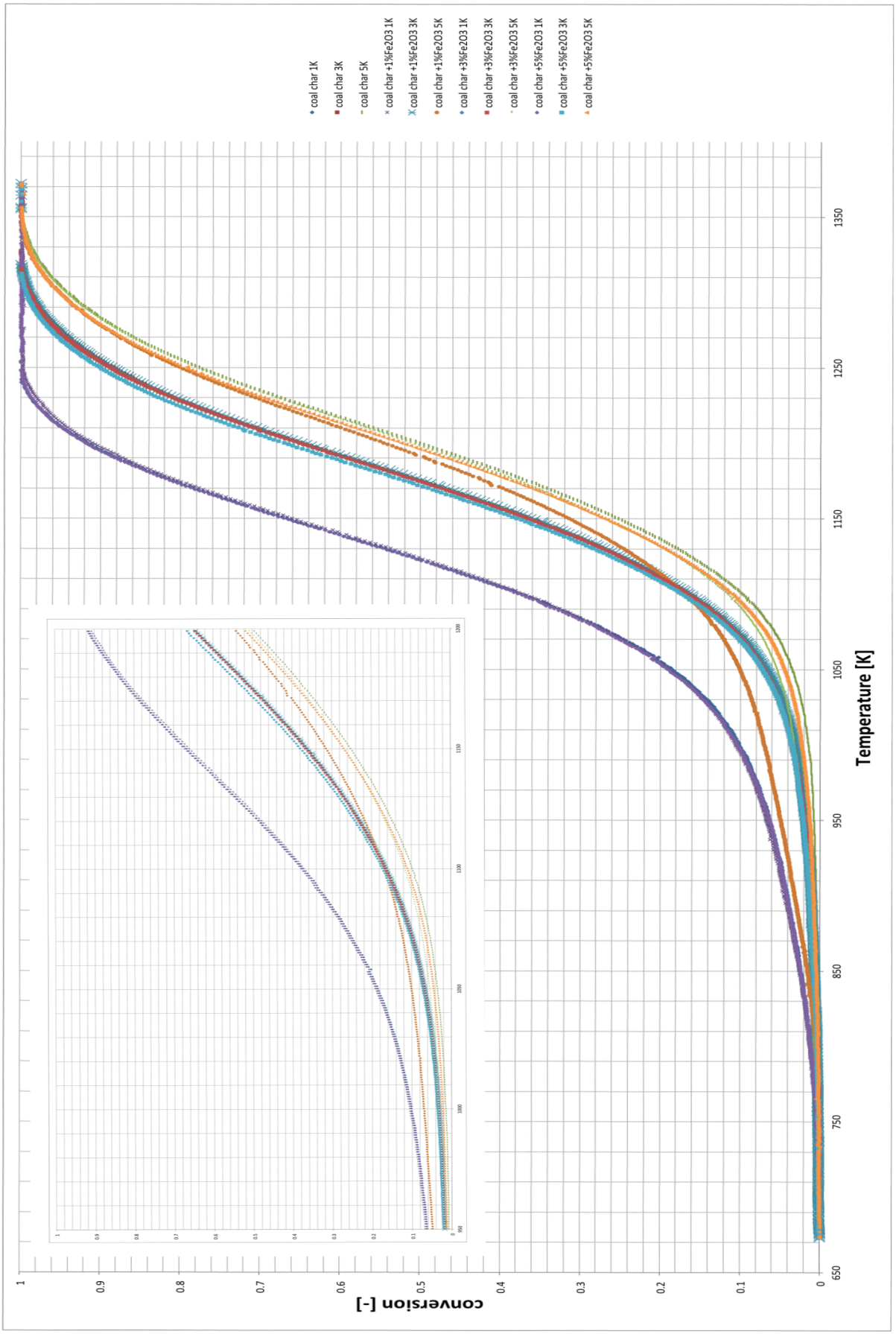

Figure 47. Coal char with Fe_2O_3 catalyst TG results conversion vs. the temperature.

5.2. KINETIC MODELS RESULTS

In order to calculate the kinetic parameters of coal char gasification, three previously described models were applied, namely: Integral Flynn-Wall-Ozawa model, maximum rate Kissinger-Akahira-Sunose model and differential Friedman model. Isoconversional models consider the activation energy to be constant, therefore discretization of fixed values of conversion for which the calculation are made. For each curve for plot of conversion dependence on the temperature, *5%* steps of conversion were calculated. Interpolated temperatures were presented before in Table 10 and Table 12, for coal char and coal char with artificial catalysts.

Series of calculations of the activation energy and pre-exponential factors using isoconversional models is as it may be seen in Figure 48, below.

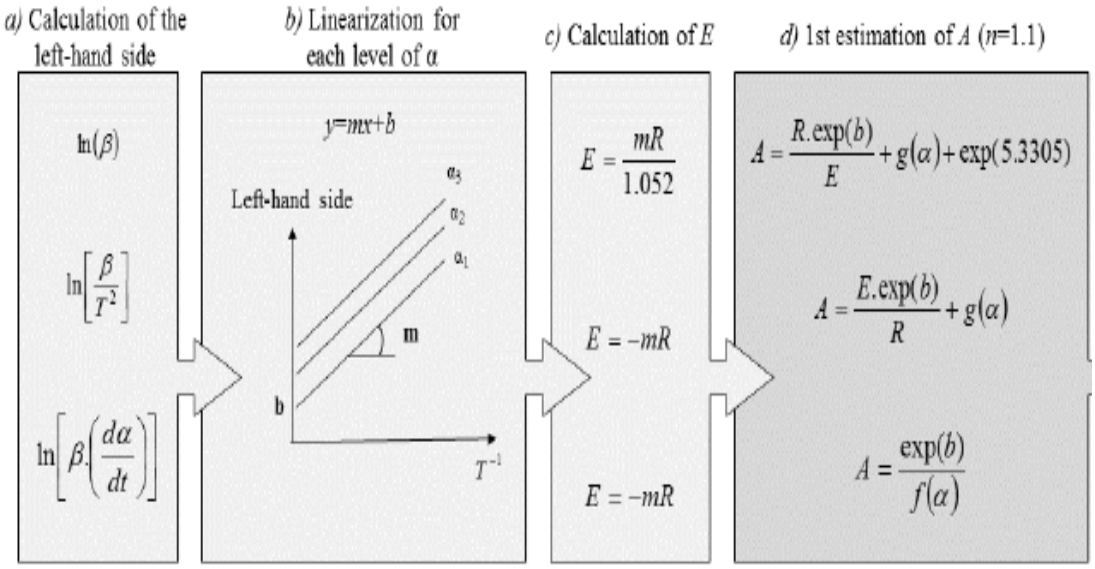

Figure 48. Flowchart for calculating the activation energy and pre-exponential factor using isoconversional models [64].

Each model is based on assuming contracting volume (*R3*) fitting model [9]. In this paper following one was used:

$$g(x) = 3\left[1 - (1-x)^{\frac{1}{3}}\right] \qquad (40)$$

$$I(E_a, T) = \int_{T_0}^{T} exp\left(\frac{-E_a}{R*T}\right) dT \qquad (41)$$

For the kinetic parameters to be estimated firstly calculations of the left-hand side with the respect of used model must be performed (step a). Secondly linearization for each level of conversion takes place (step b). Slope of line determined by plotting appropriate function with temperature at any degree of conversion. Plots differs for each method, they are listed in following Table 13 [65].

Table 13. Kinetic methods used in calculating activation energy.

Method	Final Equation	Plots
O-F-W	$\log(g(\alpha)) = \log(\frac{AE}{R}) - \log(\beta) - 2.315 - 0.4567\frac{E}{RT}$	log β against 1/T
Kissinger	$\frac{d(\ln(\beta/T_m^2))}{d(1/T_m)} = -\frac{E}{R}$	$\ln(\beta/T_m^2)$ against $1/T_m$
Friedman	$\ln(\frac{d\alpha}{dt}) = \ln(\beta(\frac{d\alpha}{dT})) = \ln A + n\ln(1-\alpha) - \frac{E}{RT}$	ln(β(dα/dT)) against 1/T

Exemplary plots, obtained for data from thermogravimetric coal char gasification at 3 different heating rates (*1,3,5 K/min*) presented below in Figures 49,50,51. From linear parameters activation energy can be established (*step c*). Further step (*step d*) is related to the optimization of the pre-exponential factor.

All plotting and final calculations were performed in *MathCAD* and *MS Excel* software. Results of activation energy and pre-exponential factor calculations for each sample are attached in a form of electronic file and exemplary ones are presented below on Figures 49-51.

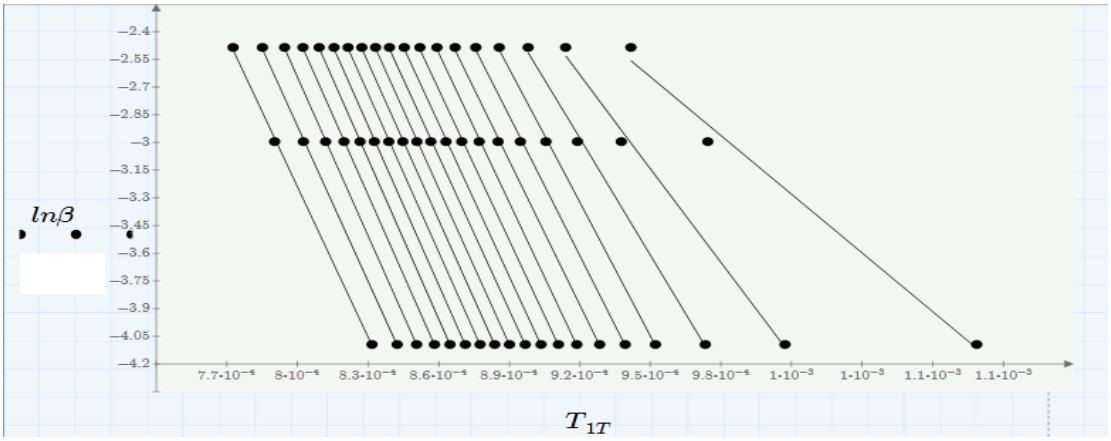

Figure 49. Iso-conversion plot of FWO method for coal char at varying degree of conversions.

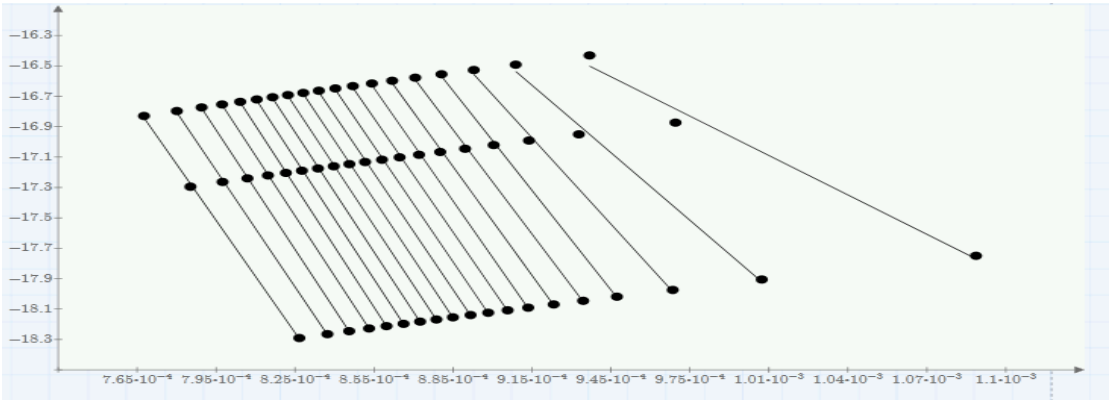

Figure 50. Iso-conversion plot of KAS method for coal char at varying degree of conversions.

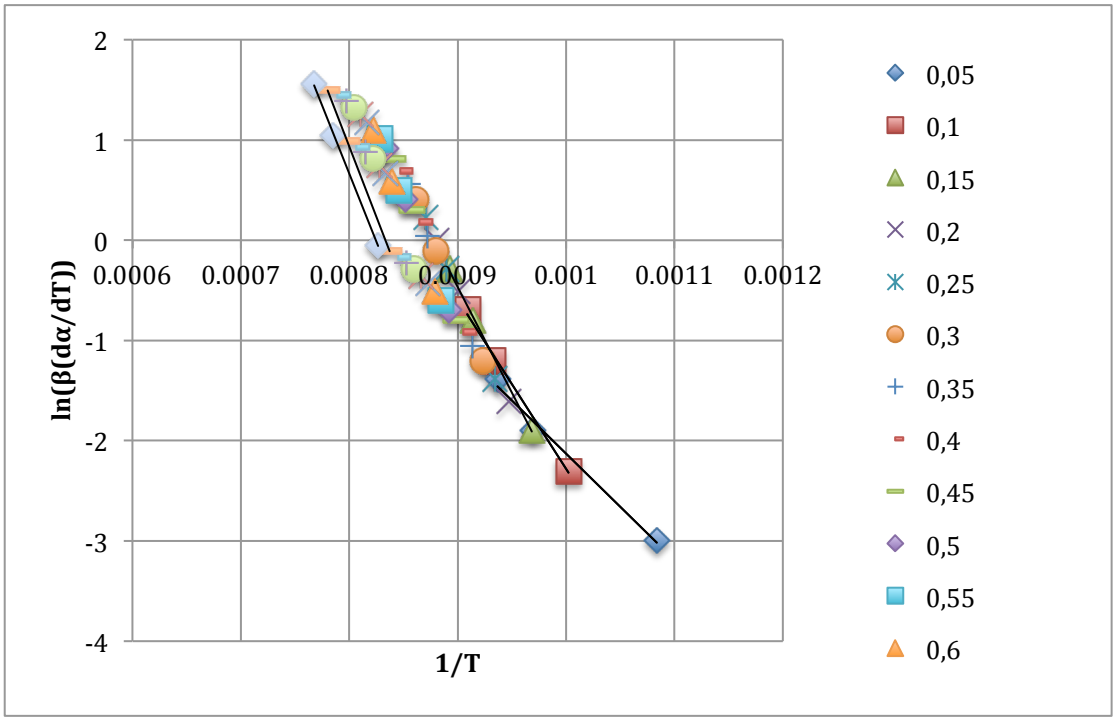

Figure 51. Iso-conversion plot of Friedman method for coal char at varying degree of conversions.

5.2.1. LIMESTONE CATALYST

As it may be seen on following Figures 52-54, the activation energy calculated using all models was in similar range. It is approximately *230-250 kJ/mol* for conversion values greater than *0.2* and pre-exponential factor *logA* are approximately *7-8* s^{-1} for FWO and KAS models and *10-12* s^{-1} for Friedman method. Those results are comparable with one obtained by other research group investigating coal char gasification [61], who calculated the activation energy *(245 kJ/mol)* and pre-exponential factor (7.41 s^{-1}) using the F1 method. Comparing to the parent coal gasification tests performed by [66], char gasification reveals a significantly higher value. It can be justified by the passivation of the char surface.

The activation energy and pre-exponential factor increase significantly for all samples in the conversion range from the beginning of the gasification to the conversion *0.4*. Then, it stabilizes and obtains above-mentioned value for the rest course of the reaction. The catalyst effect of limestone addition was observed only for *3%*$_{wt}$ limestone loading, but only in the first stage of the gasification up to *0.4* conversions. The activation energy in this range of conversion is approximately *10 kJ/mol* lower with limestone catalyst. *1%*$_{wt}$ and *5%*$_{wt}$ $CaCO_3$ loading do not only showed lack of the catalytic effect but as well inhibited coal char gasification.

Thus the small or even lack of catalytic effect of limestone addition was probably due to a relatively large limestone sample size, which resulted in transport limitations. R.C. Rimpe and R.E. Sears

concluded in their paper [67] that calcium inherent to the coal does not necessary provokes any additives.

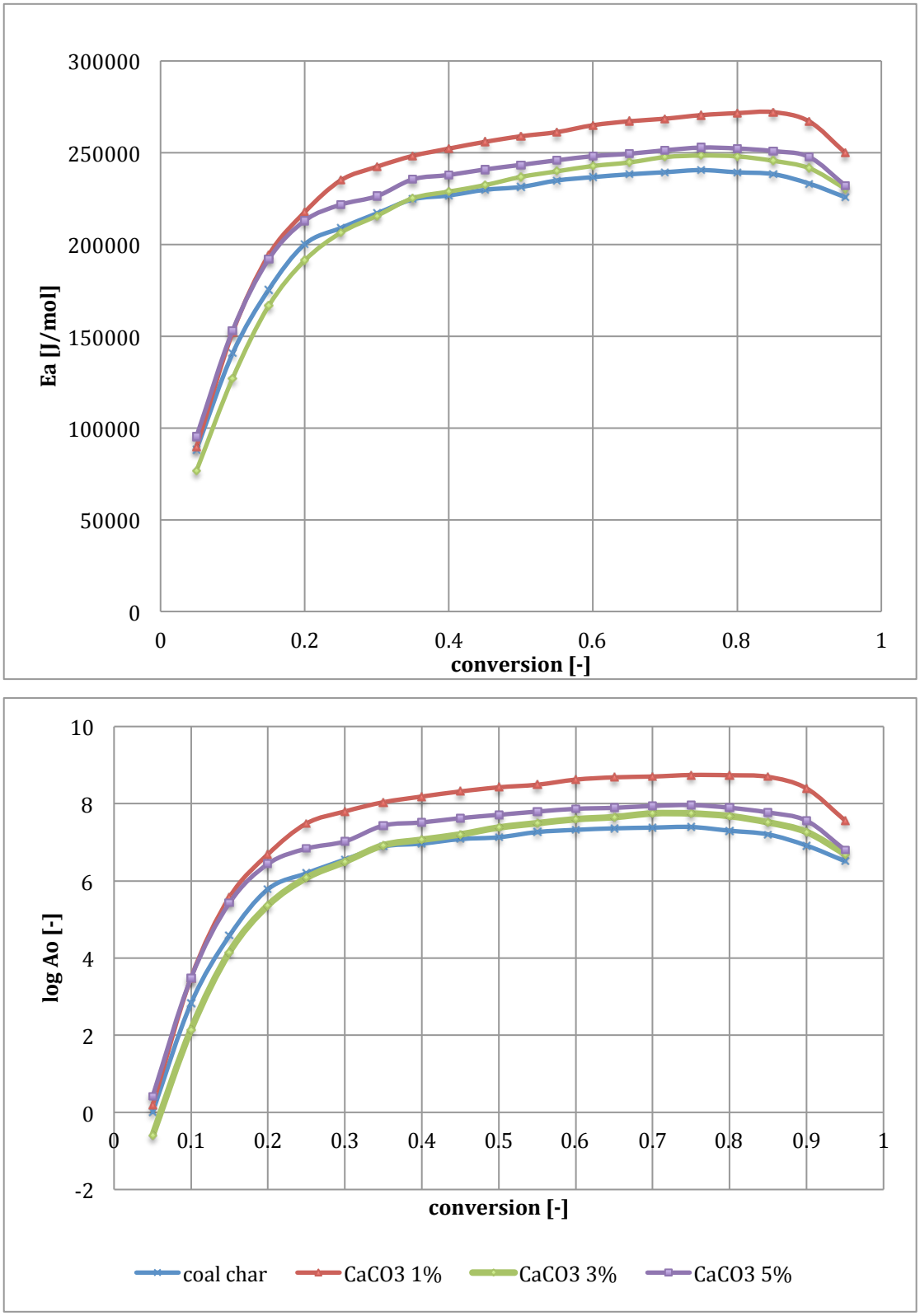

Figure 52. Coal char with limestone catalyst gasification Flynn Wall Ozawa modelling results: activation energy and pre-exponential factor.

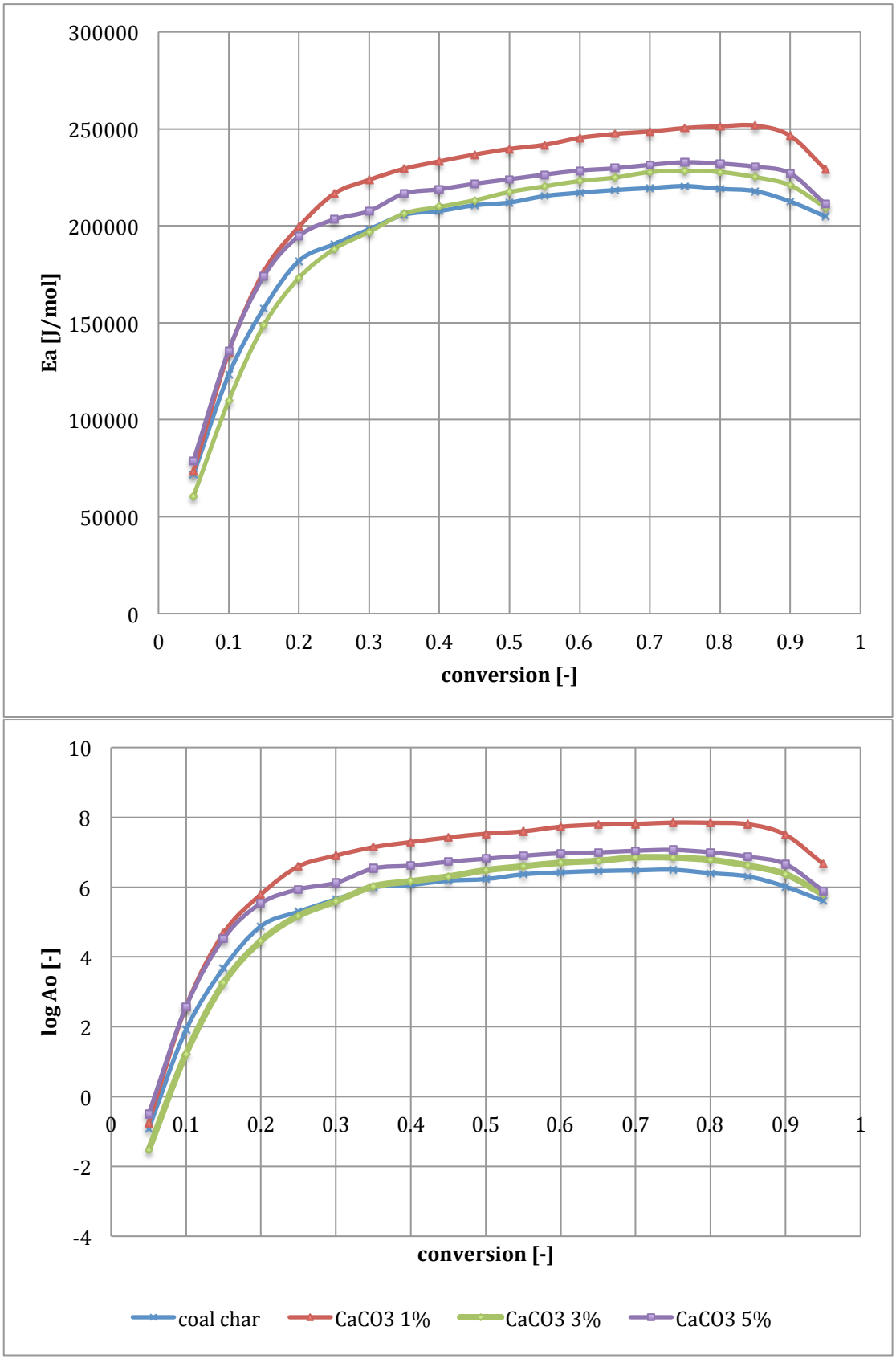

Figure 53. Coal char with limestone catalyst gasification Kissinger-Akahira-Sunose modelling results: activation energy and pre-exponential factor.

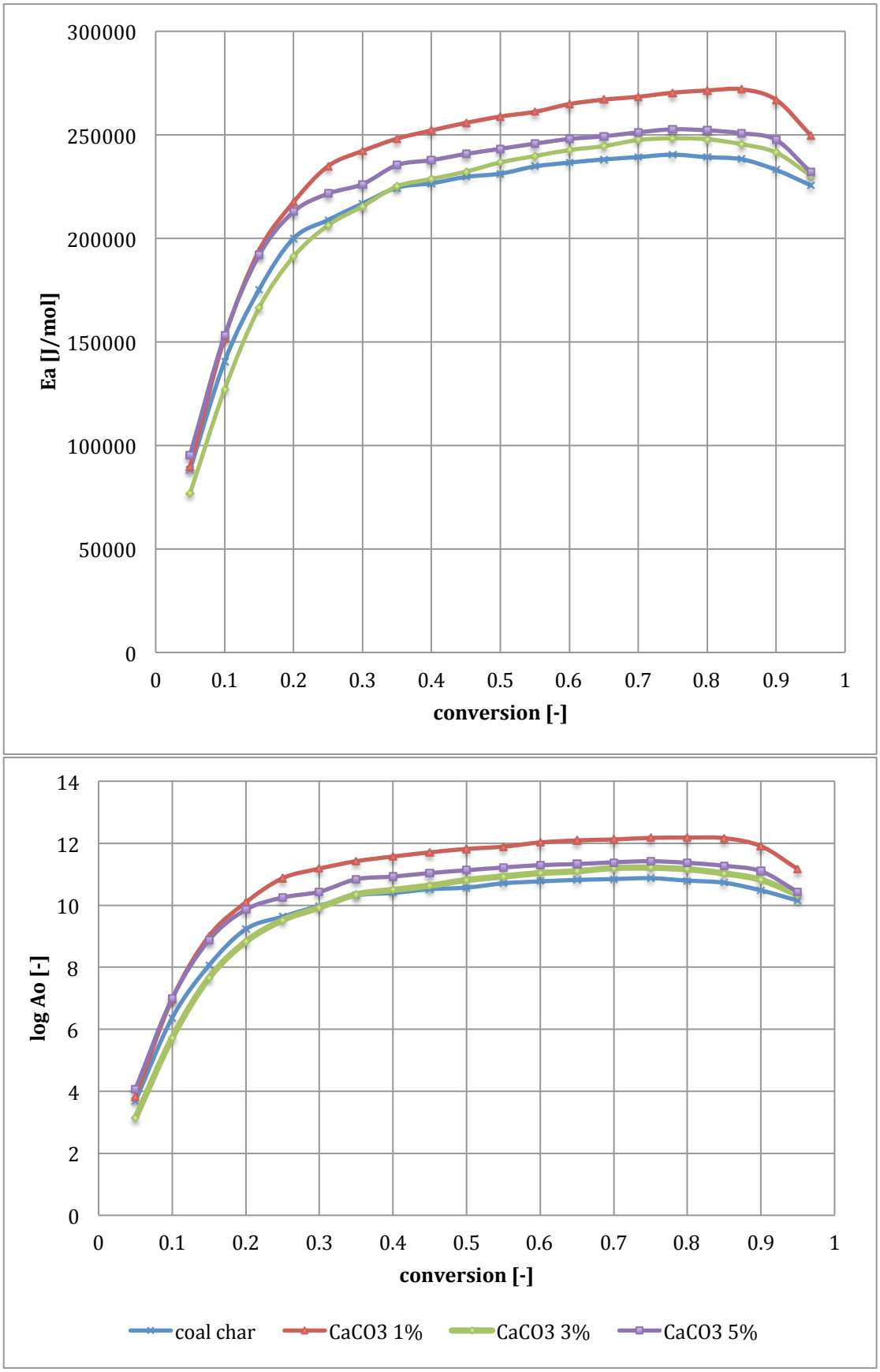

Figure 54. Coal char with limestone catalyst gasification Friedman modelling results: activation energy and pre-exponential factor.

5.2.2. IRON (III) OXIDE CATALYST

As it may be seen on following Figures 56-58, the activation energy calculated using all models were in similar range, as well comparing to the limestone catalyst tests. It is approximately *240-250 kJ/mol* for conversion values greater then *0.2* and pre-exponential factor logA is approximately *7-8* s^{-1} for FWO and *6-8* s^{-1} KAS models and *10-12* s^{-1} for Friedman method. Those results are comparable with one obtained by other research group investigating coal char gasification [61], who calculated the activation energy (*245 kJ/mol*) and pre-exponential factor (*7.41* s^{-1}) using the F1 method. Comparing to the parent coal gasification tests performed by [66], char gasification reveals a significantly higher value. It can be justified by the passivation of the char surface. The activation energy and pre-exponential factor increase significantly for all samples in the conversion range from the beginning of the gasification to the conversion *0.3*. From that moment it, stabilize and obtain above-mentioned value for the rest of course of reaction. Catalyst effect of iron (III) oxide addition was observed only in the first stage of the gasification up to *0.1* conversions for *1%*$_{wt}$ of addition, *0.2* for *3%*$_{wt}$ and *5%*$_{wt}$ addition. In the rest of conversion range Fe_2O_3 loading do not only showed lack of catalytic effect but as well inhibited coal char gasification.

Thus the small or even lack of catalytic effect of iron (oxide) addition was probably due to a relatively large iron (oxide) particle size, which resulted as well as in limestone case in transport limitations [68]. Japan scientist reached conclusion that catalysts particle size is very important factor. Finely dispersed catalyst shows highest activities. Moreover, they concluded that due to the high catalytic effect of iron dependence on the coal type. They found that iron drastically promotes brown coal, the effect is much smaller for bituminous coal. As coal char is characterized by high coal rank it may not influence its gasification. However, group supervised by Xuejun Qi [69] investigated effect of iron on Shenfu coal char gasification reactivity. They observed that carbon conversion rate increased with the rise of iron loading within *0-2 %*$_{wt}$. However, as it may be seen in following Figure 55 further increase of iron loading had no obvious catalytic effect. It may be result, as in this case, of a suppressing effect, related to the aggregation of iron catalyst [70,71], leading to the lost of the catalyst surface area. The fine iron particles have high mobility and high activity, which can promote the gasification of char. Unfortunately, the size of iron particle rises with the increase of catalyst loading, which leads to the reduction of catalytic effect on char.

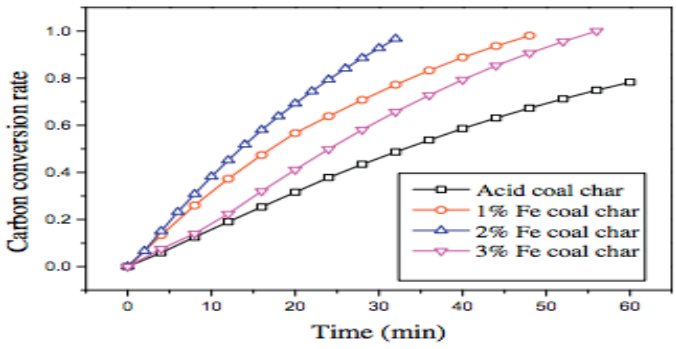

Figure 55. Carbon conversion rate during CO_2 char gasification [70,71].

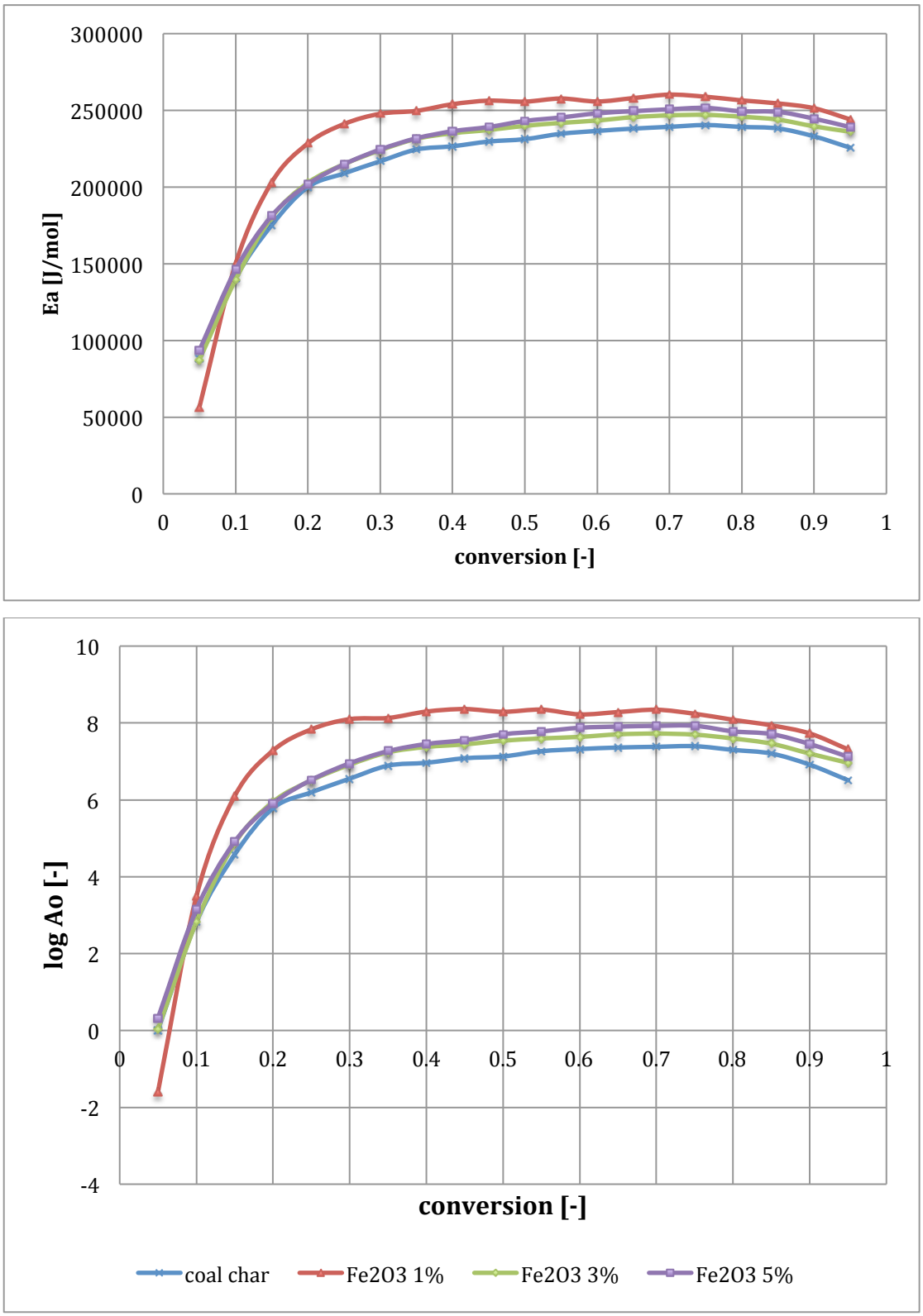

Figure 56. Coal char with Fe_2O_3 catalyst gasification Flynn Wall Ozawa modelling results: activation energy and pre-exponential factor.

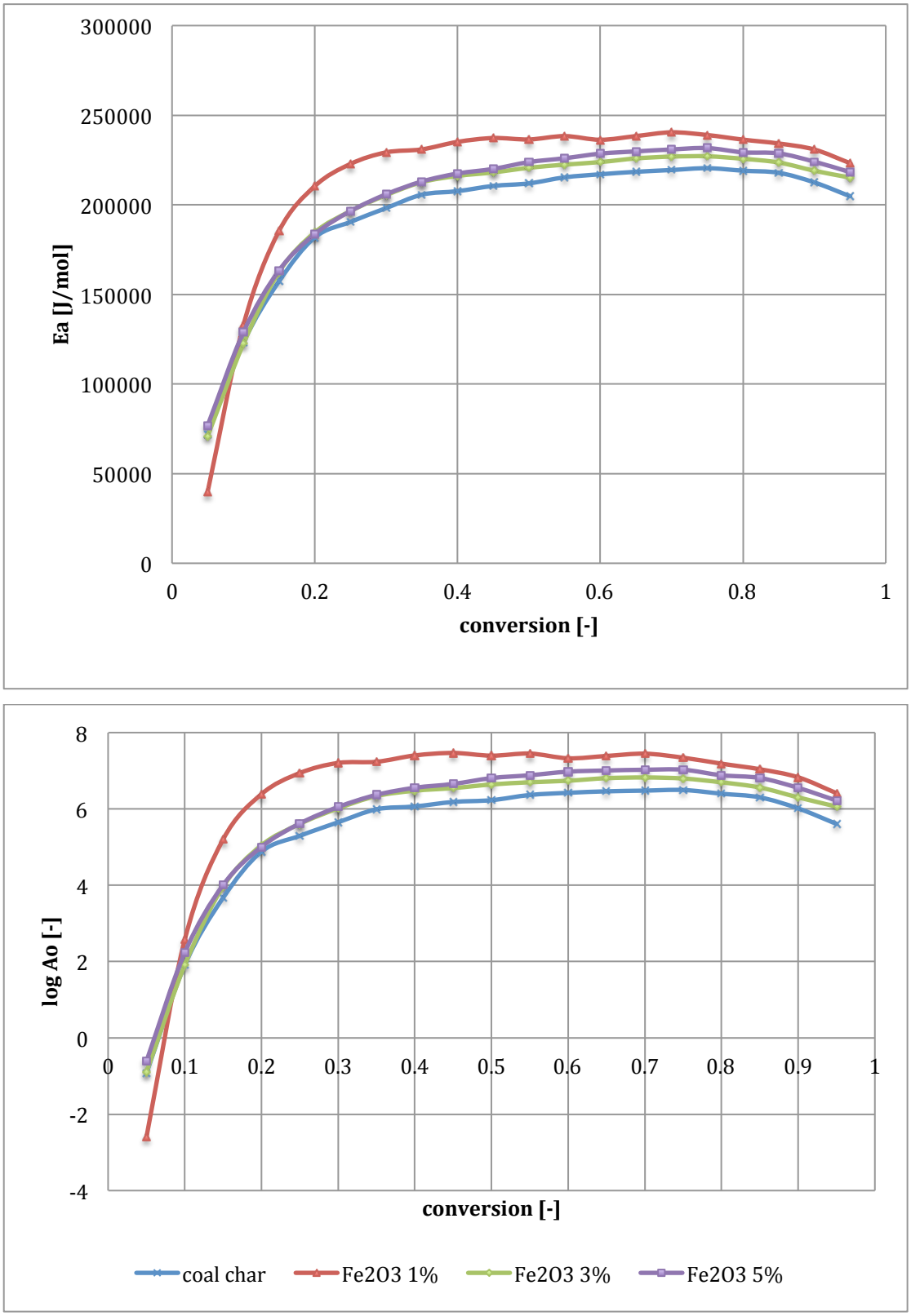

Figure 57. Coal char with Fe_2O_3 catalyst gasification Kissinger-Akahira-Sunose modelling results: activation energy and pre-exponential factor

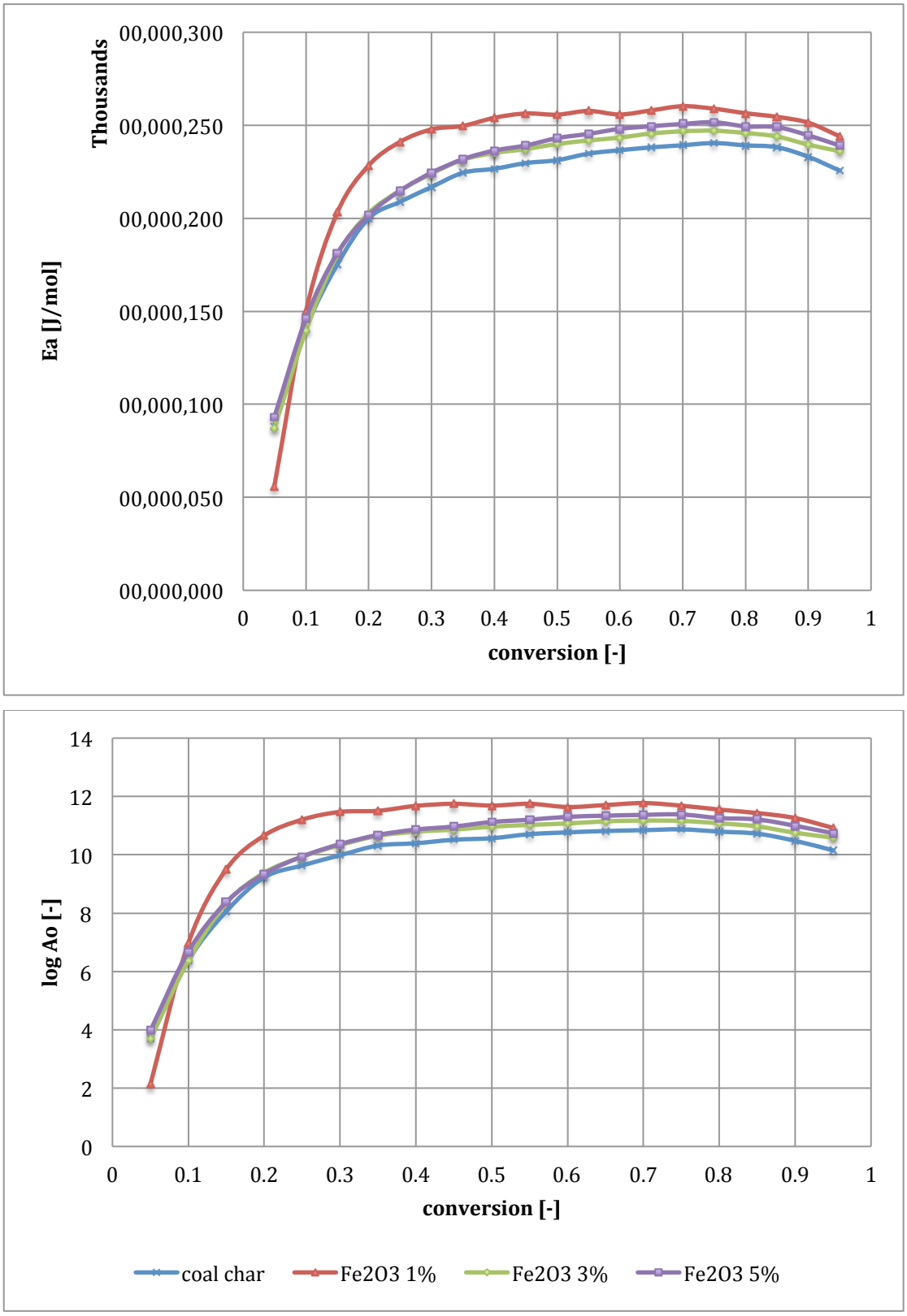

Figure 58. Coal char with Fe_2O_3 catalyst gasification Friedman modelling results: activation energy and pre-exponential factor.

5.3. COAL CHAR GASIFICATION RESULTS

Results of performed “in-situ” fixed bed coal char gasification tests are presented in Figure 59, below. They confirmed those obtained during thermogravimetric tests. It shows constant influence of mineral oxides addition while up scaling. Gasification reaction as it was concluded before, started at temperature about *1000 K*, from there carbon monoxide concentration started to be larger than *1%* in process gas. Addition of $3\%_{wt}$ of limestone inhibited coal char gasification, obtained in same temperatures CO concentrations were lower then one obtained in pure coal char gasification.. As depicted, addition of $3\%_{wt}$ of iron (III) oxide promoted CO production, its concentrations obtained in same temperatures were slightly higher then one obtained in pure coal char gasification.

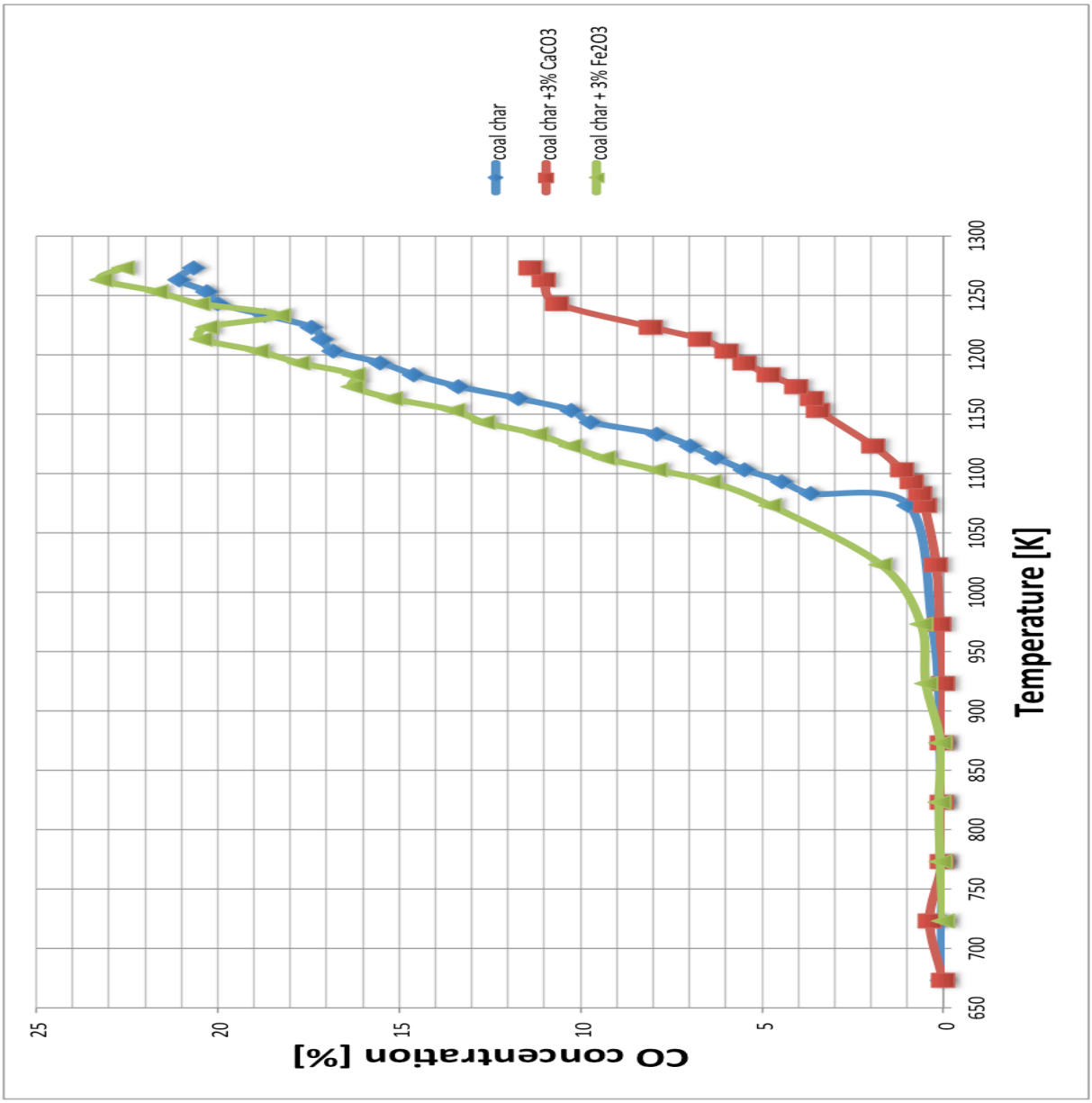

Figure 59. Concentration of carbon monoxide in syngas produced during coal char gasification dependence on the temperature.

5.4. SEM + EDS RESULTS

All samples, of coal char (before and after CO_2 gasification), coal char mixtures with artificial catalysts (before and after CO_2 gasification) were tested by Scanning Electron Microscopes (SEM) with Energy Dispersive X-ray Spectroscopy (EDS) analysis. As it may be seen in following Figures 60 and 61, coal char was milled to very small particles (*10-100* μm), its particles have coarse surface and irregular shape, even after conversion (Figure 61). After EDS test (Figure 62), it was confirmed that irregular particles were mineral matter particles. Its composition given in Table 14 by EDS was similar to one tested before. After the gasification reaction number of particles with smooth surface increase, those are pure carbon particles.

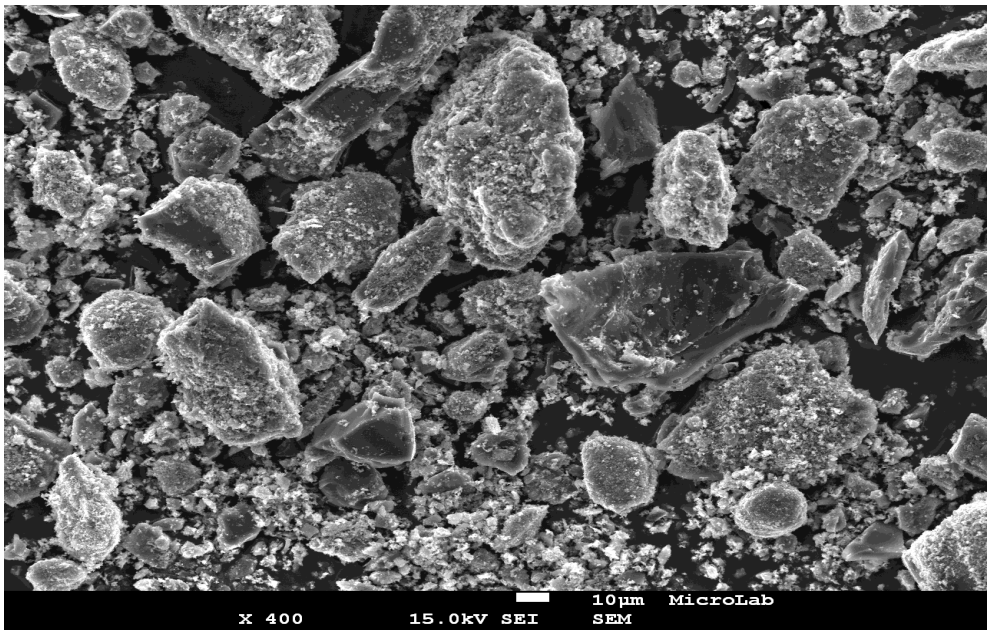

Figure 60. SEM picture of coal char samples before gasification.

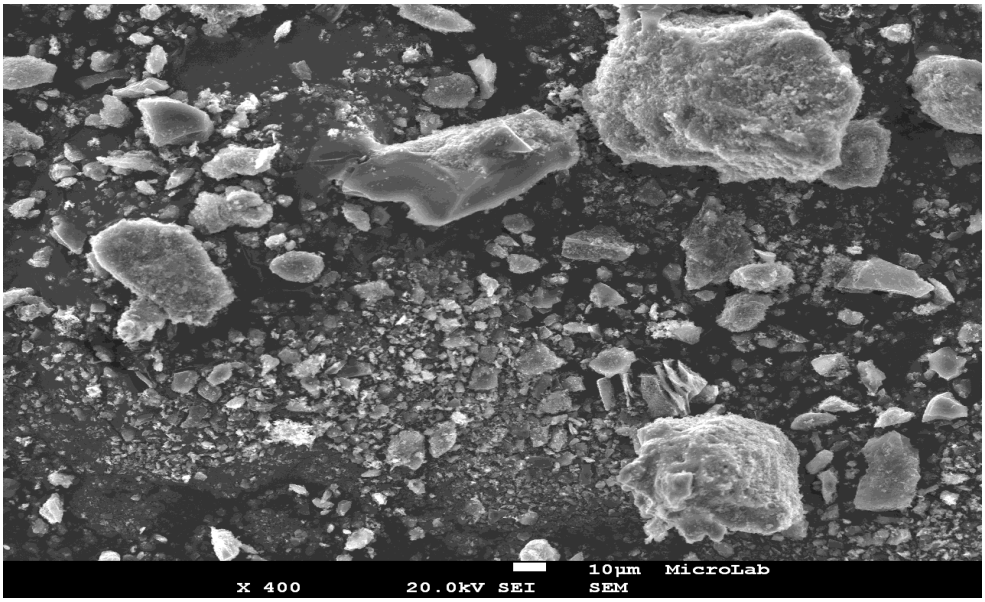

Figure 61. SEM picture of coal char samples after gasification.

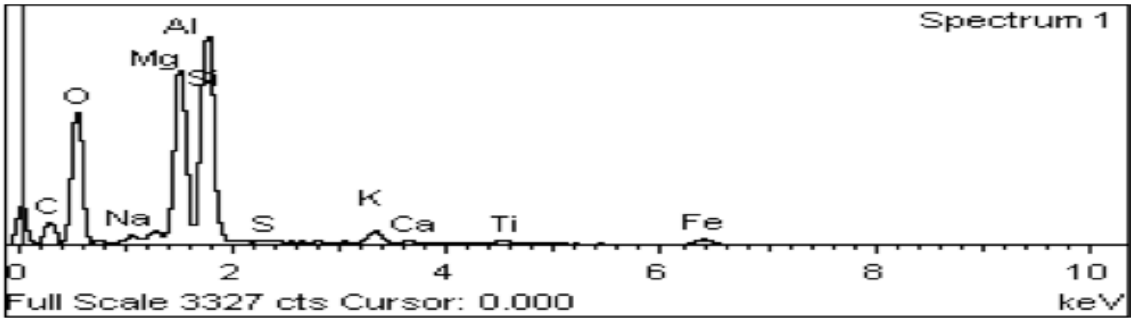

Figure 62. EDS spectrum of mineral matter after gasification.

Table 14. EDS Acquisition geometry (degrees) of mineral matter after gasification:

Element	App Conc.	Intensity Corrn.	Weight%	Weight% Sigma	Atomic%
C K	18.84	0.3442	24.11	1.74	34.00
O K	71.60	0.7011	44.96	1.11	47.61
Na K	1.14	0.8488	0.59	0.07	0.44
Mg K	1.19	0.7839	0.67	0.07	0.46
Al K	22.29	0.8750	11.22	0.29	7.04
Si K	28.53	0.8100	15.51	0.40	9.35
S K	0.29	0.8000	0.16	0.04	0.09
K K	2.55	0.9956	1.13	0.06	0.49
Ti K	0.79	0.8039	0.43	0.06	0.15
Fe K	2.25	0.8077	1.22	0.09	0.37
Totals			100.00		

Those test confirmed that after gasification mostly mineral matter composes residual sample. Performed during sample preparation milling and sieving, led to coal char sample with very small porosity. It may be seen on above Figures that coal char has lack of macro pores.

Further SEM pictures were taken on coal char with artificial limestone addition. Figure 63 shows that limestone particles are not very dense on coal char surface. Moreover, as seen in Figure 64, catalyst particles are similar to coal char size, with irregular shape, very uneven, characterized by high porosity. To confirm presence of $CaCO_3$ catalyst EDS test were performed in the area of particle believed to be the limestone. According to Figure 66, showing EDS spectrum with clear Calcium peak. Table 15 presents its high fraction (*49%*) in sample composition. As it was in pure coal char sample case, after gasification sample in Figure 65 shows smaller particles, flaked around smooth carbon particles. It shows that shrinkage of the particle carbon matrix results in the exposure of included minerals in the initial stage of the char.

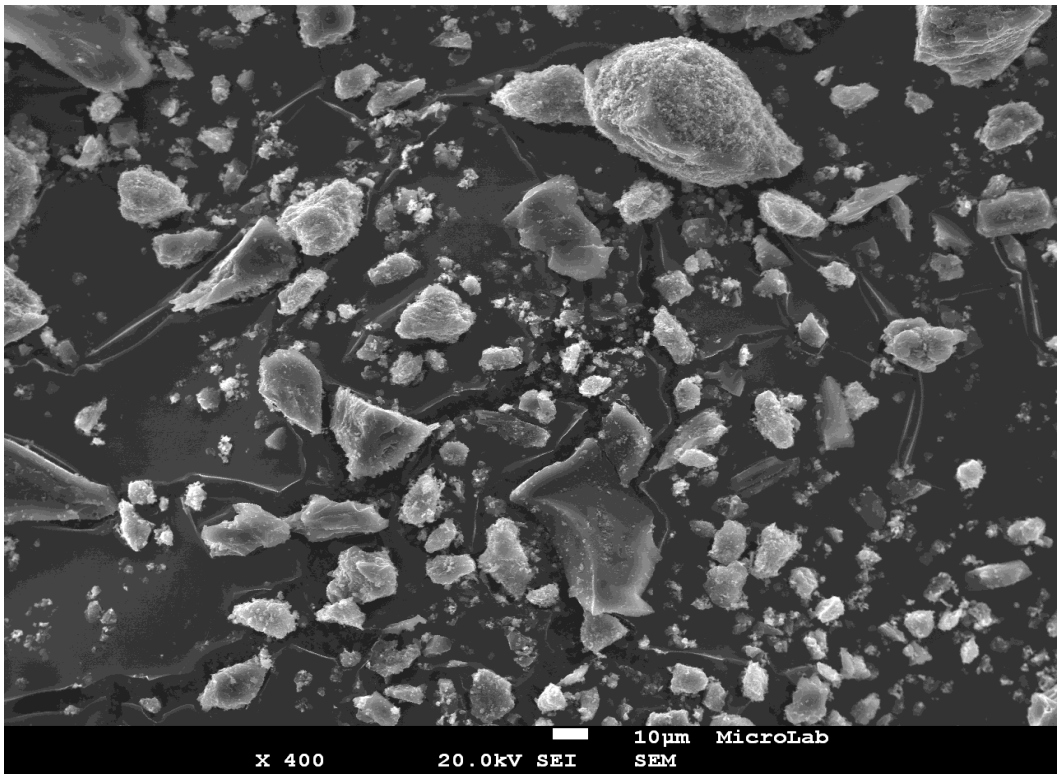

Figure 63. SEM picture of coal char with *3%* of $CaCO_3$ catalyst before gasification.

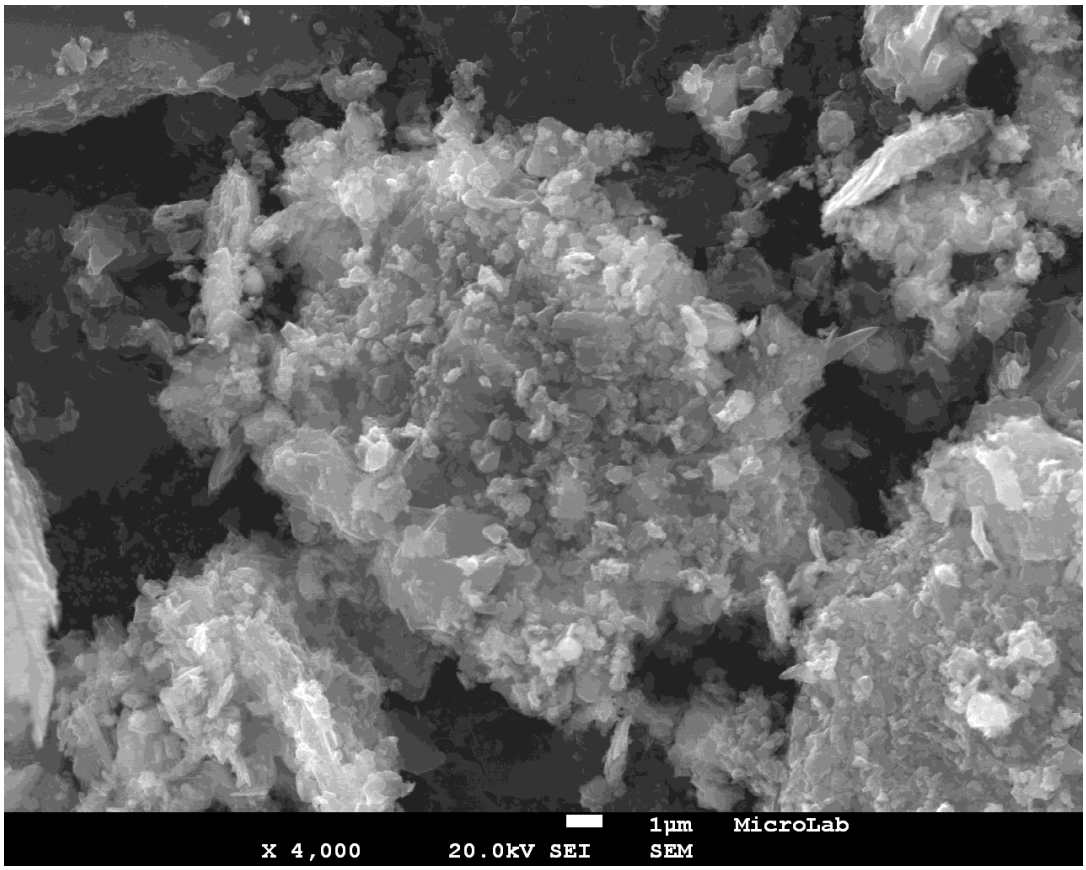

Figure 64. SEM picture of limestone catalyst.

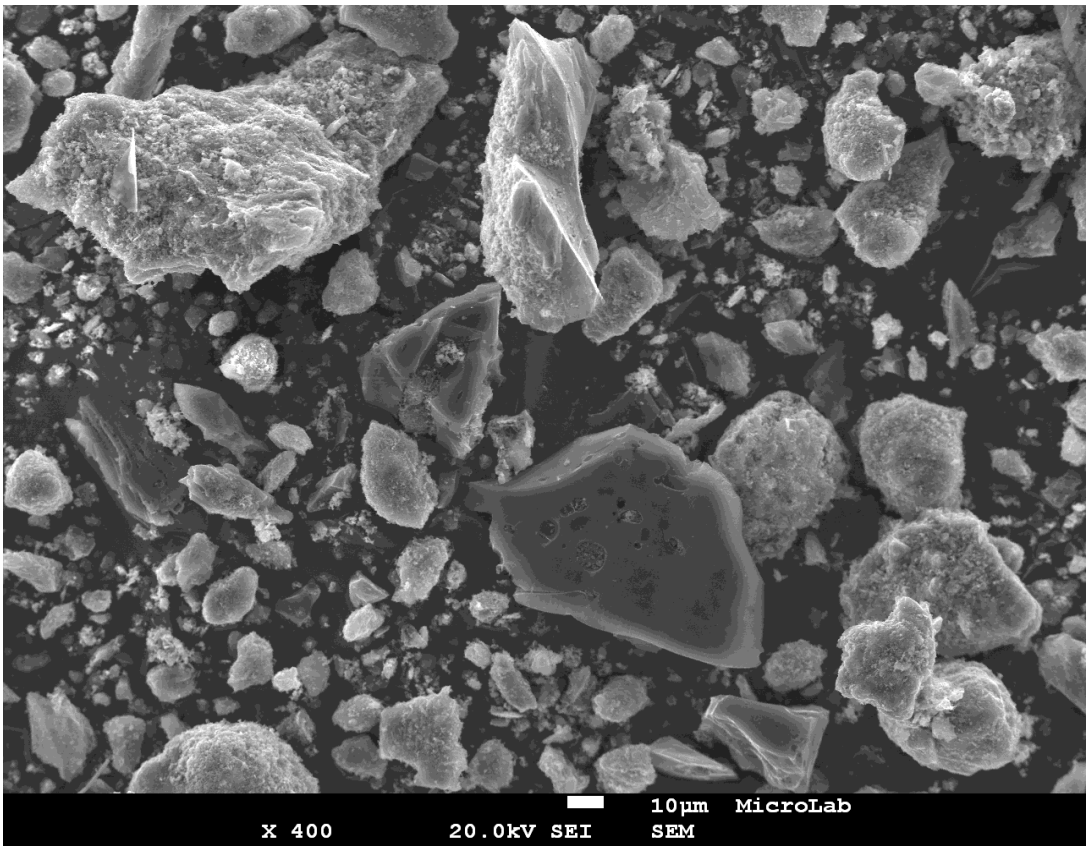

Figure 65. SEM picture of coal char samples with 3% of limestone catalyst after gasification.

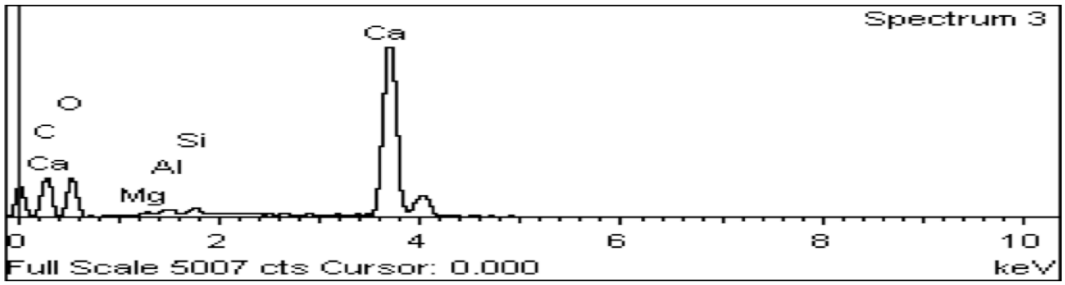

Figure 66. EDS spectrum of limestone catalyst.

Table 15. EDS Acquisition geometry (degrees) of $CaCO_3$ catalyst:

Element	App Conc.	Intensity Corrn.	Weight%	Weight% Sigma	Atomic%
C K	25.08	0.9160	18.64	0.47	28.96
O K	25.93	0.3776	46.73	0.56	54.52
Mg K	0.29	0.6620	0.30	0.06	0.23
Al K	0.83	0.7787	0.73	0.06	0.50
Si K	0.90	0.8710	0.70	0.06	0.47
Ca K	49.47	1.0234	32.90	0.38	15.32
Totals			100.00		

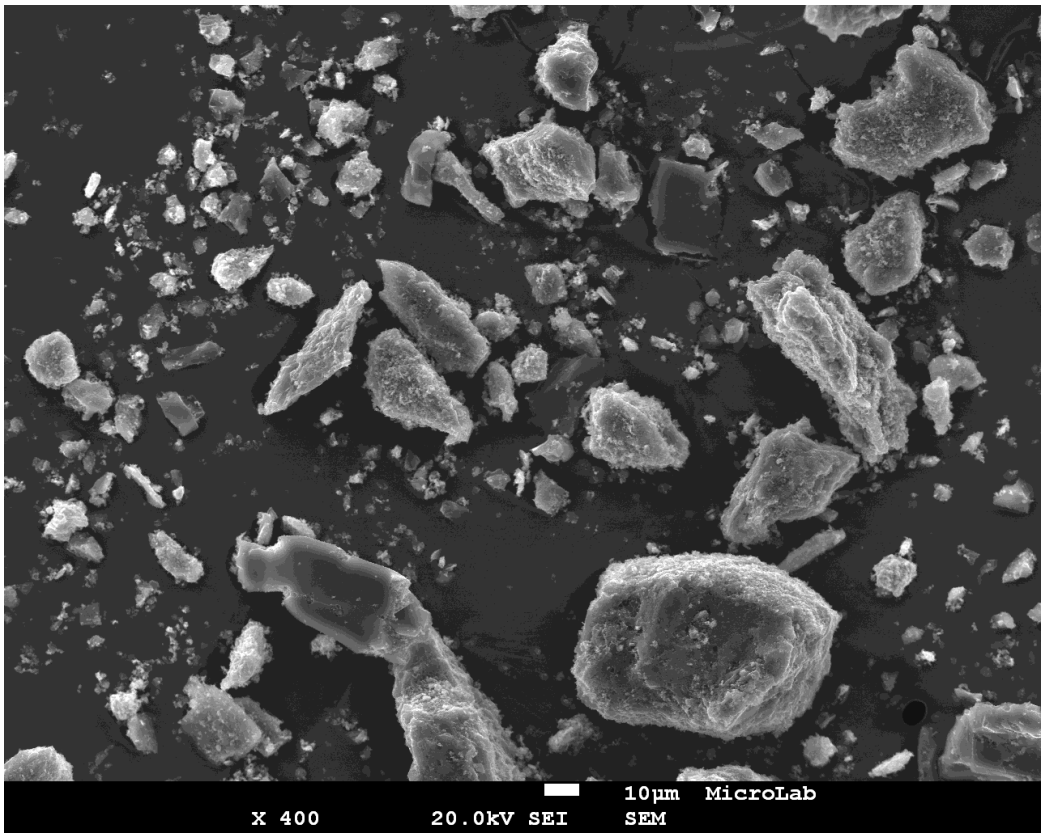

Figure 67. SEM picture of coal char with 3% of Fe_2O_3 catalyst before gasification.

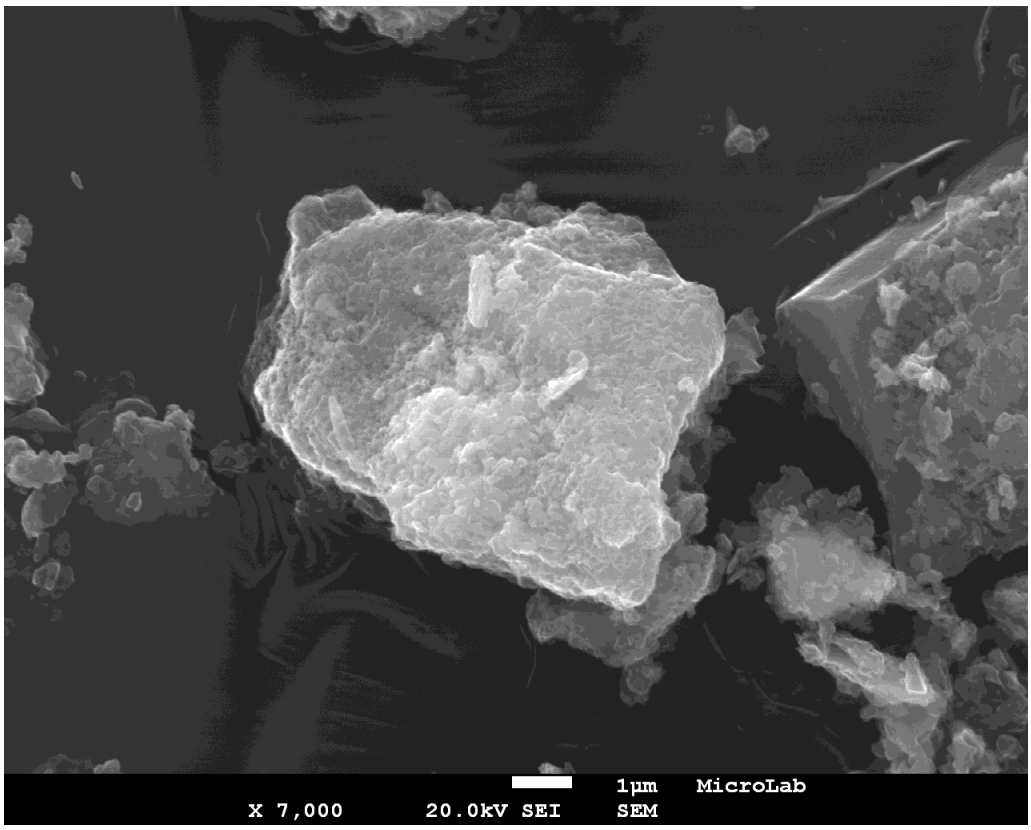

Figure 68. SEM picture of Fe_2O_3 catalyst.

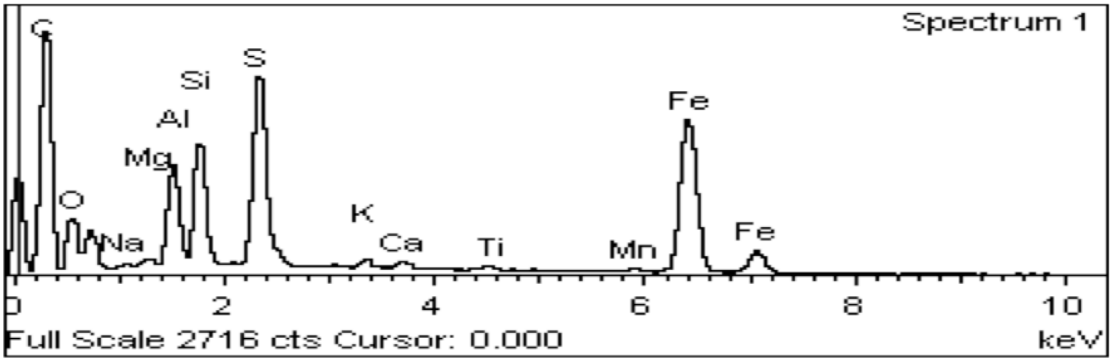

Figure 69. EDS spectrum of Fe_2O_3 catalyst.

Table 16. EDS Acquisition geometry (degrees) of Fe_2O_3 catalyst:

Element	**App Conc.**	**Intensity Corrn.**	**Weight%**	**Weight% Sigma**	**Atomic%**
C K	79.06	0.5107	59.04	0.60	75.05
O K	19.13	0.4347	16.79	0.57	16.02
Al K	2.67	0.8217	1.24	0.06	0.70
Si K	3.07	0.8911	1.31	0.06	0.71
S K	19.67	0.9493	7.90	0.15	3.76
Fe K	29.01	0.8063	13.72	0.26	3.75
Totals			100.00		

Figure 67 shows coal char with artificial 3% iron (III) oxide loading. Catalyst was very sparse on the sample surface, as it may be seen its particles are significantly smaller then coal char ones. As presented in Figure 68 iron (III) oxide has regular, low porous shape. Confirmation of catalyst presence was performed by EDS test; on its spectrum in Figure 69 iron peak is very clear. Moreover, in sample composition presented in Table 16 iron has notably higher share. However its size is not so small as it was supposed to be. Catalyst producer said that its size was supposed to be below 5 μ, but as it may be seen in Figure 68 made with high magnitude (x7000) particles are even 2-3 times bigger.

7. SUMMARY AND CONCLUSIONS

Literature reports that several factors have a great impact on coal char gasification in a CO_2 atmosphere. Among them could be considered: coal rank, process temperature, process and gas pressure, gas composition (CO_2 concentration), coal and ash chemical composition, additional mineral catalyst, pore structure, and particle size. Their impacts were briefly presented in the *Literature part* of this paper. Influence of mineral matter presence and its composition, due to its possible catalytic effect is today under great interest of research groups. In this paper impact of artificial addition of limestone and iron (III) oxide were investigated. Presented in *Experimental part* results of performed thermogravimetric, SEM, EDS, "in-situ" fixed-bed reactor tests led to several conclusions.

Firstly, prepared coal chars were stabilized and chemically deactivated. It was hard to gasify them, and conversions were achieved at the high temperatures. This was caused by the fact that they were characterized by relatively high ash content. Obtained reaction rates, conversions and activation energies were comparable to the ones presented by other research groups [61] investigation kinetics of coal char gasification in carbon dioxide.

Secondly, investigated mineral oxides additions were in most ranges inhibiting coal char gasification. In principle, two effects are expected, i.e. higher coal char conversion and shift of reaction equilibrium to carbon monoxide direction. As it may be concluded from Thermogravimetric results, there was no positive effect on gasification progress. Limestone addition only in $3\%_{wt}$ loading and up to *0.4* conversion rate showed catalysis effect. Iron (III) oxide was catalysing coal char gasification only up to *0.1* conversion rate. Those results correlates with one obtained by Tanaka S, Uemura T, Ishizaki [23]. It may by stated that mineral matter in coal needs time to be activated as catalyst and this results in a increasing rate and in a later stage catalytic effect becomes weaker because reaction surface is blocked by ash layer. However, gasification tests in the fixed bed reactor showed caused by iron oxide (III) addition desired shift of the reaction equilibrium to the carbon monoxide production direction.

Thirdly, dispersion of catalyst over the organic matrix is a major consideration when studying gasification and catalyst effects. Prepared sample were milled and sieved under *100 μm* particle-size. It was believed that it would guarantee mapping of mineral matter distribution in coal matrix. Instead small particles were deprived of macro-pores and contact area between carbon and artificial catalyst loading was hindered. Moreover, at high conversions, exposure of included minerals on the char surface was mostly caused by fragmentation. In the later stage of gasification, the char particle fragmented into a few particles of *20–30 μm* as indicated by SEM pictures [72]. Addition of limestone or iron (III) oxide catalyst did not promote coal char gasification; its particles conglomerated and blocked active sites.

Fourthly, chosen due to its simplicity and low costs, physical mixing of coal char sample with artificial mineral oxide catalyst method [73] was not the proper way to map mineral matter distribution in coal matrix. For future research, "wet-method" of loading catalyst particles on coal char surface from its solution should be taken under investigation [74].

REFERENCES

[1] Energy production and imports, Eurostat, http://ec.europa.eu/eurostat/statistics-explained/, 1.06.2014
[2] EURACOAL EU Statistics, http://www.euracoal.be/pages 1.06.2014
[3] BP Statistical Review of World Energy 3, http://www.bp.com/content/dam/bp/pdf/statistical-review 1.07.2014
[4] EA Statistics OECD/IEA, http://www.iea.org/stats/index.asp, International Energy Agency electronic files on CO2 Emissions from Fuel Combustion., 1.08.2014
[5] Kyoto Protocol, UNFCCC, 1997, http://unfccc.int/kyoto_protocol/items/2830.php 1.08.2014
[6] UE 2030 Framework, http://ec.europa.eu/clima/policies/2030/index_en.htm, 1.08.2014
[7] Coal Gasification Systems, http://www.netl.doe.gov/research/coal/energysystems/gasification, 1.10.2014
[8] http://www.gasification.org/uploads/eventLibrary/2013-GTC2013-Higman-Presentation.pdf, 1.08.2014
[9] Marek Ściażko, Lectures, Gasification, AGH 2013/2014
[10] EIA, International Energy Outlook, http://www.eia.gov/forecasts/ieo/, 1.09.2014
[11] Michał Kumor; Zgazowanie węgla - szansa na czyste jutro; AGH, 2014
[12] Tomasz Chmielniak, Marek Sciazko, Aleksander Sobolewski, Grzegorz Tomaszewicz, Józef Popowicz; Zgazowanie wegla przy zastosowaniu CO2 sposobem na poprawe wskazników emisyjnych i efektywnosci procesu; Polityka Energetyczna Tom 15 Zeszyt 4 2012
[13] IRFAN i in. 2011 – IRFAN M.F., USMAN M.R., KUSAKABE K., 2011 – Coal gasification in CO_2 atmosphere and its kinetics since 1948: A brief review. Energy, 36, 12–40
[14] H. Ono, S. Yoshida, M. Nezuka, T. Sano, M. Tsuji, Y. Tamaura, Kinetics and simulation on high-temperature solar thermochemical energy conversion process on the Boudouard reaction, Energy & Fuels 13 (1999) 579–584.
[15] CI Keattch and D. Dollimore, Introduction to Thermogravimetry, Heyden, London, UK, 1975.
[16] Nozaki T, Adschiri T, Fujimoto K. Coal char gasification under pressurized CO_2 atmosphere. Fuel 1992;71:349-50.
[17] Sha X-Z, Chen Y-G, Cao J, Yang Y-M, Ran D- Q. Effects of operating pressure on coal gasification. Fuel 1990;69:656-9.
[18] Roberts DG, Harris DJ. Char gasification with O_2, CO_2, and H_2O: effects of pressure on intrinsic reaction kinetics. Energy Fuels 2000;14:483-9.
[19] Tie-feng Liu, Yi-tian Fang, Yang Wang; An experimental investigation into the gasification reactivity of chars prepared at high temperatures; Fuel 87 (2008) 460–466
[20] R.C. Messenbock, D.R. Dugwell, R. Kandiyoti; CO2 and steam-gasification in a high-pressure wire-mesh reactor: the reactivity of Daw Mill coal and combustion reactivity of its chars; Fuel 78 (1999) 781–793
[21] Gui-Su Liu, Stephen Niksa; Coal conversion submodels for design applications at elevated pressures. Part II. Char gasification; Progress in Energy and Combustion Science 30 (2004) 679–717
[22] Ahn DH, Gibbs BM, Ko KH, Kim JJ. Gasification kinetics of an Indonesian sub- bituminous coal char with CO_2 at elevated pressure. Fuel 2001;80:1651-8.
[23] Tanaka S, Uemura T, Ishizaki S, Nagayoshi K, Ikenaga N, Ohme H, et al. CO_2 gasification of iron-loaded carbons: activation of the iron catalyst with CO. Energy Fuels 1995;9:45-52.
[24] Matsuoka K, Yamashita T, Kuramoto K, Suzuki K, Takaya A, Tomita A. Transformation of alkali and alkaline earth metals in low rank coal during gasification. Fuel 2008;87:885-93.
[25] Grigore M, Sakurovs R, French D, Sahajwalla V. Mineral reactions during coke gasification with carbon dioxide. Int J Coal Geol 2008;75:213-4.
[26] Bai J, Li W, Li C-Z, Bai Z-Q, Li B- Q. Influences of mineral matter on high temperature gasification of coal char. J Fuel Chem Technol 2009;37:134-8.
[27] Schafer HNS. Functional groups and ion exchange properties. In: Durie RA, editor. The science of Victoria brown coal: structure, properties and conse- quences for utilization. Oxford: Butterworth-Heinemann Ltd; 1991. Ch. 7.
[28] Nishiyama Y. Catalytic behavior of iron and nickel in coal gasification. Fuel 1986;65:1404-9.
[29] Ye DP, Agnew JB, Zhang DK. Gasification of a South Australian low rank coal with carbon dioxide and steam: kinetics and reactivity studies. Fuel 1998;77:1209-19.
[30] Li S, Cheng Y. Catalytic gasification of gas-coal char in CO_2. Fuel 1995;74:456-8.
[31] Asami K, Sean P, Furimsky E, Ohtsuka Y. Gasification of brown coal and char with carbon dioxide in the presence of finally dispersed iron catalysts. Fuel Process Technol 1996;47:139-41.
[32] Marco A. Saucedo, Jin Yang. Lim, John S. Dennis, Stuart A. Scott; CO2-gasification of a lignite coal in the presence of an iron-based oxygen carrier for chemical-looping combustion, Fuel 127 (2014) 186–201
[33] Setyawati Yani, Dongke Zhang An experimental study of sulphate transformation during pyrolysis of an Australian lignite, Fuel Processing Technology Volume 91, Issue 3, March 2010, Pages 313–321
[34] Biswas AK. Principles of blast furnace iron making. Brisbane: Cootha Publishing House; 1981.
[35] Hu G, Dam-Johansen K, Wedel S, Hansen JP. Decomposition and oxidation of pyrite. Progr Energy Combust Sci 2006;32:295-304.

[36] G. Skodras, G. Nenes, N. Zafeiriou; Low rank coal e CO 2 gasification: Experimental study, analysis of the kinetic parameters by Weibull distribution and compensation effect; Applied Thermal Engineering xxx (2013) p.1-8
[37] D. P. Ye, J. B. Agnew, D. K. Zhang, "Gasification of South Australian Low Rank Coal with Carbon Dioxide and Steam: Kinetics and Reactivity Studies", Fuel, 77, 1209-1219 (1998)
[38] A. Aboulkas, K. El Harfi, Study of the kinetics and mechanisms of thermal decomposition of moroccan tarfaya oil shale and its kerogen, oil shale, 2008, vol. 25, no. 4, pp. 426–443
[39] B. Jankovic, Kinetic analysis of the non-isothermal decomposition of potassium metabisulfite using the model-fitting and isoconversional (model-free) methods, Chemical Engineering Journal 139 (2008) 128–135
[40] Friedman, H. Kinetics of thermal degradation of char-forming plastics from thermogravimetry. Application to a phenolic plastic // J. Polym. Sci., Part C. 1964. Vol. 6. P. 183–195.
[41] Kissinger, H. E. Reaction kinetics in differential thermal analysis // Anal. Chem. 1957. Vol. 29, No. 11. P. 1702–1706.
[42] Akahira, T., Sunose, T. Trans. Joint Convention of Four Electrical Institutes, Paper No. 246, 1969 Research Report // Chiba Institute of Technology Sci. Technol. 1971. Vol. 16. P. 22–31.
[43] Coats, A. W., Redfern, J. P. Kinetic parameters from thermogravimetric data // Nature. 1964. Vol. 201. P. 68–69.
[44] Williams, P. T., Ahmad, N. Investigation of oil-shale pyrolysis processing conditions using thermogravimetric analysis // Appl. Energy. 2000. Vol. 66, No. 2. P. 113–133.
[45] J.H.Flynn,L.A.Wall,J.Res.Natl.Bur.Stand.,A:Phys.Chem.70A(1966) 487.
[46] T. Ozawa, Bull. Chem. Soc. Jpn. 38 (1965) 1881.
[47] C. Doyle, J. Appl. Polym. Sci. 6 (1962) 639.
[48] J.H. Flynn, J. Therm. Anal. 27 (1983) 95.1
[49] Polish Standard PN-80/G-04511
[50] Polish Standard PN-80/G-04512
[51] Polish Standard PN-G-04516:1998
[52] Polish Standard Q/LP/03/A:2011
[53] Polish Standard PN-G-04584:2001
[54] Polish Standard PN-G-04571:1998
[55] Polish Standard Q/LP/55A:2011
[56] Polish Standard PN-G-04534:1999
[57] Polish Standard PN-82/G-04543
[58] Polish Standard PN-80/PN-04511pkt.2.3.3.
[59] Polish Standard Q/LP/32/A:2011
[60] Mineral's pricelist http://minerals.usgs.gov/minerals/pubs/commodity/index.html , 1.11.2014
[61] Grzegorz Łabojko, Michalina Kotyczka-Moranska, Agnieszka Plis, Marek Sciazko, Kinetic study of polish hard coal and its char gasification using carbon dioxide, Thermochimica Acta 549(2012) p158-165
[62] Estimating kinetic parameters in TGA using B-spline smoothing and the Friedman method, X. Zhang, W. Jong, F. Preto, Biomass and Bioenergy, Vol. 33, P: 1435-1441, 2009
[63] An Approach to using agricultural waste fibers in biocomposites application: thermogravimetric analysis and activation energy study. M.S Alwani, H.P.S. Abdul Khalil, O.Sulaiman, Bioresources, 2014, 9(1) 218-230
[64] IX Congresso Brasileiro de Análise Térmica e Calorimetria 09 a 12 de novembro de 2014 – Serra Negra – SP - Brasil The applicability of isoconversional models in estimating the kinetic parameters of biomass pyrolysis
[65] Comparative degradation kinetic studies of three biopolymers: Chitin, chitosan and cellulose. S. Arora, S. Lal, S. Kumar, Archives of Applied Science Research, 2011, 3 (3):188-201
[66] David Harris, Coal Gasification Reactivity: Measurement and Application, Pittsburgh Coal Conference, 2007
[67] R.C. Timpe, R.E. Sears, anion effects on calcium catalysis of low-rank Coal char-steam gasification, Energy&Enviromental Research Center, p530-534
[68] Hiroshi Mori, Kenji Asami, and Yasuo Ohtsuka**,** Role of Iron Catalyst in Fate of Fuel Nitrogen during Coal Pyrolysis , Energy & Fuels 1996, 10, 1022-1027
[69] Xuejun Qi, Xin Guo, Lucheng Xue, Chuguang Zheng, Effect of iron on Shenfu coal char structure and its influence ongasification reactivity, Journal of Analytical and Applied Pyrolysis 110(2014), p401-407
[70] H. Mori, K. Asami, Y. Ohtsuka, Role of iron catalyst in fate of fuel nitrogen during coal pyrolysis, Energy Fuels 10 (1996) 1022–1027.
[71] K. Asami, P. Sears, E. Furimsky, Y. Ohtsuka, Gasification of brown coal and char with carbon dioxide in the presence of finely dispersed iron catalysts, Fuel Process. Technol. 47 (1996) 139–151.
[72] Suhui Li, PhD dissertation: Char–Slag Transition During Pulverized Coal Gasification; Department of Chemical Engineering; The University of Utah; May 2010
[73] Mingquan Jiang, Jie Hu, Jie Wang, Calcium-promoted catalytic activity of potassium carbonate for steam gasification of coal char: Effect of hydrothermal pretreatment, Fuel 109 (2013) 14–20
[74] J. Yu, F.J.Tian, L.J. McKenzie, C.Z.Li; Char-suppoerted nano iron catalyst from WGS Reaction: hydrogen production from coal/biomass gasification; Process Safety and Enviromental Protection; Vol. 84 Issue 2, 2006, p125-130